EXPERIMENTS IN A CYLINDRICAL MAGNETIC SHOCK TUBE

Thesis by

George C. Vlases

In Partial Fulfillment of the Requirements

For the Degree of

Doctor of Philosophy

California Institute of Technology

Pasadena, California

1963

ACKNOWLEDGMENTS

The author wishes to express his sincere appreciation to Professor H. W. Liepmann, who suggested this problem originally and under whose direction the research was carried out. He also wishes to thank Professors J. D. Cole and G. B. Whitham for their fruitful discussions on the interpretation of the experimental results. The help of Mrs. Geraldine Krentler in typing the manuscript and Mrs. Nell Kindig in preparing the figures is also gratefully acknowledged.

The author is further indebted to the National Science Foundation for their continuing fellowship support and to the Francis I. du Pont Fund for Magnetohydrodynamic Research, which supported the experiments.

ABSTRACT

An investigation has been conducted with the two-fold purpose of producing very high Mach number shock waves and studying their interaction with an external magnetic field parallel to the shock front. By means of the technique of electromagnetic driving, stable, reproducible, outward-going cylindrical shock waves in the Mach number range from 20 to 100 have been produced and studied.

Theory predicts fundamental differences between the interaction of a magnetic field with a shock moving into a highly conducting fluid and the interaction of a field with a strong gas-ionizing shock. In the former case a true mhd shock is produced. In the latter the field interacts directly only with the piston and the shock remains an ordinary one. The effect of a conducting wall surrounding the chamber also differs substantially in the two cases.

Detailed experiments have been carried out on gas-ionizing shocks. While the overall motion is very nearly that predicted by the theory, anomalies have arisen in the details of the flow and are explained in a qualitative manner.

Methods of producing sufficient initial conductivity to obtain a thin magnetohydrodynamic shock are discussed, together with some preliminary experiments along these lines.

TABLE OF CONTENTS

TABLE OF CONTENTS (Contd.)

LIST OF FIGURES

LIST OF FIGURES (Contd.)

I. Introduction

A. Scope of the Investigation

Magnetohydrodynamics (mhd) has attracted widespread attention in recent years. Scientists have become interested in processes occurring when a conducting fluid interacts with electromagnetic fields. The study of such processes has been, and will be to an even greater extent in the future, instrumental in the understanding of many problems of astro- and atmospheric physics. Engineers have been attracted by such possible applications as controlled fusion, power generation, propulsion, reduction of aerodynamic heating, and control of lift and drag.

The interest in the present experiments lies in the field of wave motion, and in particular of the motion of strong shocks, where there are some exciting prospects for the production of very high enthalpy gases and interesting aspects of the interaction of shock waves with a magnetic field. These experiments may be envisioned as an mhd analogy to a classical piston problem in ordinary gasdynamics. The early experiments [1] centered on the production of strong shock waves and it was found possible to produce ordinary gasdynamics shocks in the Mach number range from twenty to one hundred which are reproducible, stable, and travel with nearly constant velocity. This Mach number can easily be increased by up to an order of magnitude, as will be discussed below.

Subsequent experiments have been made in which the interaction of these strong shocks with a magnetic field parallel to the shock front was studied with the goal of understanding the basic interaction phenomena.

B. Production of Strong Shocks, Background Sketch

During the last decade several methods have been developed to produce strong shock waves. Conventional shock tubes are capable of producing only relatively low speed shocks, primarily because an infinite ratio of driver to driven section pressure produces only a finite (and rather low) "piston pressure", i.e. pressure immediately behind the shock, for the range of driver to driven section sound speed ratios available by ordinary means.

Stronger shocks can be produced if either the piston pressure can be increased directly or the driver gas can be substantially heated. The latter technique is the one used in chemically and electrically driven shock tubes as well as conventional shock tubes. In an electric shock tube a high current arc is created in the driver section which heats the gas very rapidly and generates a shock wave. Some of the earliest work along these lines was done by Fowler[2, 3] and his group at the University of Oklahoma. In recent years the electric shock tube has been used by many investigators for various purposes such as spectroscopic studies in high energy gases, interaction with external fields, and propulsion.

Alternatively, the "piston pressure" can be increased directly by arranging the Lorentz force resulting from the interaction between the discharge current and a magnetic field in such a way that it aids in propelling the gas; this technique is known as magnetic driving and cannot be accomplished in a conventional shock tube.

Moderately strong shocks can be produced by either electric or magnetic driving, or, as usually is the case, by a combination of

the two. However, as the gas temperature rises, and with it the electrical conductivity, the heating effect, which is inversely proportional to the conductivity, decreases. Conversely, magnetic driving becomes more effective as the temperature increases because the penetration of the field into the fluid decreases; one can think of the piston as becoming less porous. Thus the production of very high speed shocks is most easily accomplished by magnetic driving.

One of the earliest magnetically driven shock tubes was a T-tube modified by the addition of a backstrap [4] (Figure 1). In this device the interaction of the discharge current with the field of the returning current in the backstrap produces a force directed down the tube which helps to propel the gas. Although much of the driving still comes from arc heating, many experimenters have demonstrated that increased shock velocity results from the addition of the backstrap.

Another popular configuration is the conical shock tube as suggested by Josephson [5]. Here all the field, in principle, is trapped between the current in the gas and the electrodes and acts to force the gas down the tube.

As a final example one might mention the coaxial linear shock tube which has received a great deal of attention, particularly at AVCO [6]. The magnetic field in the annulus acts on the current sheet to product a shock, as illustrated in Figure 1.

While each of these devices does produce strong shock waves there are several problems which arise. In the T-tube the coupling between the field and the gas is weak and the shock attenuates rapidly. The same is true to a lesser extent in a conical shock tube. The

co-axial geometry is capable of providing a more continuous push on the gas but suffers from difficulties in obtaining a uniform current sheet around the annulus. The current sheet (plasma-vacuum interface) does not seem to be particularly stable. This fact, along with the non-uniform magnetic pressure which varies inversely with the square of the radius across the annulus, makes it difficult to create reproducible, plane shocks. If the annulus spacing is decreased to make driving field more uniform the wall losses become correspondingly greater. The T-tube and conical tube likewise suffer from poor reproducibility and severe wall effects. Experiments with T-tubes, linear coaxial accelerators, and transmission line accelerators have previously been carried out at GALCIT [7, 8].

C. The Cylindrical Magnetic Shock Tube

The experimental geometry used in the present experiments was first discussed by Anderson [9], et al., from a different viewpoint than the present one, and was suggested independently by Liepmann [10]. Current passes through a solid copper center conductor (Figure 2) and returns in a hollow cylindrical arc through the gas. The interaction of the B_θ field produced by the current in the center conductor with the returning current produces a Lorentz force, or, equivalently, a magnetic pressure, which acts radially outward in the manner of a solid cylindrical piston expanding with time and drives a shock wave into the ambient gas. The device is thus termed a cylindrical magnetic shock tube. An axial field B_{z_o} can be established prior to the discharge.

This device possesses several inherent features which make it useful for shock studies. The first of these is its gross stability and

reproducibility, which makes the experiments feasible. This feature has been extensively studied by Colgate and Furth [11] and others and will not be reconsidered here. The magnetic piston forms quickly, remains stable, and produces a continuous push on the gas. A great deal of theoretical work has been done on the flow and provides a guide for interpretation of the experimental results. Theory predicts, and experiment verifies, that the shock velocity is constant for a linearly increasing driving current.* The outward going front is very accessible for optical and probe measurements. Wall losses (to the top and bottom electrodes) are minimized. The fact that the field is confined entirely within the current sheet means not only that the magnetic driving is effective but also that pickup is greatly reduced.

There are some disadvantages to this geometry which should be pointed out. Since the area of the piston is continually expanding, a continuously increasing current must be supplied to prevent decay. This is in contrast to a linear geometry (co-axial or rail) where in principle a constant current produces a constant speed shock. In addition, contamination from the electrodes is a problem as in any discharge where electrodes are present within the discharge chamber. As a direct result of the cylindrical geometry, the ideal separation distance between the shock and contact surface is half of that in a linear geometry.

In spite of these disadvantages it is felt that the cylindrical shock tube, because of its stability and efficient driving, is the most successful magnetic shock tube configuration existing at the present time.

---

* There is an exception which is discussed in Chapter II.

II. Theoretical Predictions of Shock Tube Performance

A. Introductory Remarks

In this chapter we shall discuss various theoretical models of the flow to get an idea of expected performance. The problem of a magnetically driven shock propagating into a region of no field (i.e. the problem studied in the early experiments) is simply a sub-case of the general interaction problem and needs not be discussed separately.

By varying the axial field strength and other parameters the ratio of the ion cyclotron frequency ω_{c_i} to the collision frequency ν_c can be varied over a wide range, making possible an investigation of both the "collisionless shock" limit and the collision dominated case as well as the transition from one to the other. This paper deals mainly with flows in which $\omega_{c_i} / \nu_c \ll 1$.

It is assumed throughout that the conductivity in the arc is sufficiently high that the current runs in a relatively thin annular region, and the concept of a localized "magnetic piston" therefore has validity. This assumption is fairly well justified a posteriori by the experimental results. Single-fluid theory (mhd) is used except when it is clearly inadequate; recourse is then taken to a more elaborate description.

The nature of the flow will be seen to depend critically on whether or not the fluid ahead of the shock is appreciably conducting. For that reason the theoretical discussion is divided into two sections, the first describing the motion when the fluid is initially highly conducting throughout the chamber, and the second describing flows in which a very strong shock propagates into an essentially non-conducting gas.

Most of the experiments reported here were done without any

attempt at preionization. There are two reasons, however, for discussing both theoretical models at this time. First, a few experiments have been carried out in which the gas is rendered highly conducting before the main discharge, and preliminary results indicate that the "everywhere highly conducting" theory is applicable. Secondly, in the absence of attempted preionization, the gas ahead of the shock may become more or less conducting due to radiation and electron diffusion through the shock front[12, 13, 14].

B. Shock Moving into a Conducting Fluid

The simplest theoretical model is a gross balance of rate-of-change of momentum against pressure, suggested by Rosenbluth, and referred to frequently as snowplow theory. It is assumed that the piston moves into the fluid and sweeps it up into a very thin, dense layer on the piston surface. For a cylindrical piston the equation of motion is [15]

$$\frac{d}{dt}\left[\pi r_c^2 \rho_o \frac{dr_c}{dt}\right] = 2\pi r_c\left[p_{m_\theta} - p_{m_z}\right] \qquad (1)$$

where r_c is the piston radius, ρ_o is the ambient gas density, and p_{m_θ} and p_{m_z} are the magnetic pressures, $B^2/2\mu$, of the azimuthal and axial fields. In this equation, the radius of the inner conductor and the ambient gas pressure are assumed negligible compared to the shock radius and magnetic pressure. For the case $B_{z_o} = 0$ and $I = I_o \omega t = (V_o/L)t$, where V_o and L are the initial condenser voltage and average* inductance of a slightly damped RLC circuit, equation (1)

* The inductance varies with time as the piston expands. However, conditions are such that this variation is not important and an average inductance may be used.

possesses the conical similarity solution $r_c = u_o t$, where

$$u_o = \left\{ \frac{V_o^2}{L^2} \frac{\mu}{8\pi^2 \rho_o} \right\}^{1/4} \tag{2}$$

and will be called the characteristic snowplow velocity. For $B_{z_o} \neq 0$ it is found that the solution is again conical, $r_c = u_c t$ where u_c is related to u_o and to the Alfven speed in the ambient fluid b_o by

$$\left(\frac{u_c}{u_o}\right)^2 = -\left(\frac{b_o}{2u_o}\right)^2 + \left[\left(\frac{b_o}{2u_o}\right)^4 + 1\right]^{1/2} \tag{3}$$

Clearly $u_c/u_o \leq 1$ and the piston is retarded by the axial field.

As is shown in reference 15, snowplow theory is equivalent to the Newtonian limit in ordinary gasdynamics and thus can be expected to represent the flow only in the case of very strong shocks propagating into undisturbed fluid (and not for shock reflection, etc.). A shock wave is termed strong when it propagates with a speed large compared to the speed of corresponding infinitesimal disturbances. In the present instance, the latter speed is the combined wave speed $c = (a_o^2 + b_o^2)^{1/2} \simeq b_o$ for $a_o/b_o \ll 1$. Thus, increasing the axial field while holding the other parameters of the problem fixed is equivalent to raising the generalized acoustic speed and hence to weakening the shock. We therefore expect a breakdown in the snowplow theory for sufficiently high values of B_{z_o}.

An exact solution for the cylindrical magnetic shock tube was found by Greifinger and Cole[15] using the full mhd equations. In

their solution, the current was assumed to rise linearly and the conductivity was taken to be everywhere infinite. The main results of that solution, which of course possesses conical similarity, are summarized below:

(i) Equation 3 predicts the speed of the piston with remarkable accuracy for even very weak shocks, but is very inadequate for predicting the velocity of any shocks other than very strong ones.

(ii) For a fixed u_o the shock speed increases and the piston speed decreases (according to equation 3) as B_{z_o} increases, accompanied by a decrease in compression of the plasma across the shock. (The rate of increase of shock speed with B_{z_o} is less than the rate of increase of acoustic speed with B_{z_o} so that the shock Alfven Mach number approaches 1.)

(iii) The axial magnetic field increases in passing through the shock in the amount of the density increase, a consequence of flux conservation through a contour attached to the fluid.

In the original article by Greifinger and Cole there appeared plots of shock and piston speeds, and velocity, pressure, density, and magnetic pressure profiles as functions of the appropriate parameters for the case $\gamma = 7/5$. The present author is indebted to Dr. Greifinger for extending these calculations to the case $\gamma = 5/3$ for values of parameters pertinent to these experiments. As they are not available elsewhere, the results of the calculations are plotted (in somewhat different form from the original article) in Figures 3, 4, and 5.

In the experiments the glass chamber wall is surrounded by coils

which produce the axial field. During the short time of the experiment, these coils appear to the advancing wave motion somewhat as an infinitely conducting cylinder which might be expected to influence the electric and magnetic fields and hence the fluid motion. It is important to note that in the case considered here of a very highly conducting fluid there can be no disturbance (either electromagnetic or fluid-mechanical) ahead of the shock [16]; hence the wall has no effect until the first shock reaches it. An effect does arise, however, from the top and bottom electrodes. Being highly conducting, they tend to anchor the B_z field lines and cause them to become convex near the electrodes as the shock propagates outward. This effect has been minimized by extensive radial slotting of the electrodes (which is also necessary to establish the external field initially (see Appendix D)).

We now consider the situation where the conductivity is appreciable throughout the chamber but not infinite. In this case two new effects appear, diffusion of the magnetic field lines through the fluid and Ohmic heating.

At the shock front the diffusion of the induced azimuthal current is counterbalanced by the non-linear steepening effect familiar in shock motion, resulting in a steady profile whose thickness is determined by the transport coefficients. In experiments like these, the width is almost always of order $(\mu\sigma)^{-1}$ since the magnetic diffusivity is the largest of those involved.

The structure of mhd shocks has been studied by Marshall [17] and others. When the shock thickness is governed by conductivity, two types of profiles occur. For high field strengths, all the variables

undergo transition in a length of order $(\mu\sigma)^{-1}$; for sufficiently low fields there exists a sharp thermodynamic shock at the end of the magnetic field transition region. Thus one sees a sharp Rankine-Hugoniot shock with a tail on the low pressure side. In a cylindrical geometry, the jump conditions must be appropriately modified if the thickness of the shock is not small compared to the radial position of the shock.

Diffusion of the field into the plasma also occurs at the plasma-vacuum interface (piston) and there the diffusion depth grows continuously at $t^{1/2}$ since there is no counteracting mechanism. However, from considerations of conservation of mass it is clear that the separation between the shock and this piston grows as t so the shock should separate cleanly from the diffusing piston for sufficiently large t.

The effect of Ohmic heating is to produce a non-constant-velocity wave system, that is, to destroy the conical similarity. For example, if one imagines that most of the heating occurs near the center during the initial stages of the discharge when the conductivity is likely to be quite low, then conditions are approximated for the classical blast wave solution where the velocity decays as 1/r. Therefore, the experimentally-determined deviation from constant velocity may provide a measure of the relative importance between heating and magnetic driving.

C. Propagation of Shock Waves into a Non-Conducting Fluid

In this section we choose as a model a shock propagating into a non-conducting fluid in which there is an axial field B_{z_o}. The shock is assumed to be sufficiently strong that the gas becomes highly conducting a short distance behind it. The essential point is that now the field must be continuous through the shock and hence the jump conditions are the

ordinary Rankine-Hugoniot relations[18]. This does not mean that there is no effect of the field on the flow, for body forces arise in the region of the piston tending to retard the piston and thus produce a slower rather than the faster shock produced by the field when the fluid is everywhere highly conducting. However, the shocks are strong shocks since their strength depends on the ordinary Mach number. Thus, a snowplow theory remains valid for predicting the motion.

For the case of no wall, equation 3 is again valid for describing the piston path and the flow remains conical.

In contrast to the model discussed in Section B above, the effect of a conducting wall around the chamber is now important since electromagnetic disturbances can propagate without losses ahead of the shock through the non-conducting gas.

Consider the idealized problem of a highly conducting, thin, hollow cylindrical piston advancing with velocity u(t) into a vacuum region surrounded by a fixed, highly conducting cylindrical wall (e.g. a coil producing the field B_{z_o}). We suppose that at t = 0 the piston has a radius $r = r_c(0)$ and that a uniform axial field B exists for $r < R$ where R is the radius of the outer cylinder (see sketch), and we investigate what happens to this field as the piston advances.

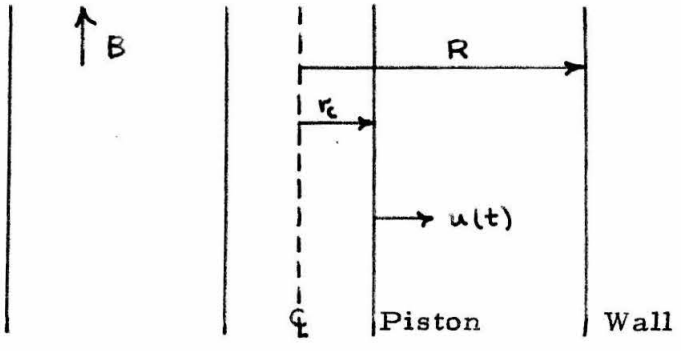

Assume

$$\vec{B} = (0,\ 0,\ B(t)) \tag{4}$$

$$\vec{E} = (0,\ E_\theta\ (r,\ t),\ 0) \tag{5}$$

and that all θ derivatives vanish, from which div $\vec{B}$ = div $\vec{E}$ = 0.

The current flows azimuthally in sheets on the piston (I_c) and on the wall (I_w). The remaining Maxwell's equations are

$$\frac{\partial B}{\partial r} = \mu j_\theta\ (r,\ t), \tag{6}$$

$$\frac{1}{r}\ \frac{\partial (rE_\theta)}{\partial r} = -\ \frac{\partial B}{\partial t} \tag{7}$$

From equation 6 there results

$$\begin{aligned} B(t) &= -\mu I_w(t);\ \text{for } r_c < r < R \\ B(t) &= -\mu\left(I_w(t) + I_c(t)\right) \text{for } r < R \end{aligned} \tag{8}$$

Equation 7 yields

$$\begin{aligned} E_\theta &= -\frac{r}{2} B'(t), \qquad r < r_c \\ E_\theta &= -\frac{r}{2} B'(t) + \frac{f(t)}{r}, \quad r_c < r < R \\ E_\theta &= \frac{g(t)}{r}, \qquad r > R \end{aligned} \tag{9}$$

where the prime denotes differentiation with respect to time.

At the wall and the piston there can exist no electric fields since the conductivity is assumed to be infinite. This implies $\vec{E} + \vec{u} \times \vec{B} = 0$. At the piston we have

$$\left.\begin{aligned} &\frac{r_c}{2} B' + r_c' B = 0 \\ &\text{or, } (r_c^2 B)' = 0, \; r_c^2 B = \text{const.} \end{aligned}\right\} \quad \text{for } r < r_p \tag{10}$$

That is, the flux through the area within the piston remains constant in time; the field decreases as $1/r_c^2$. At the piston we also have the boundary condition

$$-\frac{r_c}{2} B' - r_c' B + \frac{f}{r_c} = 0 \tag{11}$$

and at the wall, $E_\theta = 0$ implies

$$-\frac{R}{2} B' + \frac{f}{R} = 0 \tag{12}$$

and

$$g = 0. \tag{13}$$

Equations 11 and 13 can be combined to give

$$[B (R^2 - r_c^2)]' = 0$$

or

$$B (R^2 - r_c^2) = \text{const.} \qquad r_p < r < R \tag{14}$$

Thus the flux between the piston and the wall is likewise conserved, that is, the field is compressed between the advancing piston and the wall.

To apply these results to the present experiment one must reconcile two questions. First, the coils do not close on themselves but are connected to an external circuit. However, the driving capacitors are short circuited (crowbarred) during the passage of the shock across the chamber.

Secondly, there are gaps between adjacent coils so that some of the field "leaks out" instead of being compressed between the piston and the wall; the extent of this leakage will be discussed in Chapter IV.

The piston forms initially on the surface of the inner teflon insulator so that the field inside this radius is negligible and we may consider $r_c(0) = 0$ for this purpose. Then equation 14 yields

$$B_z = \frac{B_{z_o}}{(1 - r_c^2/R^2)} \tag{15}$$

and the equation of motion (1) takes the form

$$\frac{d}{dt}\left[x^2 \frac{dx}{dt}\right] = \frac{x}{R^2 \rho_o}\left[\frac{\mu I^2(t)}{4\pi^2 R_o^2 x^2} - \frac{B_{z_o}^2}{\mu (1 - x^2)^2}\right] \tag{16}$$

where $x = r_c/R$. For $I \sim t$ and $B_{z_o} = 0$ the solution is again $r_c = u_o t$. For $B_{z_o} \neq 0$, however, the piston slows down as it approaches the wall, even for a linearly rising current. That is, conical similarity is destroyed in this case by the presence of the conducting wall. The situation is now analogous to flow over a convex body rather than a

cone (compare Ref. 1).

In summary, we see that the flow pattern is quite different when the shock advances into a non-conducting fluid rather than into one which is a good conductor. In the former case the shock speed increases but its strength drops; in the latter, the shock travels more slowly but remains relatively strong.

In the foregoing discussion of expected shock tube performance the existence of an idealized fluid with scalar conductivity has been assumed. The one fluid model appears adequate to roughly describe the motion of the shock and contact surface. The fact that the fluid is composed of electrons, ions, and neutrals will, however, become important in understanding some of the detailed experimental results. In particular, the exact mechanism by which the current and field interact to produce a shock depends on three-fluid effects and is not completely understood at the present time.

III. Experimental Apparatus and Techniques

A short discussion is given here of the experimental apparatus. Details will be found in appendices C, D, and E.

A. Basic Discharge Chamber (Figure 2)

The discharge chamber consists of a Pyrex cylinder of 3/8" wall thickness closed by 1/2" thick glass end plates. Its inside dimensions are approximately: height, 4", diameter, $6\frac{1}{2}$". There are two radial probe inlets in the midplane of the chamber, spaced 60^{o} apart. A teflon tube of 5/16" outside diameter covers the 3/16" copper center conductor.

Vacuum down to about one micron is provided by a Cenco mechanical pump used in conjunction with a liquid nitrogen cold trap. All sealing is done with neoprene O-rings and the leak rate is on the order of 3 microns per hour. Pressures are measured with a Hastings thermocouple vacuum gauge whose gauge tubes have been calibrated against a McLeod gauge for Argon and Helium.

Current for the main discharge is supplied by two 15 μf capacitors in parallel. The mean inductance of the circuit results in a quarter cycle of 4.5 μs. Most of the tests were run at 12 kv initial voltage, corresponding to a peak current of 123 ka.

The axial magnetic field is produced by discharging a 1000 μ f capacitor bank charged at up to 4 kv through a four-coil system of the type described by Barker [19]. It reaches its peak value, up to 12 kilogauss, in 940 μs.

B. Instrumentation

On each firing the condenser voltage was monitored as a function of time with a capacitance type voltage divider for use as a time reference. It should be noted that, due to the changing circuit inductance, the time at which the capacitor voltage reaches zero lags the time of maximum current slightly. This must be taken into account when reducing the data. A simpler time reference is obtained by measuring the rate of change of current with a Rogovsky loop; this is the method used at present.

At the outset of the experimental investigation it seemed necessary to develop a direct pressure measuring device in order to clarify the existing speculation in the literature concerning identification of observed light fronts with shock or current sheets, etc. Barium titanate pressure probes were developed which have a rise time of $1/5\,\mu$ s. They accurately indicate the arrival of a pressure pulse but, due to pulse reflections inside the transducer, do not faithfully reproduce the complete pressure history.

Time derivatives of magnetic fields ($\dot{B}_\theta$, $\dot{B}_z$) are measured with small search coils (1mm diameter, 10 turns) encased in a Pyrex envelope inserted radially into the discharge. For sufficiently high conductivities, a glass shield is known to have a deleterious effect on probe response [20, 21]. However, for the moderate conductivities encountered in the present experiment, the probes give an accurate measurement of the fields in the plasma[21, 22]. As a check on possible electrostatic effects, a grounded center tap probe [22] used in conjunction with a differential preamplifier was used on several runs

and yielded results identical to the single coil probes.

A single-frame Kerr-Cell camera manufactured by Electro-Optical Instruments, Inc., is used to take pictures through the side and top of the chamber at given times after the onset of the discharge. Exposure times are 1/20 and 1/10 μs.

A "run" is accomplished by first discharging the B_z capacitor bank into the field coils and then firing the main bank after a suitable delay. A "set" of experiments in a given gas at a particular initial pressure and condenser voltage consists of pressure, $\dot{B}_\theta$, $\dot{B}_z$, and Kerr-Cell records for six radial probe stations and five or more values of initial axial field B_{z_o}. Two probes are used on each run.

The results presented below deal primarily with sets of experiments in Argon and Helium at 100μ and 500 μ initial pressures with all other parameters fixed. Although most of the experiments were done without preionization, some preliminary experiments with preionization will be described.

IV. Results and Interpretations for Experiments without Preionization

A. General Remarks and Illustration of the Raw Data

The purpose of this section is to illustrate some of the general results of the experiments by presenting oscillograms of the raw data. In subsequent sections a more detailed description of the results of three particular sets of runs will be discussed.

Figures 6, 7, and 8 were obtained with a Tektronix 555 dual beam oscilloscope. On each trace the sweep runs from left to right through the 1 cm^2 mesh at a rate of 1 $\mu s/cm$. The discharge occurs at about 1.4 to 1.5 μs after sweep initiation and is responsible for the pickup at that time appearing on the traces and persisting for 1 - 2 μs. (The additional small spurious signals appearing at various times are also due to pickup.) In general, preamplifier sensitivities vary from one trace to the next.

Figure 6 shows the results of a run in Helium at 500 μ initial pressure. Of particular interest here is a comparison between the $\dot{B}_\theta$ traces in figures 6a and 6b. In the former the axial field is zero and it is clear that there is some B_θ field ahead of the shock and consequently a current there also. That the signal actually represents a magnetic field and does not arise from electrostatic effects was proved by using a double coil and differential preamplifier as described above. The lower trace in figure 6b shows that in the presence of a small axial field the azimuthal field tends not to extend far forward of the shock. This is a general result which was observed in all the experiments.

The arrival of the pressure pulse at the front face of the probe

actually occurs . 2 microseconds earlier than the traces indicate due to the traversal time of a stress wave across the probe glass front plate.

Figure 7 was obtained from runs in Argon at 500 μ . In figure 7a the pressure pulse arrives after the peak in the magnetic field derivative in contrast to the situation in Helium as shown in figure 6; this anomaly is discussed below. The upper trace of figure 7b was obtained with the magnetic probe oriented to pick up $\dot{B}_z$. The positive deflection occurring until shock arrival (indicated on the lower trace) indicates compression of the axial field. The ensuing sweeping away of the axial field after the passage of the piston gives rise to the large negative deflection following the compression.

Figure 8 illustrates runs in Argon at 100 μ . It can be seen that there is some disturbance on the pressure probe trace before the sharp shock arrives. This is an electrical effect resulting from the difficulty of shielding the probe completely from electrical fields (which may become quite large due to charge separation, for example). It was shown to be an electrical effect rather than a true pressure disturbance by constructing probes of opposite polarity and noting that the "precursor" had the same polarity on different probes while the main disturbance arising from the shock reversed in polarity.

These electrical effects become more predominant in lighter gases and at lower pressures since Δp becomes smaller while the electric fields in general do not, so that the ratio of pressure-induced signal to electrical pickup becomes smaller.

Experiments have been run in air, Argon, and Helium at initial pressures of from 50μ to 500 μ. There seems to be a general tendency for the shock to be more clearly defined at the higher pressures. Below 100 μ in Helium the shock is often difficult to pick up, although the instrumentation difficulties just described are at least in part responsible. The magnetic field traces are generally good but also show a tendency to become less reproducible, with poorly defined peaks, in Helium at low pressures.

In all experiments the time of arrival of a magnetic peak or pressure pulse is repeatable to a high degree, while the shape and amplitude of the pulses are somewhat less repeatable (although still quite good in most instances).

It is perhaps worthwhile to note that at 100 μ the mean free path (for neutrals) is 1.7 mm in Helium and .7 mm in Argon, long enough to give some structure to phenomena occurring with a mean free path length scale, while at 500μ it is one fifth of these values. Thus one expects "pulses" and "discontinuities" to be less sharply defined at the higher pressures, which is no doubt in part responsible for the observed behavior below 100μ in Helium.

B. Detailed Results of Experiments in Helium and Argon at 100μ and 500 μ Initial Pressure

In this section emphasis is placed on three sets of experiments which illustrate most of the important features of the flow.

B.1. Preliminary Remarks. Table I presents some of the relevant parameters (see appendix B for sample calculations). The equilibrium temperature behind the shock ($T_{2_{eq}}$) is calculated from

Rankine-Hugoniot relations and equilibrium thermodynamics using the observed shock speeds for $B_{z_o} = 0$ and serves as a rough estimate of conditions behind the shock. It is possible, of course, that thermodynamic equilibrium is not established sufficiently quickly to make the calculation strictly applicable. (Extrapolation of the results of Petschek and Byron [23] indicates that equilibrium would be reached (in Argon) in a time between 1/2 and 1 μ s. The electric field will tend to keep the electrons hotter, enhancing the ionization rate but tending to prevent the establishment of true thermodynamic equilibrium.) The equilibrium degree of ionization behind the shock ($\alpha_{2_{eq}}$) is based on $T_{2_{eq}}$ and p_2 and is defined as the number of electrons per original neutral particle. The electrical conductivity is obtained from Spitzer's[24] result for fully ionized gases. The diffusion depth of the driving field B_θ into the gas in the time required to traverse the chamber, R/u_o, is also listed, from which it is seen that the "piston" is somewhat diffuse and a clean separation of the shock and piston is not to be expected.

In scanning Table I, one should note that a major effect of the axial field is to decrease the shock strength and hence to produce less conductivity and consequently greater departures from the idealized mode.

The state of the plasma is such that $\frac{\omega_{c_i}}{\nu_c} \ll 1$, that is, the shock is collision determined.

B. 2. Relative Front Positions. Typical r-t diagrams are shown in figures 9, 10, and 11. The legend needs a little further clarification: Circles represent the arrival at a given radius of a peak in the function $B_\theta(r, t)$ which for sharp peaks (ideal flow) correspond closely to the maximum current density j_z, i.e. to the arrival of the magnetic piston at the distance r_i. The symbols labeled "B_z null" refer to the null in $B_z(r_i, t)$ which occurs when compression of the axial field at a given radius is complete. This, according to the theoretical discussion given above, should correspond closely to the shock position. Finally, the solid circles represent the radius of the luminous front. Where deviations from cylindrical symmetry were observed, the positions of the left- and right-hand sides of the front are both shown.

These figures illustrate the relative positions of the various fronts. In Helium at 500 μ (figure 9) the shock precedes the piston as one expects. This is true both with and without the axial field. The separation between the fronts changes little with field strength, indicating a non-mhd shock flow. For no field the light front is very near the shock, while it lags slightly when a field is applied. Figure 10 illustrates a result which at first appears somewhat paradoxical. For For $B_{z_o} = 0$, the piston appears to be slightly ahead of the shock, while for $B_{z_o} = 4950$ the "piston" is definitely ahead of the shock. It should be recalled that the "piston" is really a relatively thick annular region in which volume currents flow, rather than a current sheet at a well-defined location. Thus, the shock is located near the rear of the current-carrying region in Argon (figure 10) and near the front in Helium

(figure 9). Figure 11 shows that a similar tendency for the piston to precede the shock occurs in Argon at 100 μ, although it is not so pronounced.

A possible explanation of the piston "preceding" the shock can be given as follows. The electrons are the primary recipients of the Lorentz force acting on the gas because they carry most of the current. Thus they tend to move away from the ions which are pulled along behind them by the electrostatic force arising from the charge separation which occurs. As the ions are heavier, they are more effective in transferring energy to the neutrals and the principal "shock" disturbance is associated with the ions. The separation which can be maintained between electrons and ions depends in part on the relative ease with which the electrons and ions can move through the neutrals, as well as on the product of the Debye length times the Mach number. (Since the electron concentration varies by several orders of magnitude in passing through the shock region, the Debye length is difficult to determine even approximately.) Now the electron-atom collision cross sections for Helium and Argon are quite different in the energy range of 1 to 3 e.v. which is characteristic of these experiments. The electron-atom cross section for Argon as a function of energy displays a very pronounced dip at 1 e.v. (Ramsauer effect) to a value less than 1/6 that of Helium, whose electron-atom cross section is approximately independent of energy in this range (Massey and Burhop[25]). Above 1 e.v. the Argon cross section increases rapidly, becoming equal to that of Helium at around 4 e.v. From Table I it is seen that the characteristic

temperature in Argon at 500 μ for no axial field is about 2 e. v. The presence of a field slows the shock (see below) and moves the temperature toward 1 e. v., where the cross section is the smallest; this is precisely where the largest separation of the fronts occurs. The experiments in Argon at 100 μ correspond to a cross section intermediate between that of the experiments in Helium at 500 μ, where the piston lags as in a normal shock-piston flow, and Argon at 500 μ. As seen in figure 11, the relative positions of the fronts in this case are consistent with the above reasoning.

The foregoing explanation is certainly an over-simplification of a complicated phenomenon, but does suggest the importance of the Ramsauer effect in the piston mechanism. Obviously a great deal of work remains to be done before the process whereby a magnetic piston drives a gas and produces a shock wave is thoroughly understood.

B. 3. Kerr-Cell Photographs. Several interesting features of the flow are shown in figure 12. As is evident, the light front is straighter and more clearly defined at high initial pressures. In Argon, with no axial field applied, small offshoots or flares of luminosity are present which disappear when even a slight initial field is used. In general, the presence of the axial field is to enhance the stability of the luminous front.

A slight tendency was noted, particularly in Argon in the absence of a B_z field, for the radius of the cylindrical light front at a given time to be slightly greater at the cathode than at the anode. This effect disappears upon application of the axial field. Most of the luminosity is due to line radiation from excited states and thus the light front

corresponds closely to the ionization front and shock, as is apparent from figures 9, 10, and 11.

Figures 13 and 14 show quite well the effect of the axial field on the radius of the luminous front and also give a good overall view of the difference between the high and low initial pressure experiments. (The extraneous light at the edge of the photographs is due to reflection in the Kerr-Cell caused by the omission of a collimating lens from the optical system.) Photographs were also taken in Helium, but due to the lower intensity of visible radiation emitted the pictures do not show enough contrast for good reproduction.

Figure 15 was taken through the top of the chamber and illustrates the outstanding cylindrical symmetry of the flow.

In figures 12, 13, and 14, some curvature of the light front near the electrodes due to the anchoring of the field lines is observed, however, the effect is quite small.

B.4. Wave Speeds. Figures 16, 17, and 18 illustrate the influence of the axial field strength on the motion of the shock and piston. In each case, the shock is slowed by the axial field. This is fairly conclusive evidence that the shock is an ordinary one propagating into an essentially non-conducting fluid, as discussed in Chapter II. The increasing deviation from conical similarity as the field increases indicates further that the effect of the conducting wall (coils) is being felt. Note that although the shock slows down in fairly good agreement with snowplow theory, the velocity of the piston follows a peculiar behavior as described above. A power series integration of equation 16 has been carried out for the parameters corresponding to figure 11 and good agreement with the

experimental points is obtained.

B.5. Pressure Pulse. As the shock slows, the pressure jump must drop. Calibration of the pressure probes in an ordinary shock tube shows that the output is roughly proportional to the reflected shock pressure jump. For strong shocks, this is proportional to the square of the shock Mach number, so that output falls rapidly as the shock speed drops. Comparison of figure 19 with figures 16 and 17 shows this to be qualitatively experimentally verified.

B.6. Magnetic Field Profiles. The magnetic probe traces can be integrated to give $B_\theta(r_i, t)$, where r_i is the probe location on a given run. By cross plotting the results for several runs one obtains magnetic field profiles $B(r, t_i)$ for several times during the propagation of the wave system across the chamber.

At any given instant the azimuthal field, B_θ, should decay as $1/r$ in the region between the center conductor and the piston and drop to zero through the piston. Therefore a plot of rB_θ vs r for a given t should resemble a negative step; i.e. rB_θ = const for $r_o < r < r_c$, and $rB_\theta = 0$ for $r > r_c$ for the idealized case of a current sheet piston. Since $j_z = \frac{1}{\mu r} \frac{\partial (rB_\theta)}{\partial r}$, a current flows wherever the slope is non-zero.

Such plots are presented in figures 20 through 25 (the times denoted on the curves should be increased by 0.2μ sec.). As above, examination of the flow details reveals some anomalous results.

The magnetic field profiles shown in figure 20 are very similar to the step described above. As time increases the position of the current front advances nearly to the wall. Figure 21 shows that in the presence of an axial field, the motion of the piston is sharply inhibited

and the current diffuses slowly to the wall.

We next consider figure 24. The curves indicate that as the driving current builds up, additional currents begin to flow in the "vacuum" region behind the piston, in the direction of the current in the center conductor near the center of the chamber, and in the opposite direction further out.

One's first inclination is to distrust the results for two reasons: first because the experimental errors are the largest near the center, and secondly, because the curves depend on the assumption of detailed repeatability of the magnetic traces. Repeated experiments, however, indicate the same qualitative behavior.

There are several comments to be made: First, in order for a current to flow there must be some plasma left behind the piston. The density can be quite small since the conductivity of a fully ionized gas is essentially independent of density [24]. Thus it is possible that the mass of plasma left behind the piston is small enough that the total momentum balance is not significantly disturbed, i.e. the snowplow theory given above remains valid. The "leakiness" of the piston depends on the conductivity, which is lower for Helium than for Argon for the conditions of the experiments (Table I).

Although j_z can get very large near the center (larger than in the piston, for example), the current carrying area is relatively small and the total "induced additional current" never exceeds 15 per cent of the main drive current.

The plots for Argon at 500 μ show a behavior intermediate between that observed in Argon at 100 μ and Helium at 500 μ ; it is

interesting to note from Table I that the conductivity here is also intermediate between those of the other experiments.

One notes also that the "induced current" is reduced in the presence of an axial field, an effect which is apparently due to the tendency of the axial field to inhibit plasma motion.

It remains to be shown that an electric field exists which could produce such a current. Consider the idealized problem of the electric field between the elements of a co-axial conductor separated by vacuum. The current is assumed to rise linearly with time and the boundary conditions are

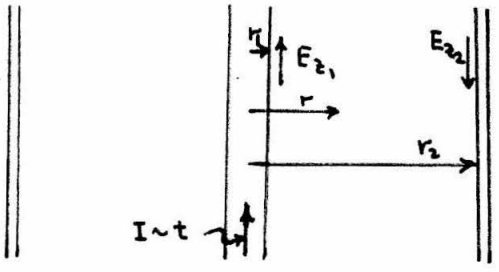

$$E_z = E_{z_1}(t) \text{ at } r = r_1,$$

$$E_z = E_{z_2}(t) \text{ at } r = r_2,$$

$$E_r = 0 \text{ at } z = z_o.$$

Under such conditions the electric field is given by

$$E_z = \frac{E_{z_1}(t) + E_{z_2}(t)}{\ell n\, r_2/r_1} \ell n \frac{r_2}{r} - E_{z_2}(t)$$

$$E_r = -\frac{1}{r}\left[\left(\frac{\mu_o\, dI/dt}{2\pi} + \frac{E_{z_1}(t) + E_{z_2}(t)}{\ell n\, r_2/r_1}\right)(z - z_o)\right]$$

Although this idealized model does not correspond exactly to the experimental conditions, it is believed to incorporate the essential features and shows that a field E_z exists which changes sign in the

interval $r_1 < r < r_2$ and which could therefore give rise to the observed current pattern.

The fields E_{z_1} and E_{z_2} are simply equal to j_z/σ in the two conductors. Rough calculation shows that the values of E_{z_1} and E_{z_2} computed for the conditions of the experiments are somewhat less than that required to produce the observed results. Alternatively, the conductivity of the plasma would have to be a factor of five or so greater than the equilibrium conductivity listed in Table I; this is not inconceivable because the electric field tends to maintain the electron temperature at a higher value than that given by equilibrium thermodynamics.

It is felt that these arguments give a general indication of the observed phenomena. However, because of the inaccuracy of the measurements near the center conductor and the over simplified model which was chosen, further attempts at quantitative description on this level are not justified. Clearly, more work must be done before a detailed understanding is achieved.

Finally, we return to the point of conservation of flux as discussed in Chapter III. In order for flux to be conserved in the chamber as the piston advances, we must have

$$\int_{\text{center}}^{\text{coil}} r\,(B_z - B_{z_o})\,dr = 0$$

at any given time. In figure 26 the quantity $r(B_z - B_{z_o})$ is plotted versus r for several times after the initiation of the discharge. It can be seen that there is a definite tendency towards flux conservation,

but that some flux is lost from within the chamber as the piston advances.

C. Conclusions

The experiments performed without preionization indicate that an ordinary shock wave propagates into the ambient fluid at a rate governed by the speed of the magnetic piston, whose motion is retarded in the presence of an axial magnetic field.

The gross motion is very well predicted by snowplow theory. In examining the details, however, one encounters anomalies which have thus far been explained only qualitatively. A thorough understanding of the phenomena occurring within the discharge chamber would form the basis for several interesting future investigations.

V. Preliminary Experiments with Preionization

A. General Discussion

From the discussion in the foregoing chapter it is clear that the gas ahead of the shock wave is not sufficiently conducting for an mhd shock to be produced. In order to create a shock whose thickness is small compared to the chamber dimensions the ambient gas must have a conductivity of at least 10^4 to 10^5 mhos/meter.

Preionization by means of r-f induction has been used in many experiments. In most of these, however, the goal has been simply to produce some electrons so that the main discharge proceeds smoothly. Measurements have shown that conductivities produced by r-f heating in general are less than that required here. In addition, the tendency of the electrodes in the present experiment to exclude high frequency external fields makes it very unlikely that either the desired magnitude or uniformity of the conductivity could be attained, so that r-f heating appears to be unsatisfactory for the present purposes.

One of the most effective ways to heat a gas is by passing a strong shock or repeated strong shocks through it. In the cylindrical shock tube a shock wave is generated each time the condenser rings through a half-cycle. Thus the first shock can be used to heat the gas and measurements made on the second, for example. In this method the state of neither the axial field nor the fluid is known since the second shock comes so soon after the first; conditions are probably very non-uniform. Some measurements have been made on the "second-half-cycle shock" and will be discussed below.

In order to surmount these difficulties a system has been

constructed which utilizes two capacitor banks firing through the same electrodes (Fig. 28). The second bank can be delayed an arbitrary amount with respect to the first, and thus two series of shock waves can be generated. The first is used to render the gas conducting. After the gas comes to some sort of equilibrium the second bank is fired and measurements are made on the first shock resulting therefrom.

B. Preliminary Results

B.1. "Second-Half-Cycle" Experiments. Measurements of the wave originating from the second-half-cycle oscillation of the main condenser (separate preionization bank disconnected) in the absence of an external magnetic field show that the shock forms immediately and travels outward, with the snowplow velocity based on original ambient pressure, to a radius of approximately 2". Beyond that distance it attenuates rapidly and disappears before reaching the wall. Preliminary runs with an axial field failed to give conclusive evidence of a true mhd shock. Because of the uncertainties involving the initial conditions for the second shock, this method of preionization has not been further pursued.

B.2. Preionization by Means of a Separate Condenser. Initial tests without an axial field were made with a series inductance of 7.5 μh, (see Fig. 28 and App. E) with a resulting ringing time for the preionization bank of 47 μs. It was found immediately that initiation of the main discharge at a time other than that of a null in the preionization current resulted in the main arc starting at the place where the preionization current was flowing. The main bank was therefore fired

94 μs after the preionization bank, corresponding to two full cycles of preionization current.

For radii greater than 2" the pressure and magnetic traces are extremely reproducible. Within 2" of the center a pressure pulse in general can not be detected and the magnetic traces are not very well defined or repeatable. Kerr-Cell photographs reveal that the luminous front initiates near the center and spreads very quickly to a radius of 1" to 1 1/2", after which a stable front forms and travels at the snowplow speed. However, even for radii greater than 2" the luminous front remains an approximately constant distance ahead of the shock and magnetic fronts.

One can explain this behavior qualitatively as follows. The electrodes are initially nearly equipotential surfaces and apply a uniform electric field across the gap. The discharge tends to originate at the center for reasons of minimum inductance, after which the electric field becomes small. If the plasma is very highly conducting the field and current diffuse very little and the behavior is nearly ideal, i.e. a "piston" forms. If the gas is initially non-conducting the arc is again confined to a narrow region where the conductivity is non-zero and an effective piston is formed. In the intermediate case, however, the diffusion speed is initially great and the current diffuses rapidly into the moderately conducting plasma, and distributed body forces begin acting to form a shock, which then overtakes the diffusing piston. Thus the conductivity must be made quite high to get a piston-like behavior in the initial stages.

In order to increase the conductivity the series inductor was

removed from the preionization circuit, resulting in a ringing period of 16 μ s. The capacitor is allowed to oscillate through six complete cycles, after which it is nearly completely damped. This sends many strong shock waves through the chamber, heating the gas to a high degree. The main discharge is then initiated. An upper bound to the energy deposited in the gas is just the energy stored originally in the capacitor (most of the dissipation is in the gas so that this should be a fairly good estimate). This amounts to 85 ev/particle at 500 μ initial pressure, and 420 ev/particle at 100 μ , for a 7.5 μf capacitor charged to 12 kv. This energy is more than sufficient to attain the desired conductivity.

There will, of course, be losses, and these must be calculated or measured. Most of the loss is due to radiation. Calculations show that losses from Bremsstrahlung are negligible but that those from optical radiation may not be. In future experiments the electron temperature will be measured, either spectroscopically or with Langmuir-type probes, to determine the time at which conductivity is a maximum.

One set of runs has been carried out with this circuit, in Argon at 500 μ, in which pressure and magnetic probes were placed at a fixed radius while the axial field was increased in successive runs in steps of 500 gauss. A sharp shock exists at the lowest field strengths. At higher fields the tendency is for the leading edge of the shock to deteriorate while remaining sharp at the back. At the highest fields only a slow pressure transition is observed. This is in qualitative agreement with Marshall's prediction of shock structure[17]. In addition, the shock seems

to move slightly ahead of the piston as the field is increased. Although these initial results are encouraging, a great deal of work remains to be done before any definite conclusions can be reached.

C. Preionization by Ohmic Heating

One final method of preionization, involving an ordinary discharge between the top and bottom electrodes without the use of the center conductor, should be noted. This method, in which there is now no outward Lorentz force (indeed, the Lorentz force is radially inward, i.e. it pinches, but is rather small for small currents and no outer return cylinder), has been used in "inverse pinch experiments" at the University of Illinois[26], and may be effective in the present experiments for the following reasons. Electrical conductivity depends primarily on electron temperature[24], which in a discharge tends to remain higher than ion temperature due to the poor electron-ion energy transfer cross section. Thus it may be possible to establish a uniform discharge throughout the chamber with a current small enough that the Lorentz force is negligible, but large enough to ionize the gas to a high degree and heat the electrons sufficiently to achieve the required conductivity. This would have the additional advantage of not greatly disturbing the gas density distribution and initial axial field.

D. Conclusion

Heating the gas by means of multiple strong shocks seems to hold promise as an effective way to produce the initial conductivities required for an mhd shock whose thickness is small compared to chamber dimensions. Initial experiments along this line have been

encouraging, but instrumentation must be developed to measure conductivities achieved by the preionization bank. A direct Ohmic heating discharge without the use of the center conductor may be an alternate method of achieving the desired results.

Appendix A. Parametric Study of the Cylindrical Magnetic Shock Tube

The purpose of this appendix is to illustrate the dependence of various quantities such as the shock speed, Mach number, enthalpy, conductivity, testing time, etc., on the relevant parameters, which include the circuit inductance, capacitance, and voltage and the type of gas and its initial pressure.

Remarks will be confined to the case of no axial field. We will assume the shocks are strong, in which case snowplow theory is valid.

The characteristic shock speed, which we have seen to be experimentally verified, is

$$u_o = \left\{ \frac{V^2}{L^2} \frac{\mu_o}{8\pi^2 \rho_1} \right\}^{1/4} \sim \frac{V^{\frac{1}{2}}}{L^{\frac{1}{2}}} \frac{(k T_1)^{1/4}}{p_1^{1/4} m^{1/4}} \qquad \text{(A. 1)*}$$

where the subscript 1 denotes conditions ahead of the shock** and the ambient gas has been assumed perfect,

$$\rho_1 = \frac{p_1 m}{k T_1} \qquad \text{(A. 2)}$$

Thus, to achieve the highest velocity, one uses a high voltage and low inductance and a light gas at low initial pressure. The initial temperature, T_1, will be taken to be room temperature.

The capacitance does not enter into equation 1 directly because the assumption of a linearly rising current is equivalent to assuming a

---

*Equation numbers within an appendix include the letter of the appendix.

**This is in contrast to previous sections, where the subscript o was used to denote conditions ahead of the shock.

constant voltage source (very large capacitance). It has been found that if the quarter cycle of this discharge is greater than or equal to the time required for a wave to traverse the chamber, i.e. $\frac{\pi}{2}\sqrt{LC} \geq \frac{R}{u_o}$, then the front travels with nearly constant speed all the way across the chamber. The capacitance should therefore be chosen large enough that this inequality holds for the smallest values of u_o which will be encountered in the experiments, that is

$$C \geq \left(\frac{R^2 \rho_1^{\frac{1}{2}} 8\sqrt{2}}{\mu_o^{\frac{1}{2}} V \pi} \right)_{max} \tag{A.3}$$

Diffusion of the driving field into the plasma is minimized by making the conductivity behind the shock as high as possible. The conductivity depends on the temperature and hence on the enthalpy and pressure, which are functions of the shock Mach number.

The speed of sound in the ambient gas is

$$a_1 = \left(\frac{\gamma_1 k T_1}{m} \right)^{1/2}$$

so that the Mach number is

$$M_s \equiv \frac{u_o}{a_1} \sim \frac{V^{\frac{1}{2}}}{L^{\frac{1}{2}}} \frac{m^{1/4}}{p^{1/4}} \tag{A.4}$$

Thus, for a given V, L, and p_1, the Mach number is higher for a heavier gas than for a light one.

The enthalpy and pressure behind the shock are related to those in front by the strong shock relations [27]

$$h_2/h_1 \approx \frac{\gamma_1 + 1}{2} M_s^2 \left(1 - 1/\eta^2\right)$$

$$p_2/p_1 \approx \gamma_1 M_s^2 (1 - 1/\eta)$$

where η is the density ratio and is of the order of 10 for strong gas-ionizing shocks. Since $h_1 = (5/2)\, k\, T_1$, we have

$$mh_2 \approx M_s^2 \left(\frac{5}{2}\, k\, T_1\right) \frac{\gamma_1 + 1}{2} \sim M_s^2 \qquad \text{(A.5)}$$

and

$$p_2 \approx p_1 \gamma_1 M_s^2 \sim p_1 M_s^2 \qquad \text{(A.6)}$$

Notice that mh_2 is the enthalpy in region 2 per original particle and that p_2 is the actual pressure. A study of the Mollier chart shows that in the region where (multiple) ionization is occurring these two quantities must be maximized to maximize the temperature. Combining (4) with (5) and (6) we find

$$mh_2 \sim \frac{V}{L} \frac{m^{\frac{1}{2}}}{p_1^{\frac{1}{2}}} \qquad \text{(A.7)}$$

$$p_2 \sim \frac{V}{L}\, m^{\frac{1}{2}}\, p_1^{\frac{1}{2}} \qquad \text{(A.8)}$$

Thus a high initial pressure tends to lower the enthalpy per particle but to increase the pressure behind the shock. One can not therefore draw any general conclusions from (7) and (8) as to whether a high or low initial pressure in a given gas will produce the highest conductivity.

Similarly one can not ascertain from these relations whether a higher conductivity will be produced in a heavier or lighter gas at a given initial pressure because of the complicated relationship between pressure, enthalpy, temperature, ionization energies, number of ionizable electrons, etc. A glance at Table I shows that for the range of parameters used in the present experiments, the conductivity is higher in Argon than in Helium at a given p_1, V, and L, and higher in a particular gas at lower pressure than it is at higher pressure. Once the gas is completely ionized (all stages), the temperature depends only on the enthalpy and a low initial pressure is dictated.

To achieve a very high conductivity the gas must first be completely ionized and then its temperature raised by several electron volts. The energy requirements for complete ionization in Helium or Argon are very high. Hydrogen, which requires only about 35 ev per original particle for complete ionization, is the only gas in which this could be achieved easily.

The "ideal separation distance", Δ, defined as the separation between the piston and the shock for infinite conductivity (no diffusion), is easily shown to be

$$\Delta/r_c = (1 - 1/\overline{\eta})^{-\frac{1}{2}} \approx 1/2\overline{\eta} \quad \text{for } \overline{\eta} \gg 1, \qquad (A.9)$$

where $\overline{\eta}$ is based on the mean density between the fronts. In a linear geometry, $\Delta/r_c \approx 1/\overline{\eta}$, thus the cylindrical geometry inherently yields half the "testing length" available in an ordinary shock tube of comparable dimensions. In order to realize this ideal separation the diffusion length must be small compared to Δ.

The diffusion depth grows parabolically with time while the ideal separation grows linearly. Thus, near the edge of the chamber, where the comparison is most favorable, we require

$$\delta_o/\Delta \sim \frac{\eta}{(\mu\sigma u_o R)^{\frac{1}{2}}} \ll 1 \qquad \text{(A.10)}$$

Calculations (Table I) show that in the experiments reported here this condition is not satisfied.

In closing let us consider the conditions under which the plasma may be collisionless in the sense that the ratio of the electron-ion mean free path is much longer than the Larmor radius, that is

$$\lambda_{e-i}/\Lambda_L \gg 1 \qquad \text{(A.11)}$$

The mean free path for charged particles is*

$$\lambda_{e-i} \approx \frac{1}{n\Omega} \quad \text{where} \quad \Omega = \pi\left(\frac{e^2}{4\pi\,\epsilon_o W}\right)^2 \qquad \text{(A.12)}$$

and W is the kinetic energy of a particle, $W = (1/2)mv^2 = (3/2)kT$. The Larmor radius is

$$\Lambda_L = \frac{v_{th}}{\omega_{c_i}} = \frac{\frac{3kT}{m}}{\frac{B}{m}} \qquad \text{(A.13)}$$

Therefore the plasma will be collisionless provided that

$$\frac{36\pi}{3}\left(\frac{\epsilon_o}{e}\right)^3 \frac{(kT)^{3/2}B}{n\,m^{1/2}} \gg 1, \text{ or}$$

*The cross section used here was given by R. D. Gould[28] and corresponds to a deflection of 52°. Compare with Spitzer[24].

$$\text{const.} \cdot \frac{T^{3/2}B}{n\,m^{1/2}} \gg 1 \qquad \text{(A. 14)}$$

Thus the gas should be hot, light, and have a low density and the magnetic field should be high. From this it appears that Hydrogen is the best choice for the study of a collisionless plasma.

Appendix B. Sample Calculations of Relevant Plasma Parameters

This appendix contains some calculations of the state of the plasma and is intended to illustrate the methods and approximate range of parameters involved.

1. Equilibrium Conditions Behind the Shock. Consider Helium at 100 μ initial pressure. Using equations A. 1 and the definition of sound speed one finds $M_s = 34$. Let the subscript o denote the conditions p_o = 1 atm. and $T_o = 0^oC$. Then, for $T_1 = 300^o$ K we have

$$\frac{h_2}{RT_o} = \frac{\gamma_1}{\gamma_1 - 1}\,\frac{T_1}{T_o}\,\frac{h_2}{h_1} = 2.75\,\frac{h_2}{h_1}\;;\; p_2/p_o = p_2/p_1 \cdot p_1/p_o$$

Using the strong shock relations(from Appendix A) we have

$$\frac{h_2}{RT_o} = 2.75\,(\tfrac{1}{3})\,M_s^{\,2}\,(1 - 1/\eta^2)\;;\; \frac{p_2}{p_o} = \frac{p_1}{p_o}\,M_s^{\,2}\,(1 - 1/\eta^2)$$

At 100 μ , $p_1/p_o = (7.6 \times 10^3)^{-1}$, so

$$\frac{h_2}{RT_o} = 1050; \qquad \log_{10}\frac{p_2}{p_o} = -.64$$

where a value of $\eta^{(o)} = 10$ has been assumed for the first iteration.

Using the Mollier chart of Cann and Ducati[29] one finds $T_2 = 21,900^oK$ and, from page 42 of the same reference, $\alpha = 0.68$. From the equation of state for an ionized gas, $p = (1 + \alpha)R_{at}T$, one finds $\eta^{(1)} = 14$. Repeating the procedure with the new value of η gives essentially the same results, i. e. the iteration converges very rapidly, primarily because of the weak dependence of the pressure and enthalpy ratios on η.

For Argon the quantities h_2 and p_2 lie beyond the range of the Plasmadyne Argon Mollier chart[30] for the conditions of these experiments, and the temperature was estimated by means of an "educated guess" based on the 2nd and 3rd ionization potentials and the enthalpy per particle. Extended charts have appeared recently which cover the range up to 10^5 ^oK[31, 32].

2. Plasma Quantities. Consider Argon at 12 kv and 500μ initial pressure. The number density of atoms in the ambient fluid is 1.6×10^{16} per cm^3. Assuming $\eta = 10$ and complete (single) ionization, the ion density in the shocked gas is $n_i \approx 10^{17}$ cm^{-3}.

The corresponding Debye length, based on $T_2 = 23,000^oK$, is

$$\lambda_D = \left(\frac{\epsilon_o \, kT}{n_o \, e^2} \right)^{\frac{1}{2}} = 6.9 \left(\frac{T}{n_e} \right)^{\frac{1}{2}} = 3.3 \times 10^{-6} \text{ cm.},$$

which is smaller than any other relevant dimension in the experiment (note, however, $\lambda_D \to \infty$ in the ambient fluid).

The cyclotron frequencies are

$$\omega_c = \frac{e}{m} B \begin{cases} 1.76 \times 10^{11} \, B, & \text{electrons} \\ 2.4 \times 10^{6} \, B, & \text{ions,} \end{cases}$$

where B is in webers/m^2. The gyration frequencies are therefore as follows for two typical field strengths:

$$\left. \begin{aligned} \omega_{c_e} &= 1.76 \times 10^{10} \\ \omega_{c_{A^+}} &= 2.4 \times 10^{5} \end{aligned} \right\} \text{ at 1000 gauss,}$$

$$\left.\begin{aligned} \omega_{c_e} &= 1.05 \times 10^{11} \\ \omega_{c_{A+}} &= 1.44 \times 10^{6} \end{aligned}\right\} \text{ at 6000 gauss}$$

To find a radius of gyration (Larmor radius) one must first define a particle speed. The directed velocity is of the order of u_o and is larger than the thermal velocity; however the field is "frozen" in the plasma and thus may be thought of as being convected with it. Therefore the proper velocity to choose is the thermal velocity since that is the average velocity of the charged particles relative to the field lines.

At low fields the shock velocity is nearly u_o and the equilibrium temperature behind the shock is about 2 ev. At high fields the temperature is about the same, at least near the center, and if a true mhd shock is to be produced in the future, preheating to at least 2 ev will be required, so we will base both the high and low field estimates on this temperature. At 2 ev the thermal speed is about 3.8×10^3 m/sec for the ions and 1.0×10^6 m/sec for the electrons. Therefore the Larmor radii are

$$\Lambda_{L_e} \quad \frac{v_{Th_e}}{\omega_{c_e}} = \begin{cases} .057 \text{ mm at 1000 gauss} \\ .011 \text{ mm at 6000 gauss} \end{cases}$$

$$\Lambda_{L_{A+}} \quad \frac{v_{Th_{A+}}}{\omega_{e_{A+}}} = \begin{cases} 1.58 \text{ cm at 1000 gauss} \\ .27 \text{ cm at 6000 gauss} \end{cases}$$

The mean free path for charged particles is, from equation A. 12,

$$\lambda_{e\,-\,A+} = \left[n_i \pi \left(\frac{e^2}{4\pi\epsilon_o W} \right)^2 \right]^{-1}$$

Thus

$$\lambda_{e\,-\,A+} = 2.6 \times 10^9 \frac{T^2}{n_i} = .013 \text{ mm}$$

and the ratio of mean free path to Larmor radius is

$$\frac{\lambda_{e\,-\,A+}}{\mathcal{L}_{L_e}} = \begin{cases} .23 \text{ at 1000 gauss} \\ 1.3 \text{ at 6000 gauss} \end{cases}$$

for electrons, and

$$\frac{\lambda_{e\,-\,A+}}{\mathcal{L}_{L_i}} = \begin{cases} .001 \text{ at 1000 gauss} \\ .005 \text{ at 6000 gauss} \end{cases}$$

for the ions. We are therefore in the collision dominated regime.

The number of particles in a Debye sphere is

$$n_e \lambda_D^3 \approx 3$$

This means that the interparticle distance, the 90° impact parameter, and the shielding distance are all of the same order so that the basic assumptions involved in deriving the "continuum equations" from the Liouville equation are violated (see Appendix F). We note that $n \lambda_D^3 \sim \frac{T^{3/2}}{n^{1/2}}$ so that, for example, in Hydrogen at higher temperatures the assumption $n \lambda_D^3 \gg 1$ is well justified.

Appendix C. Development of Pressure Probes

There are two requirements that a pressure transducer intended for use in a short duration plasma discharge experiment must meet. First, it must have an extremely fast rise time, of the order of a fraction of a microsecond, in order to make meaningful measurements in an experiment which lasts a total of perhaps five microseconds. Secondly, it must be well shielded against the electrical currents and electrostatic fields of the discharge.

These requirements led to the selection of a piezoelectric ceramic as the active element of the transducer. Because of the pickup problems associated with locating a crystal within the chamber it was first decided to use a probe consisting of a long glass rod inserted radially into the discharge with a crystal bonded to the end protruding from the chamber. Such probes were constructed and tested, but were discarded because the dispersion of the shock-induced stress wave in traveling down the rod limits the rise time to about 1.5 μs.

It was then decided to construct a probe in which the crystal is located at the front, facing the oncoming shock. A cross section of such a probe is shown in figure 27.

The strong fields encountered in the discharge dictate co-axial construction in which the outer element, which is connected electrically to the front face of the crystal, is grounded.

The crystals are $BaTiO_3$ and are supplied in 1" squares of 1 mm thickness by the Clevite Corporation. They are cut into discs of about 1/4" diameter using a hollow cylinder and grinding compound on a drill press and are then cemented to the brass backing plate, to which has

previously been soldered a length of hookup wire, with Eccobond non-conducting epoxy cement. The crystal is then lapped to the same diameter as the brass. Next this assembly is bonded to an insulating washer which in turn is bonded to a brass tube about 8" in length. A piece of thin Mylar is then wrapped around the crystal and backing rod and fastened with radio cement. After the cement has dried the sheath is attached and the silver paint applied. Final assembly involves cementing the glass envelope and front plate to the probe.

The probe output is about 1 volt for a pressure step of 1 atmosphere. Pickup originating from the initial gas breakdown can be reduced greatly by keeping the leads from the scope to the probe as short as possible. Alternatively, one can probably achieve the same results with a cathode follower.

The probes were designed to detect the arrival of a pressure pulse for timing shock arrival, but not necessarily to faithfully reproduce the pressure history at the probe face. Because of the short length of the backing rod there are reflections and consequently extraneous voltages produced after shock arrival. These signals can be eliminated by making the backing rod sufficiently long that the reflected wave does not arrive at the crystal during the time of the experiment. There are additional reflections, however, arising from the impedance mismatch between the glass front plate and the crystal, which cannot be easily eliminated. In the early probes a brass plate was cemented to the front of the crystal in place of the silver paint used later, but this did not significantly improve performance and made construction more difficult.

There was an attempt made to calibrate the initial voltage output of the probes against Δp in a conventional shock tube. This investigation confirmed the theoretical rise time of 0.2 μsec and did yield a relation between Δp and voltage output. The calibration was not completely successful, however, in that the voltage depends slightly on the initial pressure and not only on Δp, so that one cannot calculate Δp from the voltage alone. Part of the calibration problem lies in computing p on the face of a probe extending into a flow.

Application of the recent work of D. S. Johnson[33] on piezoelectric pressure transducers should improve the performance of future probes. In particular, the availability of PZT 5 and conducting epoxy cement makes possible the construction of probes with significantly increased sensitivity. This will be important in the measurement of mhd shocks as they tend toward the weak wave limit.

Appendix D. Design, Construction, and Calibration of Axial Field Coils

1. Design. Calculations based on the Greifinger-Cole solution indicate that a field on the order of 10,000 gauss is sufficient to produce measurable effects on the flow. It is necessary that this field be as uniform as possible throughout the chamber and that it be steady during the duration of the experiment.

Because the experiment lasts only about 10 microseconds, a pulsed field is used which eliminates the cooling problems associated with producing steady state fields of this magnitude. On the deficit side, the pulsed mode of operation gives rise to eddy currents which must be minimized through careful design.

An 8000 Joule capacitor bank complete with switching and timing circuits was designed by J. Wilson[34]. This unit is described briefly in appendix E. In the present appendix we shall concern ourselves with the design of the coils.

Magnetic fields of a specified configuration can be obtained by several methods including permanent magnets, electromagnets, and air-core coils. Permanent magnets are in general not capable of producing fields of the size and strength required here. Electromagnets are usually very expensive and have other disadvantages for application in this experiment. Thus it was decided to use an open (air-core) coil.

The customary method of producing a uniform field in a cylindrical volume is by means of a uniform solenoid. This is unsatisfactory for a short coil since the field strength at the end of a solenoid is only 1/2 that at the center. End windings can be added to

alleviate this effect; however, this method is not very satisfactory for coils of length to diameter ratio of about one, such as required here. The coil system chosen was one proposed by Barker[19] and uses four elements.

The field produced by a system of co-axial circular coils of small cross section arranged symmetrically about the center plane (z = 0) can be written as an infinite series of Legendre polynomials, i.e.

$$B_z = 2\pi \{ C_1 + C_3 r^2 P_2(\cos\theta) + C_5 r^4 P_4(\cos\theta) + \ldots \}$$

$$B_r = 2\pi \sin\theta \{ \frac{C_3}{3} r^2 P_2'(\cos\theta) + \frac{C_5}{5} r^4 P_4'(\cos\theta) + \ldots \}$$

where r and θ are spherical coordinates and the coefficients C_n depend on the coil currents, radii, and position. Barker applies the constraint that all coils shall have the same radius and then solves for the relative currents and spacing of the coils in a four-coil system which make C_3, C_5, and C_7 vanish. He finds that this can be accomplished by placing the inner and outer coils .243a and .941a from the center plane, where a is the coil radius, and passing current through the inner coil and outer coil in the ratio of .442:1. If the cross section is square and relatively small the field remains uniform and is given by

$$H_r = \frac{2\pi i_o}{a} \{ 1.58 - .89 \frac{r}{a}^8 P_8(\cos\theta) + \ldots \}$$

where i_o is the total current through the outer coil.

On applying these results to the present experiment one chooses a mean coil radius of 3.75" so that the distances of the inner and outer coils from the mid-plane are .912" and 3.78" respectively (Figure 31). The inner coils consist of 16 turns of #8 formvar wire while the outer

coils consist of 36 turns of #12 wire. The coils are connected in series which results in a current ratio of .444:1, sufficiently close to the prescribed value. To minimize heating they consist of two parallel systems of 8 and 18 turns wound together. The predicted output for the system is

$$B = 1.875\ I \text{ gauss},$$

where I is the current drawn from the capacitor bank.

2. Construction. The coils are wound initially on steel forms and potted in epoxy resin (Epoxylite #3101 general purpose fluid adhesive). After drying under a heat lamp for several hours they are removed from the form and cemented (with Eccobond epoxy) to lucite cylinders of length necessary to effect the desired spacing.

3. Field Calibration. The field was calibrated by recording the output of small search coils (3mm, 100 turns) whose effective diameter was accurately determined by simultaneous comparison with the output of a coil of precisely known area. Traces were recorded on Polaroid transparency film, enlarged and traced on graph paper, and integrated numerically.

The first calibration was made with no metal present within the coil volume and the field was found to be uniform within the accuracy of the measurements.

When the electrodes were inserted into the chamber it was found that the field strength was severely reduced due to eddy currents. Slotting greatly reduced the losses. The electrode configuration ultimately adopted consists of 1/16" stainless steel discs with 72 radial slots. With

these electrodes it is possible to achieve nearly the same field strength as occurs with no electrodes present.

The final field calibration was made with all electrodes and associated equipment in place. Samplings were taken in three planes at several condenser bank voltages. The field was found to be very nearly equal to the theoretical value and to be uniform to within 5 per cent over most of the chamber volume.

Appendix E. Circuitry

1. Basic Discharge Circuit. The basic discharge circuit is shown in figure 28, without any of the accessory circuits used to charge the capacitors and fire the ignitrons in the proper sequence, etc.

The main bank consists of two Tobe Deutschmann 15 μ f capacitors rated at 20 kv, which are connected in parallel. Switching is handled by two GL 77 03 Ignitrons rated at 20 kv and 100,000 amps peak current. The preionization condenser is a G. E. 7.5 μf 20 kv unit and is switched by a single GL 77 03. A series inductor (L_p) was used in the preionization circuit in some preliminary experiments but has since been removed (see text Ch. V).

The leads from the main bank to the experiment consist of two copper sheets, 1/16" by 4", separated by three layers of 10 mil Mylar film. The self-inductance of such an arrangement is quite low. (One can alternatively use low inductance twin braid co-axial cable, such as that manufactured by the Rex Corporation, in parallel to achieve a very low inductance. This has certain advantages including greater flexibility, less pickup, and no exposed leads.) The capacitors are placed about three feet from the discharge chamber in order to keep the region in the vicinity of the field coils as free from extraneous conducting material as possible.

2. Axial Field Generator. The axial field bank uses ten 100 μ f, 5 kv capacitors in parallel. The relatively low currents are switched by a single GL 7071 ignitron. The bank is crowbarred by another GL 7071 at the time of maximum current by means of a timing and triggering

circuit contained within the unit. For further details on the design, construction, and operation of this unit see reference 33.

3. High Voltage Units. The main bank and preionization bank are charged simultaneously to the same voltage by a General Electric 35 kv, 32 ma power supply. The axial field bank is charged independently by a 15 kv, 500 ma power supply.

4. Timing and Triggering Circuits. Timing and triggering circuits are required to initiate the various phases of the experiment at prescribed times. The timing sequence is described in Chapter III and illustrated in figure 28. Figure 29 shows a schematic diagram of the circuitry involved.

The ignitrons are fired by a large current pulse (300 amps, 10 μ s) initiated by 4C35 thyratrons, which in turn are fired by a 300 volt pulse from 2050 thyratrons. The latter are triggered by pulses of about 25 volts from the delay generators. The scope is triggered through a 10 to 1 attenuator probe connected to the output of the 2050 thyratron which fires the main bank 4C35 thyratrons.

Three delay units are used. The first is one designed by G. Skinner (GALCIT) and has a manual initiation which fires the axial field thyratrons and, after a pre-set delay, sends a pulse to the second delay generator. This unit consists of Tektronix 162 and 161 wave-form and pulse generators used together as a delay unit, and is used to fire first the preionization bank and then the main bank and oscilloscopes simultaneously. The internal delay generator of a Tektronix 555 scope is used to trigger the E.O.I. Kerr-Cell camera.

5. Ignitron Firing Circuits. While most of the units described above are straightforward, the design of circuits used to trigger capacitor discharge ignitrons is sufficiently new and unavailable in the literature to be worthy of comment here.

The ignitrons (both GL 7703 and 7101) require a half sine wave current pulse of 250 - 300 amps amplitude and 5 - 10 μs duration with the ignitor short circuited, and an open circuit voltage of 3 kv between ignitor and cathode.

These requirements are satisfied by the circuit shown in figure 30. The capacitor is charged to about 3 1/2 kv and discharges through the 4C35 thyratron which also acts as a rectifier. The inductor is a five-layer coil of five turns per layer of #12 insulated wire and has an inner diameter of .59".

In the present instance the ignitron cases are grounded. In some applications it is necessary to let the cases float at the potential of the discharge circuit, i.e. they may be at several kilovolts. In this case there are two ways of modifying the above circuit. The first method is to use the thyratrons as shown in figure 30 and to insert a pulse transformer between the ignitron and the thyratron. This is the method used in the magnetic cylindrical shock tube employed by H. Groenig in precursor studies[35]. The second scheme involves letting the thyratron float with the ignitron and using a pulse transformer in the grid circuit. Here the heater must also be insulated for several kilovolts. The large thyratron circuits presently in existence in this lab do have heater transformers insulated for either 10 kv or 15 kv and insulated tube sockets and thus can easily be adapted to a variety of future applications.

Appendix F. The Equations of Plasma Physics

1. Purpose. It is the purpose of this appendix to examine the assumptions leading to the set of equations known variously as the "hydromagnetic", "single-fluid", or "continuum" equations, which have been extensively investigated by workers in fluid mechanics, chiefly with regard to "magnetohydrodynamic flow" problems, and, in a linearized form, by plasma physicists in regard to stability problems. The discussion draws heavily on the work of other authors. It is included here for the sake of completeness and is intended to serve as a reference to the widespread research in this field that has taken place over the last decade.

The equations in question can be elegantly written in conservation form[36]:

$$\frac{\partial \rho}{\partial t} + \operatorname{div}(\rho \vec{u}) = 0$$

$$\frac{\partial(\rho \vec{u})}{\partial t} + \operatorname{div}\left[\rho \vec{u}\vec{u} + \mathbb{P} + \mathbb{T}\right] = 0$$

$$\frac{\partial\left[\rho\left(e^2 + \frac{u}{2}^2\right) + W\right]}{\partial t} + \operatorname{div}\left[\rho \vec{u}\left(e^* + \frac{u^2}{2}\right) + \mathbb{P}u + \vec{q} + \vec{S}\right] = 0 \quad \text{(F.1)}$$

where

$\mathbb{T}$ = Maxwell stress tensor

$\mathbb{P}$ = ordinary stress tensor

W = electromagnetic energy density, $W = \frac{1}{2}\left[\vec{E} \cdot \vec{D} + \vec{B} \cdot \vec{H}\right]$

$\vec{q}$ = heat flux vector

e^* = internal energy per unit mass

$\vec{S}$ = Poynting flux vector

and the rest of the symbols have their usual meanings. To these equations we must add Maxwell's equations and an equation of state. Even then the equations do not form a closed set, for we have not specified the so-called transport relations. In an ordinary fluid, the Chapman-Enskog expansion for a gas near local Maxwellian equilibrum leads to the familiar Navier-Stokes equations, where the transport relations are

$$\mathbb{P}_{ij} = (p + \lambda \operatorname{div} \vec{u})\,\delta_{ij} + \mu\left(\frac{\partial u_i}{\partial x_j} + \frac{\partial u_j}{\partial x_i}\right)$$

and

$$q_i = k^* \frac{\partial T}{\partial x_i}$$

in Cartesian coordinates.

In the simplest single-fluid equations for flow of a gas of charged particles one puts

$$\mathbb{P} = p\mathbb{I} \ , \ \vec{q} = 0 \qquad \text{(F. 2)}$$

and

$$\vec{j} = \sigma(\vec{E} + \vec{u} \times \vec{B}) \qquad \text{(F. 3)}$$

From the nature of the interaction of charged particles one has good reasons to believe that these assumptions will <u>not</u> be valid in many cases of physical interest. For example, one would expect that in the presence of a strong magnetic field the pressure would be non-isotropic and that $\vec{j}$ will not just be in the direction of $\vec{E} + \vec{u} \times \vec{B}$. The conservation equations must certainly be correct as they can be derived without regard to the type of collisions occurring (including no collisions); it is assumptions (F. 2) and (F. 3) which makes the use of

"single-fluid" theory questionable in some cases and which we wish to investigate here.

2. The Liouville Equation. The logical starting point for describing the motion of a group of particles is the Liouville equation, which describes the evolution in time and space of a function f_N which is defined such that $f_N(\vec{x}_1, \ldots \vec{x}_N, \vec{v}_1, \ldots \vec{v}_N, t)\, d\vec{x}_1 \ldots dt$ is the probability of finding a system of N particles in the state $\vec{x}_1, \ldots \vec{x}_N, \vec{v}_1 \ldots \vec{v}_N$ at a time t. The equation is [37]

$$\frac{\partial f_N}{\partial t} + \sum_{i=1}^{N} \vec{v}_i \cdot \frac{\partial f_N}{\partial \vec{x}_i} - \frac{1}{m} \sum_{i=1}^{N} \sum_{j=1}^{N} \frac{\partial \phi(|\vec{x}_i - \vec{x}_j|)}{\partial \vec{x}_i} \cdot \frac{\partial f_N}{\partial \vec{v}_i} = 0 \quad \text{(F.4)}$$

and can be derived directly from the conservation of particles and involves Hamilton's equations of motion[38]. One introduces the s-particle distribution function such that $f_s\, d\vec{x}_1 \ldots d\vec{x}_s d\vec{v}_1 \ldots d\vec{v}_s$ is the probability that particles 1 to s are in the state $\vec{x}_1 \ldots \vec{x}_s, \vec{v}_1 \ldots \vec{v}_s$ regardless of the state of the other particles. Then

$$f_s = \int f_N\, d\vec{x}_{s+1} \ldots d\vec{x}_N d\vec{v}_{s+1} \ldots d\vec{v}_N \quad \text{(F.5)}$$

and

$$f_1 = \int d\vec{x}_2 \ldots d\vec{x}_N d\vec{v}_2 \ldots d\vec{v}_N\, f_N = \int f_2\, d\vec{x}_2\, d\vec{v}_2, \text{ etc.}$$

On multiplying by the appropriate differentials and integrating, one obtains the B-B-G-K-Y hierarchy of coupled equations for the f_s:

$$\frac{\partial f_1}{\partial t} + \vec{v}_1 \cdot \frac{\partial f_1}{\partial \vec{x}_1} = \frac{N-1}{mV} \int d\vec{x}_2\, d\vec{v}_2\, \frac{\partial \phi}{\partial \vec{x}_1} \cdot \frac{\partial f_2}{\partial \vec{v}_1} \quad \text{(F.6a)}$$

$$\frac{\partial f_2}{\partial t} + \ldots \qquad \text{(F. 6b)}$$

$$\vdots$$

If independence is assumed, i.e. $f_2 = f_1 f_1$, etc., the first equation uncouples and yields the Vlasov equation (see below). $\vec{B}$ may be incorporated into these equations as a vector magnetic potential[37]. The problem of truncating these equations to describe a given class of physical phenomena is a difficult one. The Boltzmann equation, which deals with the motion of particles with very short range forces, can be derived from equations (F. 6a) and F. 6b) when f_3 is set identically zero. In a plasma, where the force fields are long range, research is currently active in trying to develop a tractable set of equations on this level of description.

We shall here simply write equation (F. 6a) in the form

$$\frac{\partial f_i}{\partial t} + \frac{\partial}{\partial \vec{x}} \cdot (f_i \vec{v}) + \frac{\partial}{\partial \vec{v}} \cdot (f_i \vec{a}_i) = 0 \qquad \text{(F. 7)}$$

where i denotes the species (electron, ion, etc.) and $\vec{a}_i$ denotes the particle acceleration, which in general depends on the two particle distribution function and hence indirectly on all the f_s. Equation (F. 7) is often written down directly rather than derived from the Liouville equation.

3. Manipulation of Equation (F. 7). The acceleration term of equation (F. 7) is customarily split into acceleration arising from "macroscopic" force fields (including externally applied force fields)

and "microscopic" or collisional force fields. In a gas of billard-ball molecules this dichotomy is easy to envision, in a plasma it is a difficult distinction to pin down precisely. Thus equation (F. 7) is usually written as

$$\frac{\partial f_i}{\partial t} + \frac{\partial}{\partial \vec{x}} \cdot (f_i \vec{v}) + \frac{\partial}{\partial \vec{v}} \left[\frac{e_i}{m_i} (\vec{E} + \vec{v} \times \vec{B}) f_i \right] = \left(\frac{\partial f_i}{\partial t} \right)_{\text{coll.}} \qquad \text{(F. 8)}$$

for a plasma, and the question arises as to the precise meaning of the last two terms. This point has been very nicely discussed by Green[39], and we shall summarize his findings here. Consider for simplicity a fully ionized two component gas consisting of singly charged ions and electrons. For each species one can define a distribution function f_i whose propagation in time is governed by equation (F. 7). We define the following macroscopic velocities, which we shall use throughout this appendix:

$$\begin{aligned} n_i \vec{u}_i &= f_i \int \vec{v}\, d^3 v = \text{species mean velocity} \\ \rho \vec{u}_o &= \sum_{i=1}^{2} m_i n_i \vec{u}_i = \text{center of mass velocity} \end{aligned} \qquad \text{(F. 9)}$$

where $n_i = \int f_i d^3 v$ is the species number density. The charge and current densities are defined as

$$\begin{aligned} q &= \sum_i e_i n_i \\ \vec{j} &= \sum_i e_i n_i \vec{u}_i \end{aligned} \qquad \text{(F. 10)}$$

where e_i is the charge of a particle of the i^{th} species.

Let $\vec{E}_o$ and $\vec{B}_o$ represent the fields imposed by external means, i.e. from outside the system of particles under consideration. Then the acceleration of a given particle arises from these fields plus the interaction with every other particle, that is

$$\frac{m_i \vec{a}_i}{e_i} = \vec{E}_o + \vec{v} \times \vec{B}_o + \sum_j \iint f_{j,i} (\vec{E}_j + \vec{v} \times \vec{B}_j) \, d^3x' d^3v' \qquad \text{(F. 11)}$$

Here $\vec{E}_j$ and $\vec{B}_j$ are the fields at the i^{th} particle arising from the particle at $\vec{x}'$, t' and $f_{j,i}$ is the conditional two particle distribution function. From probability theory $f_{j,i} = f_{ij}/f_i$ where f_{ij} is the joint probability. By simple addition and subtraction of terms, equation (F. 11) becomes

$$\frac{m_i \vec{a}_i}{e_i} = \vec{E} + \vec{v} + \vec{B} + \sum_j \iint \frac{(f_{ij} - f_i f_j')}{f_i} (\vec{E}_j + \vec{v} \times \vec{B}_j) \, d^3x' d^3v' \qquad \text{(F. 12)}$$

where

$$\vec{E} = \vec{E}_o + \sum_j \iint f_j' \vec{E}_j \, d^3x' d^3v'$$

$$\vec{B} = \vec{B}_o + \sum_j \iint f_j' \vec{B}_j d^3x' d^3v' \qquad \text{(F. 13)}$$

Green then points out the important fact that the $\vec{E}$ and $\vec{B}$ so defined satisfy Maxwell's equations for a continuous medium exactly, when the definitions of charge and current densities given above are used, i.e. the fields are self-consistent. Equation (F. 7) then becomes

$$\frac{\partial f_i}{\partial t} + \vec{v} \cdot \frac{\partial f_i}{\partial \vec{x}} + \frac{\partial}{\partial v} \cdot \left[\frac{e_i}{m_i} (\vec{E} + \vec{v} \times \vec{B}) f_i \right]$$

$$= - \frac{\partial}{\partial v_i} \cdot \left\{ \frac{e_i}{m_i} f_i \sum_j \iint \left(\frac{f_{ij} - f_i f_j}{f_i} \right) (\vec{E}_j + \vec{v} \times \vec{B}_j) d^3x' d^3v' \right. \qquad \text{(F. 14)}$$

$$= - \operatorname{div}_v \vec{\Gamma} = \left(\frac{\partial f_i}{\partial t} \right)_{\text{coll.}}$$

which has the same form of equation (F. 8). Notice that the statement made above that the Vlasov equation results from choosing $f_2 = f_1 f_1$ is now easily verified. While the problem has not been "solved" in the sense that f_{ij} is still unknown and involves the higher order distribution functions, Green's analysis has served the useful purpose of clearly defining E and B appearing on the left and thus of elucidating the nature of a collision in a gas of particles with long range force fields.

The right hand side of equation (F. 14) has been the subject of much investigation. For most plasmas the Debye length λ_D is much larger than the 90° impact parameter p_o (this also implies that the number of particles in a Debye sphere is large). For "collisions" with an impact parameter larger than the Debye length there is very little "individual" interaction since the particle charge is effectively shielded, rather these are the "collective" effects which appear on the left side of the equation. The cumulative effect of small-angle collisions with impact parameters between p_o and λ_D has been shown to outweigh the relatively few (since $n\lambda_D^3$ is large) large angle collisions (for example see Spitzer, Ref. 24). These collisions are described by the Fokker-Planck form of the collision term, which we shall discuss very briefly in section 6.

4. The Moment Equations. For most purposes one is interested only in the mean values of quantities such as density and velocity*; these are "moments" of the distribution function f_i. Equations governing the propagation of these quantities in time and space may be obtained by multiplying equation (F. 8) by some function of $\vec{v}$ and integrating over velocity space. In this section we shall show that the conservation equations can be derived in this manner. In taking moments we shall make repeated use of Gauss' theorem:

$$\int_{\text{volume}} \text{div } A \, d\tau = \int_{\text{surface}} \vec{n} \cdot A \, d\sigma$$

where A may be a vector or tensor.

The zeroeth moment is

$$\frac{\partial n_i}{\partial t} + \frac{\partial \cdot (n_i \vec{u}_i)}{\partial \vec{x}} = 0 \qquad \text{(F. 15)}$$

where the right hand side vanishes because collisions do not transfer particles in physical space. On multiplying equation (F. 15) by m_i and summing over species there results

$$\frac{\partial \rho}{\partial t} + \text{div } (\rho \vec{u}_o) = 0 \qquad \text{(F. 16)}$$

which is the familiar continuity equation of fluid mechanics. We next multiply equation (F. 8) by $\vec{v}$ and integrate over velocity space, assuming that f_i vanishes sufficiently quickly at ∞ that the surface

---

*There are cases of interest in plasma physics where the moment description does not contain the essential features. For example the phenomenon of Landau "damping" in a collisionless plasma does not appear in the moment equations to any order[40]. In addition, stability studies of the Vlasov equation have revealed "microscopic instabilities" which are unique to the kinetic theory description[41].

integrals vanish. This yields

$$\frac{\partial}{\partial t}\left(n_i \vec{u}_i\right) + \frac{\partial}{\partial \vec{x}} \cdot \left[n_i \vec{u}_i \vec{u}_i \right] - n_i \frac{e_i}{m_i}\left[\vec{E} + \vec{u}_i \times \vec{B} \right] = \vec{F}_{ij} \qquad \text{(F. 17)}$$

where $\vec{F}_{ij}$ represents the force per unit volume exerted by species j on species i ($i \neq j$).

Following Chapman and Cowling[42] we define a stress tensor relative to the center of mass velocity,

$$\mathbb{P}_i = m_i \int (\vec{v} - \vec{u}_o)(\vec{v} - \vec{u}_o) f_i d^3v \qquad \text{(F. 18)}$$

As Oberman[43] and others have noted, there is an alternative definition,

$$\mathbb{P}_i^* = m_i \int (\vec{v} - \vec{u}_i)(\vec{v} - \vec{u}_i) f_i d^3v, \qquad \text{(F. 19)}$$

frequently used in the literature. In some problems (usually those in which the species equations are used separately), $\mathbb{P}_i^*$ may be more convenient. If we now multiply equation (F. 17) by m_i, sum over species, and write $\mathbb{P} = \sum_i \mathbb{P}_i$, there results

$$\frac{\partial}{\partial t}\left(\rho \vec{u}_o\right) + \frac{\partial}{\partial \vec{x}} \cdot \left(\rho \vec{u}_o \vec{u}_o + \mathbb{P}\right) = q\vec{E} + \vec{j} \times \vec{B} \qquad \text{(F. 20)}$$

where the collision term vanishes because of Newton's third law. By definition, $-\operatorname{div}\mathbb{T} = q\vec{E} + \vec{j} \times \vec{B}$ when the electromagnetic momentum can be neglected, as is assumed here. Therefore equation (F. 20) is identical to equation F. 1b).

There are still fewer equations than unknowns. It is clear that multiplying equation (F. 8) by $\vec{v}\vec{v}$ and integrating will yield an

equation for $\mathbb{P}$. Before proceeding with this we note that the contraction of $\mathbb{P}$ is

$$\mathrm{Tr}\ \mathbb{P}_i = m_i \int (\vec{v} - \vec{u}_o)^2 f_i d^3v$$

and represents the kinetic energy of the molecules relative to the mean velocity. We may thus define a generalized temperature as

$$\mathrm{Tr}\ \frac{1}{2}(\mathbb{P}_1 + \mathbb{P}_2) = \mathrm{Tr}\left(\frac{1}{2}\mathbb{P}\right) = \frac{3}{2}(n_1 + n_2)\,kT \qquad \text{(F.21)}$$

The next moment can be derived in a similar fashion. The algebra involved is tedious and will be omitted here; the results are[43]

$$\frac{\partial \mathbb{P}_i}{\partial t} + \frac{\partial}{\partial \vec{x}} \cdot (\mathbb{Q} + \vec{u}_o \mathbb{P}_i) + \mathbb{P}_i \cdot \nabla u_o + (\mathbb{P}_i \cdot \nabla u_o)^T$$

$$+ \rho_i \vec{u}_o \frac{d\vec{u}_o}{dt} + e_i (\vec{B} \times \mathbb{P}_i - \mathbb{P}_i \times \vec{B}) - e_i n_i \vec{w} (\vec{E} + \vec{u}_o \times \vec{B}) \qquad \text{(F.22)}$$

$$- e_i n_i (\vec{E} + \vec{u}_o \times \vec{B}) \vec{w} = \left(\frac{\delta \mathbb{P}_i}{\delta t}\right)_{\text{coll.}}$$

where

$$\mathbb{Q} = m_i \int d^3v\, (\vec{v} - \vec{u}_o)(\vec{v} - \vec{u}_o)(\vec{v} - \vec{u}_o) f_i = \text{"heat flow" triadic}$$

$$\vec{w}_i = \vec{u}_i - \vec{u}_o = \text{species diffusion velocity}$$

and the operator $B \times \mathbb{P}$ is defined (in Cartesian coordinates) by

$$(B \times \mathbb{P}) = \sum_{j,k,\ell} B_j \mathbb{P}_{k\ell} (i_j \times i_k)\, i_\ell$$

Summing over species and contracting, one obtains the scalar equation[43]

$$\frac{\partial}{\partial t}\left(\frac{3}{2} n \theta\right) + \frac{\partial}{\partial \vec{x}}\left(\vec{q} + \frac{3}{2} n \theta \vec{u}_o\right) + \mathbb{P} : \nabla \vec{u}_o - \left(\vec{j} - q \vec{u}_o\right) \cdot \left(\vec{E} + \vec{u}_o \times \vec{B}\right) = 0 \qquad \text{(F. 23)}$$

where the right hand side vanishes because elastic collisions conserve energy, and

$$\vec{q} = \frac{1}{2} \sum_i \int m_i \, d^3 v (\vec{v} - \vec{u}_o)^2 (\vec{v} - \vec{u}_o) f_i \qquad \text{(F. 24)}$$

is the heat flux vector.

Equations (F. 16), (F. 20), and (F. 23) are completely equivalent to the conservation equations (F. 1), and were derived without consideration of the collision terms. There are still, however, more unknowns than equations. It is clear that simply taking further moments introduces new variables so that the system can not be closed in this manner and different methods of attack must be developed. It will be seen that there are two limits in which the system can be satisfactorily truncated, namely in the case of "collision dominated" flows and in the opposite limit of flows with no collisions. We will treat the first of these in some detail and simply make reference to the second.

5. The "Generalized Ohm's Law". One of the earliest schemes for closing the set is that adopted by Spitzer[24]. It is often called the "two-fluid" model and involves the derivation of a "generalized Ohm's law" and the assumption of an isotropic pressure tensor for closure.

The species momentum equations were added above to combine the $\vec{u}_i$ in such a way as to derive an equation for $\vec{u}_o$. We can now manipulate the same equations to get an expression for the rate of change of $\vec{j}$. The following assumptions are made.

(1) Terms quadratic in $\vec{u}_o$ can be neglected. (This linearization destroys the essential features of many interesting fluid dynamical problems.)

(2) $m_1/m_2 \ll 1$, where 1 denotes electrons.

(3) $n_1 \approx n_2$, i.e. the fluid is macroscopically neutral; this is valid if the Debye length is small compared to any other relevant length and is often included in the definition of a plasma.

(4) $p_1 \approx p_2$. This is valid assuming (3) holds if the further restriction $T_1 = T_2$ is made. This may be a poor approximation in some cases, for instance where a strong electric field is present.

(5) $e_i = e_2$, consistent with (3).

If we now multiply by e_i/m_i the equations analogous to (F. 17), but based on Φ_i^*, and sum over species, there results [43]

$$\frac{m_1}{e^2 n} \frac{\partial \vec{J}}{\partial t} = \vec{E} + \vec{u}_o \times \vec{B} - \frac{\vec{J} \times \vec{B}}{en} + \frac{1}{en} \nabla p_1 - \frac{m_1 \vec{F}_{12}}{en} \qquad \text{(F. 25)}$$

One now argues that the last term should be proportional to the difference in velocities of the species, i.e.

$$\left| \frac{m_1 \vec{F}_{12}}{en} \right| \sim \vec{u}_1 - \vec{u}_2 ; \quad \left| \frac{m F_{12}}{en} \right| = \eta e n (\vec{u}_1 - \vec{u}_2) = \eta \vec{J}$$

where η is defined by this equation. This step is perhaps the weakest in the entire derivation since the whole collision integral has been discarded and replaced by a very crude model. The resulting equation

is called the generalized Ohm's law and reads

$$-\frac{\eta}{\nu_c}\frac{\partial \vec{j}}{\partial t} + \vec{E} + \vec{u}_o \times \vec{B} - \frac{\vec{j} \times \vec{B}}{en} - \frac{1}{en}\nabla p_1 - \eta \vec{j} = 0 \qquad \text{(F. 26)}$$

One usually neglects the heat flow vector q (consistent with diagonalizing the pressure tensor), and thus replaces the energy equation with the isentropic equation for a monatomic gas

$$\frac{d}{dt}\left(p\,\rho^{-5/3}\right) = 0 \qquad \text{(F. 27)}$$

Thus, the equations for conservation of mass and momentum, along with equations (F. 26), (F. 27), and Maxwell's equations form a complete set.

We now wish to examine the relative magnitudes of terms in equation (F. 26). The $\vec{j} \times \vec{B}$ can be eliminated by use of the momentum equation and the resulting equation non-dimensionalized. Let ω^{-1} and L signify a characteristic time and length for a problem under consideration. Let us assume $\vec{u}_o \times \vec{B}$ and $\vec{E}$ are of order 1. Then the inertial terms can be neglected for $\omega/\nu_c \ll 1$, and the $\vec{j} \times \vec{B}$ term is small when $\omega/\omega_{c_i} \ll 1$. Under the assumption that $\frac{\lambda c_i}{L} \cdot \frac{a}{u_o} \ll 1$ the pressure gradient term is also small (note that we have previously assumed that u_o/a is small in making the linearization leading to equation (F. 26) so that λ_{c_i}/L must be very small), and there remains

$$n\vec{j} = \vec{E} + \vec{u}_o \times \vec{B} \qquad \text{(F. 28)}$$

In "ideal hydromagnetics" the term $n\vec{j}$ is also dropped, since η is supposed to vanish. This implies that collisions become infrequent

which tends to contradict the assumption of pressure isotropy. For the special case where all quantities of the linearized equations vary as $e^{i\omega t}$, Liist[44] concludes that the n_j term may be dropped when $\frac{\omega}{\omega_{c_i}} \ll \frac{\omega_{c_i}}{\nu_c}$. For pressure isotropy $\frac{\omega_{c_i}}{\nu_c}$ must be small, so ω / ω_{c_i} must be even smaller.

In summary, the transport equation (F. 28) which is used in the one-fluid theory (equation(F. 3)) can be derived under a set of some questionable assumptions and restrictive limitations on characteristic frequencies and lengths. It is often applied to problems in which the required conditions do not obtain. Fortunately, a far more rigorous theory has been used to close the equations for collision dominated flows, which we shall now discuss.

6. Plasma Transport Theory. In an ordinary fluid the relation between the flux of momentum and the velocity gradients, and between energy flux and temperature gradients, can be worked out rigorously* by setting the distribution function equal to a local Maxwellian plus a small correction, $f = F(1 + \phi)$ and solving for ϕ. This is known as the Chapman-Enskog procedure and leads to the Navier-Stokes and Fourier "laws" given on page 2 of this appendix.

We have seen that the conservation equations (F. 1) are true independent of the type of collisions which occur, and that to close the set we need to derive the appropriate transport relations, which do depend on collisions. Using a procedure analogous to the Chapman-Enskog expansion, Marshall[46] and Robinson and Bernstein[47] have studied the transport properties of a plasma, starting from the

*Some questions as to the uniformity of convergence of this method have been raised recently, for example by Liepmann, Narasimha, and Chahine[45].

Fokker-Planck form of the collision integral. As in the case of ordinary fluids the generalized fluxes and forces are found to be linearly related; in a plasma this means that thermo-electric effects, for example, are present. By way of illustration, the equation for current becomes (Ref. 8, eqn. IV-37)

$$\vec{J} = \sigma_o (\vec{E}' \cdot \hat{b})\hat{b} + \sigma_1 (\hat{b} \times (\vec{E}' \times \hat{b})) + \sigma_2 (\vec{E}' \times \hat{b})$$

$$+ \alpha_o (\nabla T \cdot \hat{b})\hat{b} + \alpha_1 (\hat{b} \times (\nabla T \times \hat{b})) + \alpha_2 (\nabla T \times \hat{b}), \qquad (F.29)$$

where $\hat{b}$ is a unit vector in the direction of $\vec{B}$

$$\vec{E}' = \vec{E} + \frac{\vec{u}_o}{c} \times \vec{B} - \frac{kT}{e} \frac{\partial}{\partial x} \left(\ell n \, (n \, k \, T) \right) \quad (c.g.s)$$

T is the temperature,

The σ's are components of a conductivity tensor and the α's are thermo-electric coefficients, both of which are tabulated in reference 8. The limitations of the method seem to be associated mainly with the limitations of the Fokker-Planck equation, which are not yet completely understood. For details the reader is referred to the original papers[46, 47] and the summary by Bernstein and Trehan[48].

7. Collisionless Plasma Theory. Although, as has been pointed out, the important "collisions" in a plasma are those which result in small-angle scattering, one can still define an effective mean free path in terms of the mean square scattering angle, etc.[24]. If the gas is sufficiently rarefied that the mean free path is larger than any other relevant length in the problem, or the collision frequency is less than any other relevant frequency, the collision terms in the kinetic equations vanish and the plasma is termed collisionless or collision-free. It should

be noted that whether or not a particular plasma is "collisionless" depends on the problem under consideration. For example, nearly all plasmas are collisionless insofar as plasma oscillations are concerned, since $\frac{\omega_p}{\nu_c}$ is almost always much greater than one. For slower phenomena many laboratory plasmas can not be considered collisionless.

The conservation equations(F. 1) are of course still valid, but again do not form a closed set. In attempting to relate $\mathbb{P}$, $\vec{q}$ and $\vec{j}$ to the other field variables one can no longer assume that the distribution function will be nearly locally Maxwellian, even if it is so initially.

Two methods of closing the equations in this limit have been studied. As they are readily available in the literature and not of direct interest in the present experiments, we shall mention them only briefly.

The Chew-Goldberger-Low theory[49] is an attempt to derive a closed set of macroscopic equations for a collisionless plasma, starting from the Vlasov equation. The main results of the theory are that two dimensional motion across the field lines can be described by the macroscopic equations with a scalar pressure and an isentropic relation with $\gamma = 2$, while motion along the field lines in general must be handled directly by the kinetic equation and can be treated fluid dynamically (i.e. with macroscopic equations) only when the additional assumption is made that the longitudinal adiabatic invariant of orbit theory exists[50].

The "low temperature approximation"[43] starts with the macroscopic equations and makes use of the fact that the successive moments ($\mathbb{P}, \mathbb{Q}, \ldots$) differ in order of magnitude by the quantity

$\frac{v_{thermal}}{u_{phase}}$. Thus if this quantity is small, $\mathbb{P}$ and $\mathbb{O}$ may be dropped completely in the first approximation. The next approximation retains $\mathbb{P}$ but discards $\mathbb{O}$ and so forth. The method can be extended to include corrections to any order.

REFERENCES

1. Liepmann, H. W., and G. Vlases, Physics of Fluids (1961), 4 pp. 927-928

2. Clauser, F. (editor), Plasma Dynamics, Addison-Wesley Publishing Co., Reading, Mass. (1960), p. 13

3. Fowler, R.G., W. Atkinson, W. Compton, and R. Lee, Physical Review (1952), 88, pp. 137-138

4. Kolb, A.D., Physical Review (1957), 107, pp. 345-350

5. Josephson, V., Journal of Applied Physics (1958), 29, pp. 30-32

6. Patrick, R.M., Physics of Fluids (1959), 2, pp. 589-598

7. Wilson, J.L., GALCIT Rept., Contract NAw-6553, (June, 1960)

8. Jones, T.G., unpublished (1961)

9. Anderson, O.A., et al., Physics of Fluids (1958), 1, pp. 489-494.

10. Liepmann, H.W., Private communication (1959)

11. Colgate, S.A., and H.P. Furth, Physics of Fluids (1960), pp. 982-1000

12. McLean, E. A., et al., Physics of Fluids (1960), 3, pp. 843-856

13. Wiese, W., H. F. Berg, and H. R. Griem, Physics of Fluids (1961), 4, pp. 250-253

14. McLean, E. A., A. C. Kolb, and H. R. Griem, Physics of Fluids (1961), 4, pp. 1055-1056

15. Greifinger, C., and J. D. Cole, Physics of Fluids (1961), 4, pp. 527-534

16. Whitham, G. B., Communications on Pure and Applied Mathematics (1959), 12, pp. 113-158

17. Marshall, W., Proceedings of the Royal Society, Series A (1955), 233, pp. 367-376

18. Burgers, J.M., U. of Md. Tech. Note BN-102 (1957)

19. Barker, J. R., Journal of Scientific Instruments (1949), 26, pp. 273-275

20. Camac, M., et al., AVCO-Everett Research Report 107 (1961)

REFERENCES (Contd.)

21. Lovberg, R. H., Annals of Physics (1959), 8, pp. 311-324

22. Dippel, K. H. and Teckenberg, Proceedings of the Fourth International Conference on Ionization Phenomena In Gases, North Holland Publishing Company (1959), Vol. I, pp. 533-536

23. Petschek, H., and S. Byron, Annals of Physics (1957), 1, pp. 270-315

24. Spitzer, L. Jr., Physics of Fully Ionized Gases, Interscience Publishers, New York (1956)

25. Massey, H. S. W., and E. H. S. Burhop, Electronic and Ionic Impact Phenomena in Gases, Oxford (1952)

26. Poeschel, R. L., Private communication (1962)

27. Liepmann, H. W., and A. Roshko, Elements of Gasdynamics, John Wiley and Sons, Inc., New York, 1957

28. Gould, R. D., Class notes, E. E. 260, Caltech (Fall 1961)

29. Cann, G. L. and A. C. Ducati, Plasmadyne Report P-4TN 069-54, AFOSR TN 59-633

30. Cann, G. L., and A. C. Ducati, Plasmadyne Report P-3TN 029-54, AFOSR TN 59-247 (1959)

31. Knocke, K-F, U.S.A.F. Rept. ARL 171 (Dec. 1961)

32. Cann, G. L., Private communication (1962)

33. Johnson, D. S., Ae Thesis, Caltech (1962)

34. Wilson, J. L., "A Pulsed Magnetic Field", unpublished report, GALCIT (1960)

35. Groenig, H., "Precursor Photoionization and Electrons", submitted to Physics of Fluids

36. Liepmann, H. W., Class notes, Ae 235, Caltech (Fall 1961)

37. Frieman, E. A., "Derivation of Kinetic Equations for a Plasma", lecture, Summer Institute in Plasma Physics, Princeton University, (Summer 1962)

38. Born, M., Natural Philosophy of Cause and Chance, Oxford Press, London (1948)

REFERENCES (Contd.)

39. Green, H. S., Physics of Fluids (1959), 2, pp. 341-349

40. Dawson, J., lecture, Summer Institute in Plasma Physics, Princeton University, (Summer 1962)

41. Frieman, E. A., "Microscopic Instabilities", lecture, Summer Institute in Plasma Physics, Princeton University, (Summer 1962)

42. Chapman, S., and T. G. Cowling, The Mathematical Theory of Non-Uniform Gases, Cambridge University Press, London (1961)

43. Oberman, C. R., "Macroscopic Equations", lecture notes, Summer Institute in Plasma Physics, Princeton University, (Summer 1962)

44. Lüst, R., Class notes, Ae 236, Caltech (Winter, 1961-62)

45. Liepmann, H. W., R. Narasimha, M. Chahine, Physics of Fluids, (1962), 5, pp. 1313-1324

46. Marshall, W., Report AERE T/R 24 19, Atomic Energy Research Establishment, Harwell, England

47. Robinson, B. B., and I. B. Bernstein, Annals of Physics (1962) 18, pp. 110-169

48. Bernstein, I. B., and S. K. Trehan, Nuclear Fusion (1960) 1, pp. 3-41

49. Chew, G. F., Proceedings of the Royal Society, (1956), A236, pp. 112-118

50. Frieman, E. A., "Orbit Theory", lecture notes, Summer Institute in Plasma Physics, Princeton University, (Summer 1962).

TABLE I

Experiment	B_{z_0} (gauss)	b_0/u_0	$T_{2\,eq.}$ (°K)	$a_{2eq.}$	σ_2 (mhos/m)	δ_c (cm)
Argon, 100μ, 12 kv u_0 = 1.95 cm/μ sec M_0 = 60	0 1350 2750 4125 5500	0 0.42 0.86 1.29 1.72	≈30,000	Doubly Ionized	13,000	1.6
Argon, 500μ, 12 kv u_0 = 1.30 cm/μ sec M_0 = 40	0 1650 3300 4950 6600	0 0.35 0.69 1.04 1.38	≈23,000	Nearly Double	8,750	2.3
Helium, 100μ, 12 kv u_0 = 3.47 cm/μ sec M_0 = 34	0 680 1350 2050 2700	0 0.38 0.75 1.14 1.53	21,900	0.68	8,000	1.5
Helium, 500μ, 12 kv u_0 = 2.32 cm/μ sec M_0 = 22.7	0 1100 2200 3300 4350	0 0.41 0.82 1.22 1.61	19,500	0.25	7,000	2.0

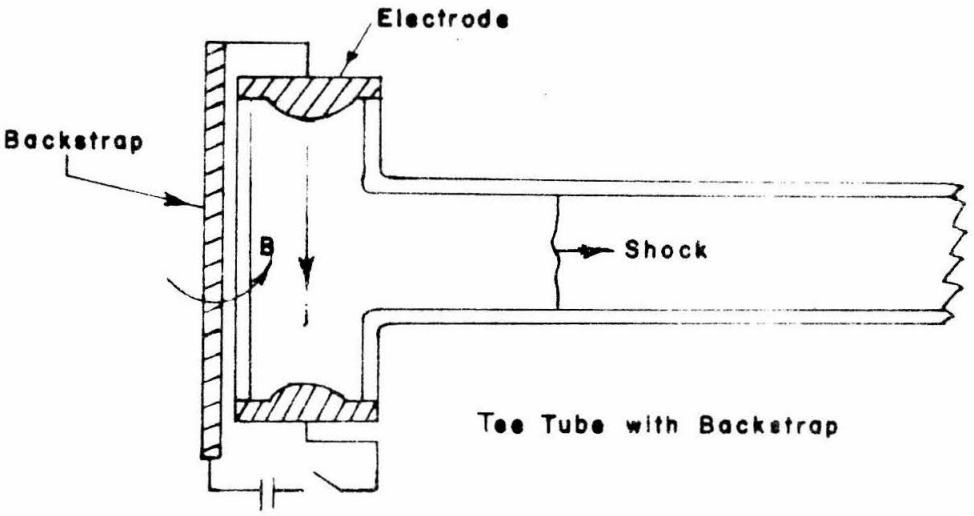

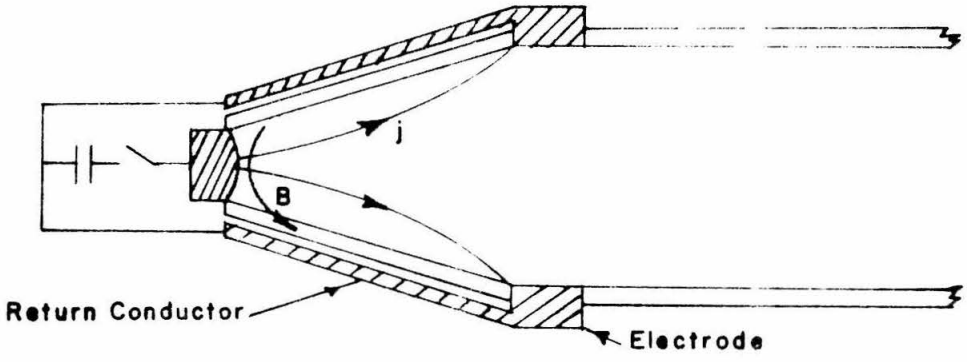

Conical Magnetic Shock Tube

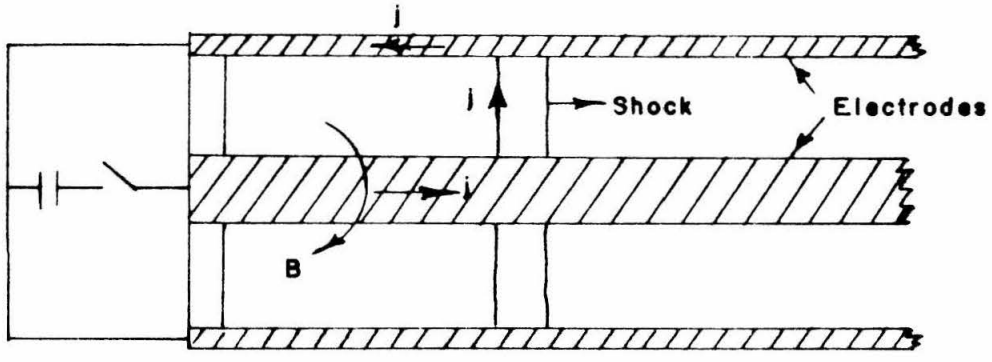

Linear Coaxial Magnetic Shock Tube

FIG. 1 VARIOUS MAGNETIC SHOCK TUBE CONFIGURATIONS

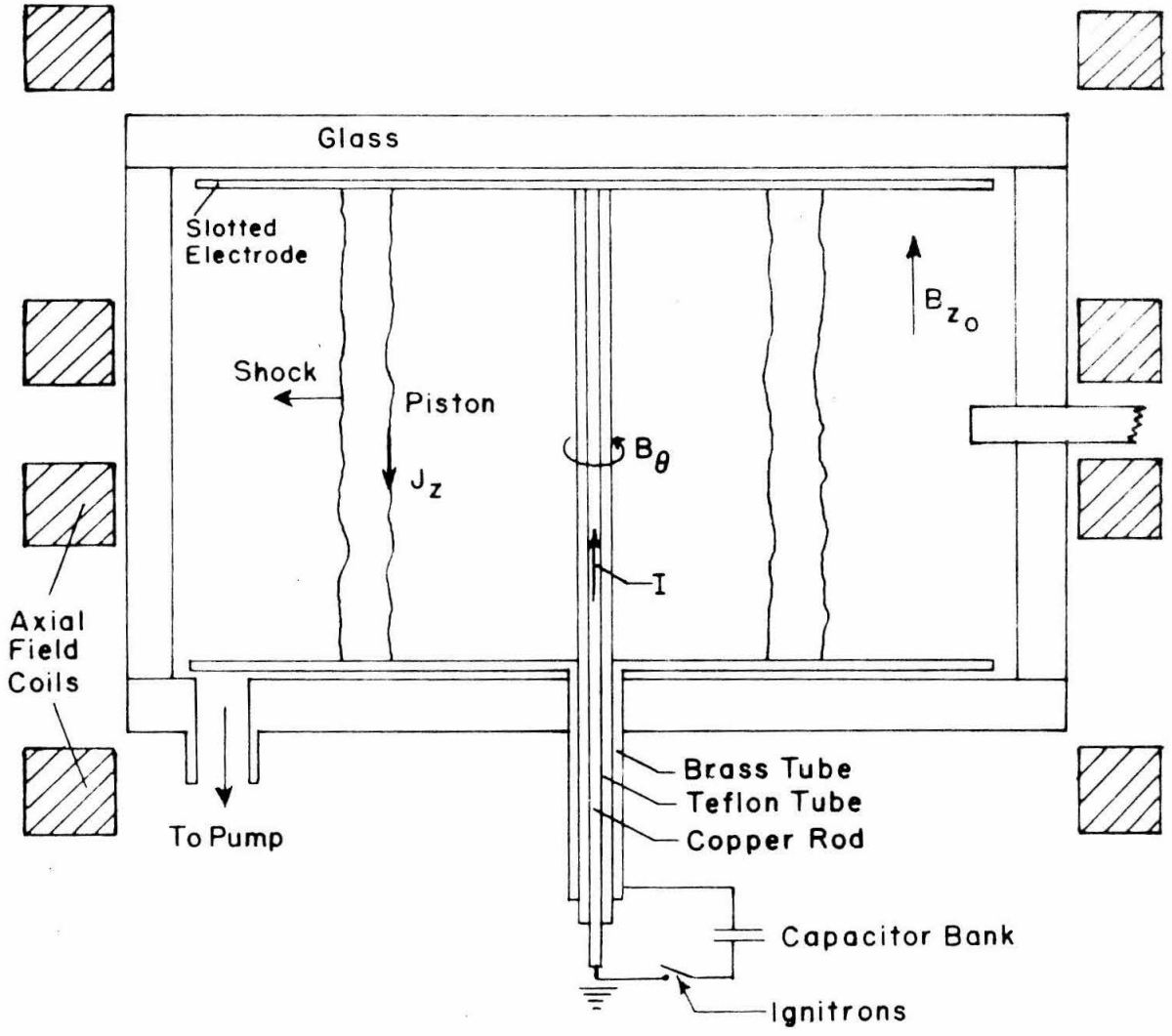

FIG. 2 SCHEMATIC VIEW OF CYLINDRICAL MAGNETIC SHOCK TUBE

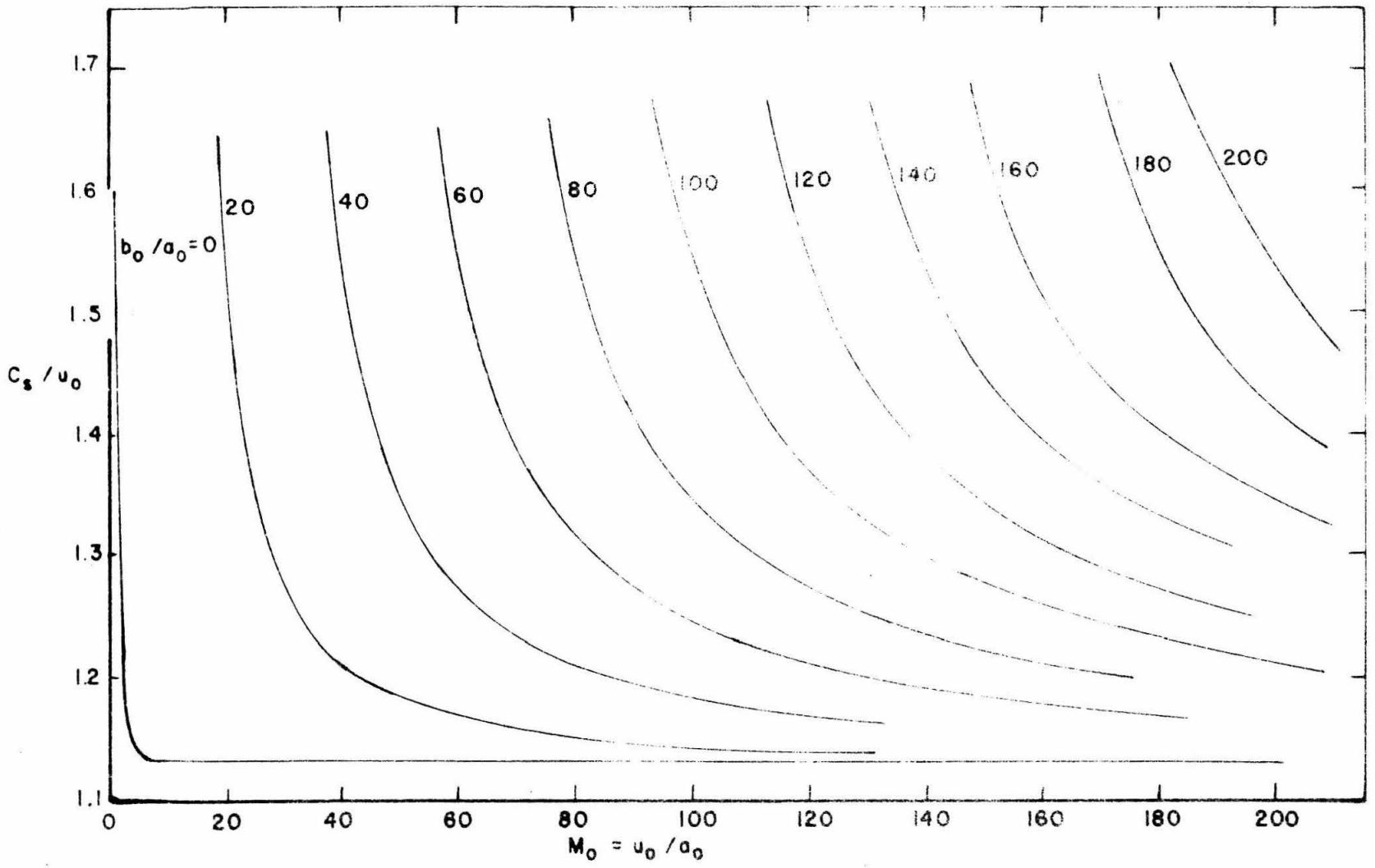

FIG. 3 SHOCK SPEED, GREIFINGER AND COLE SOLUTION, $\gamma = 5/3$

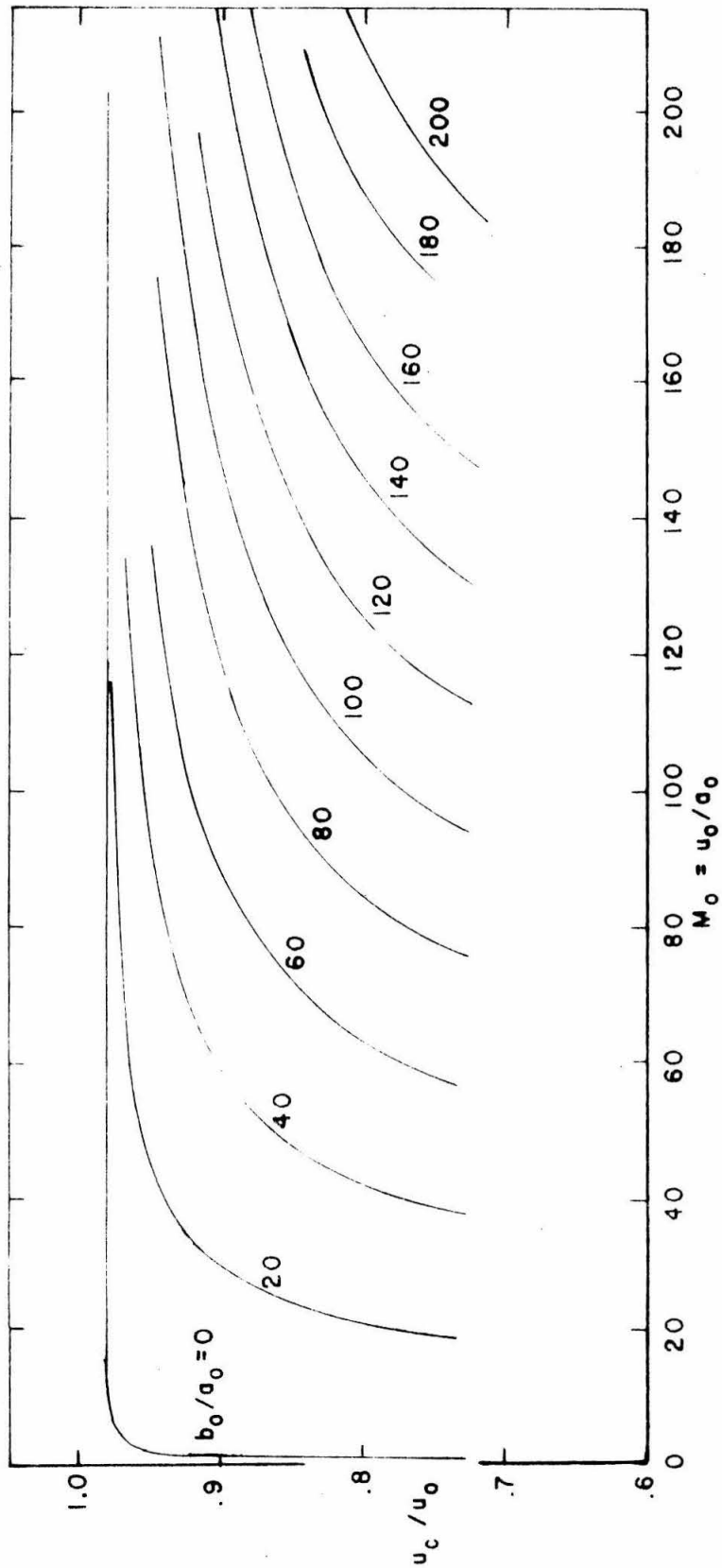

FIG. 4 PISTON SPEED, GREIFINGER AND COLE SOLUTION, $\gamma = 5/3$

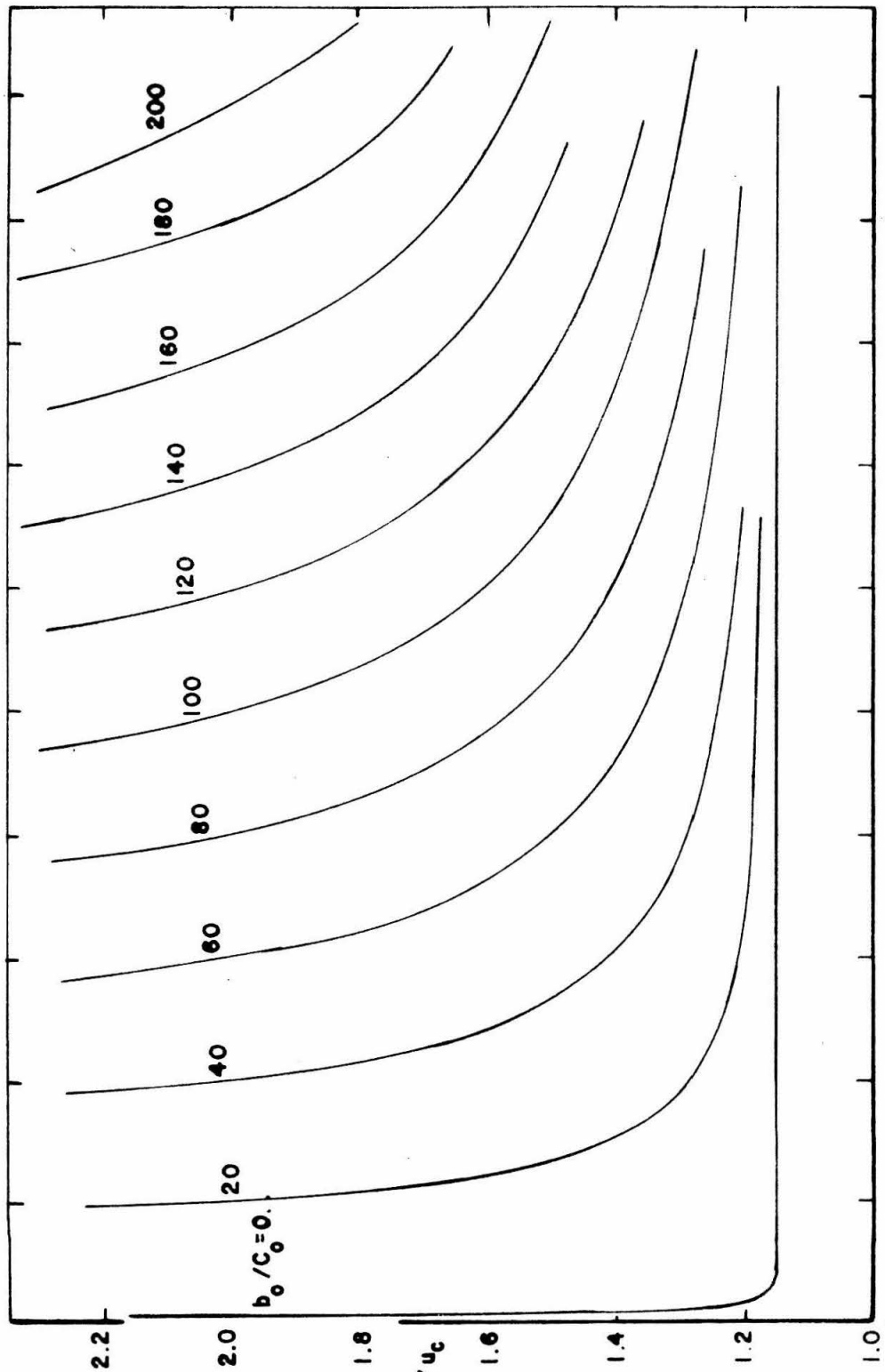

FIG.5 RATIO OF SHOCK SPEED TO PISTON SPEED, GREIFINGER AND COLE SOLUTION, $\gamma = 5/3$

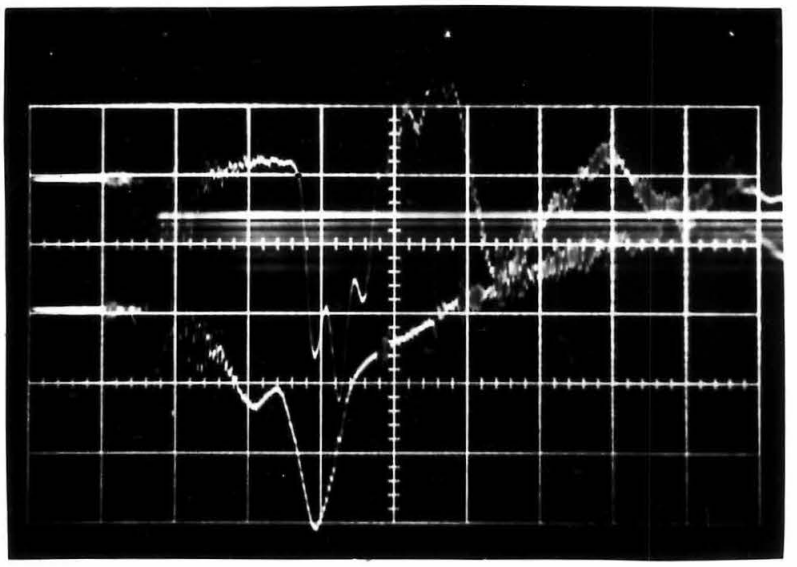

(a) $B_{z_o} = 0$

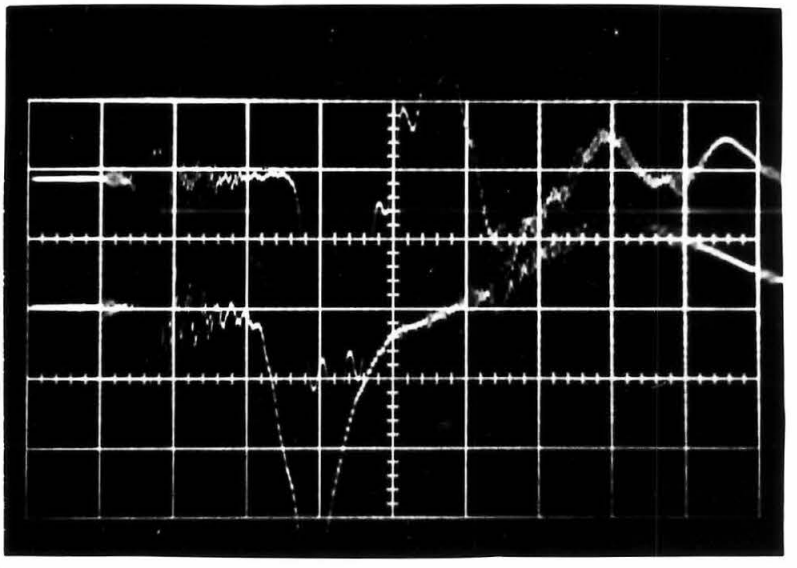

(b) $B_{z_o} = 2200$ g.

Fig. 6. Oscillograms from Helium at 500 μ. Upper beam, pressure probe. Lower beam, $\dot{B}_\theta$ probe. Sweep rate, 1 μsec/cm. Probes 1.67" from center.

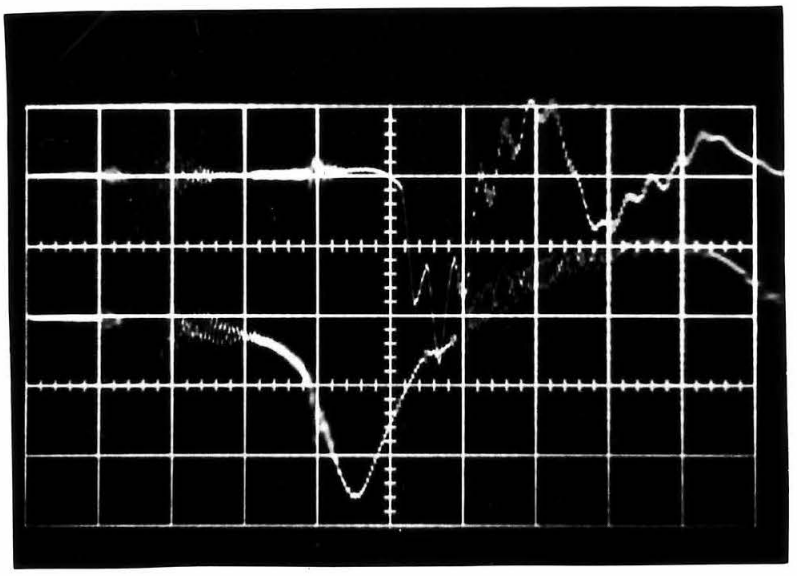

(a) B_{z_o} = 1650 g. Upper beam, pressure probe. Lower beam, $\dot{B}_\theta$ probe. Probes 1.67" from center.

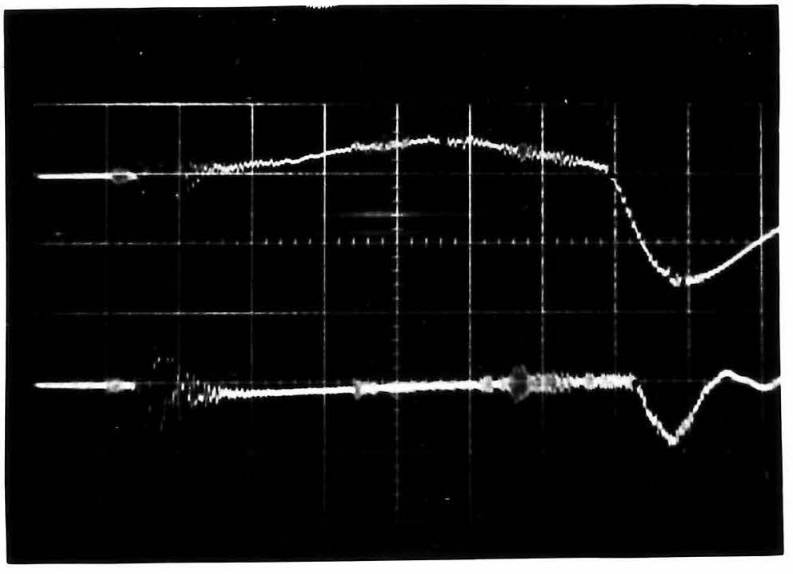

(b) B_{z_o} = 3300 g. Upper beam, $\dot{B}_z$ probe. Lower beam, pressure probe.

Fig. 7. Oscillograms from Argon at 500 μ. Sweep rate 1 μs/cm.

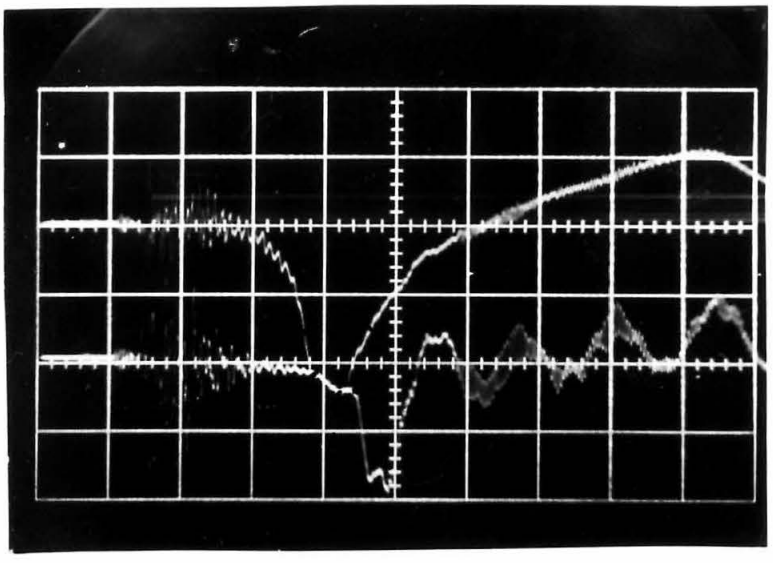

(a) Probes 1.67" from center

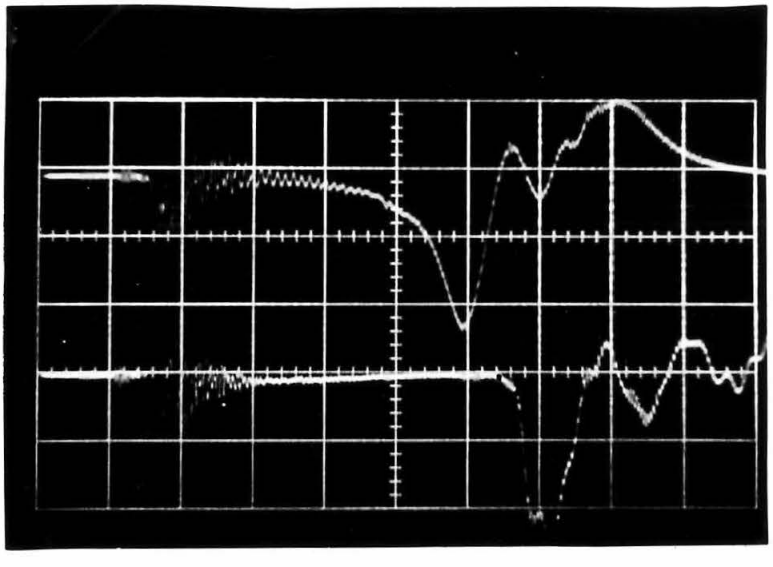

(b) Probes 3.17" from center

Fig. 8. Oscillograms from Argon at 100μ. Sweep rate 1μs/cm left to right. Upper beam, $\dot{B}_\theta$ Probe. Lower Beam, Pressure Probe. B_{z_o} = 1350 g.

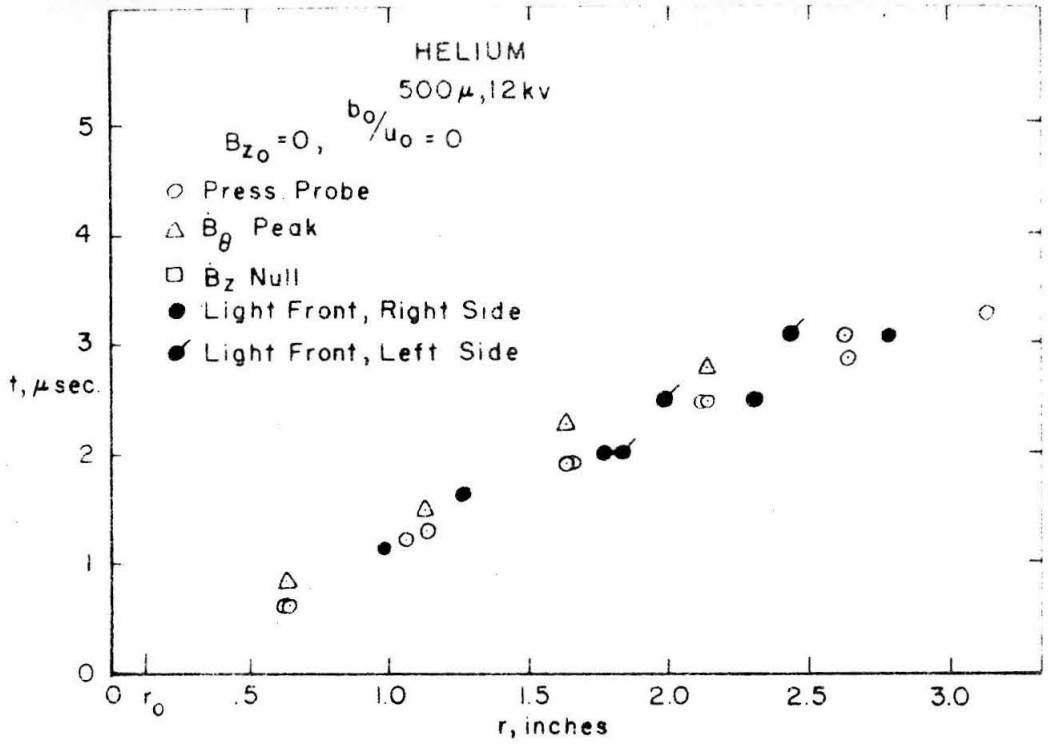

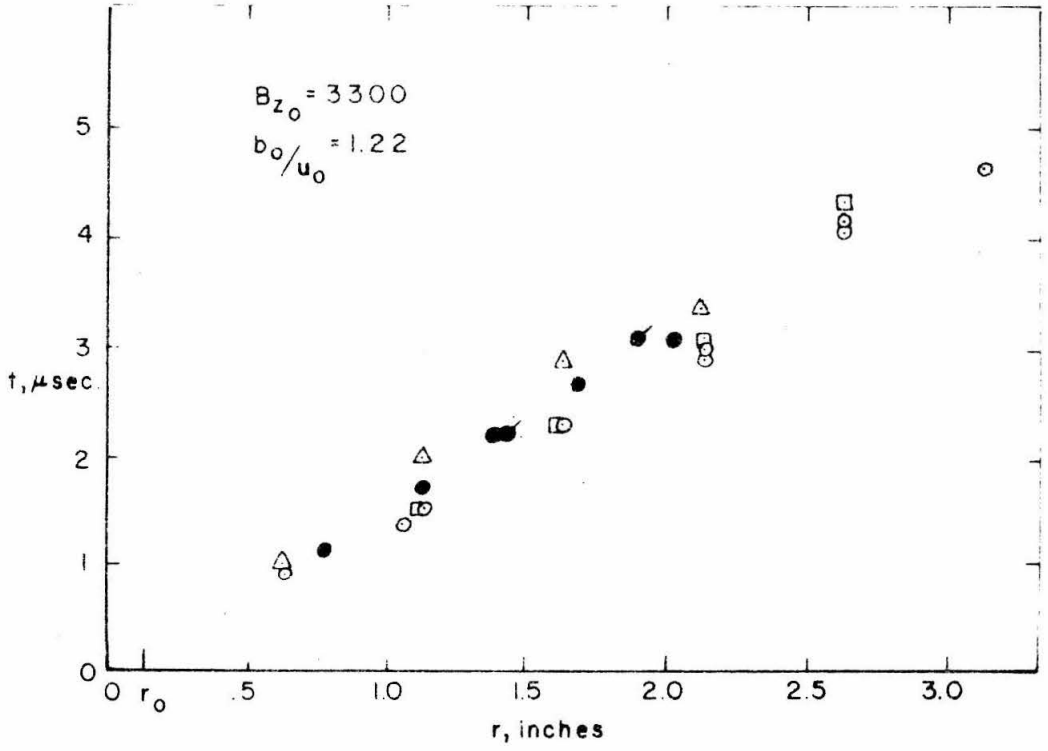

FIG. 9 RELATIVE FRONT POSITIONS

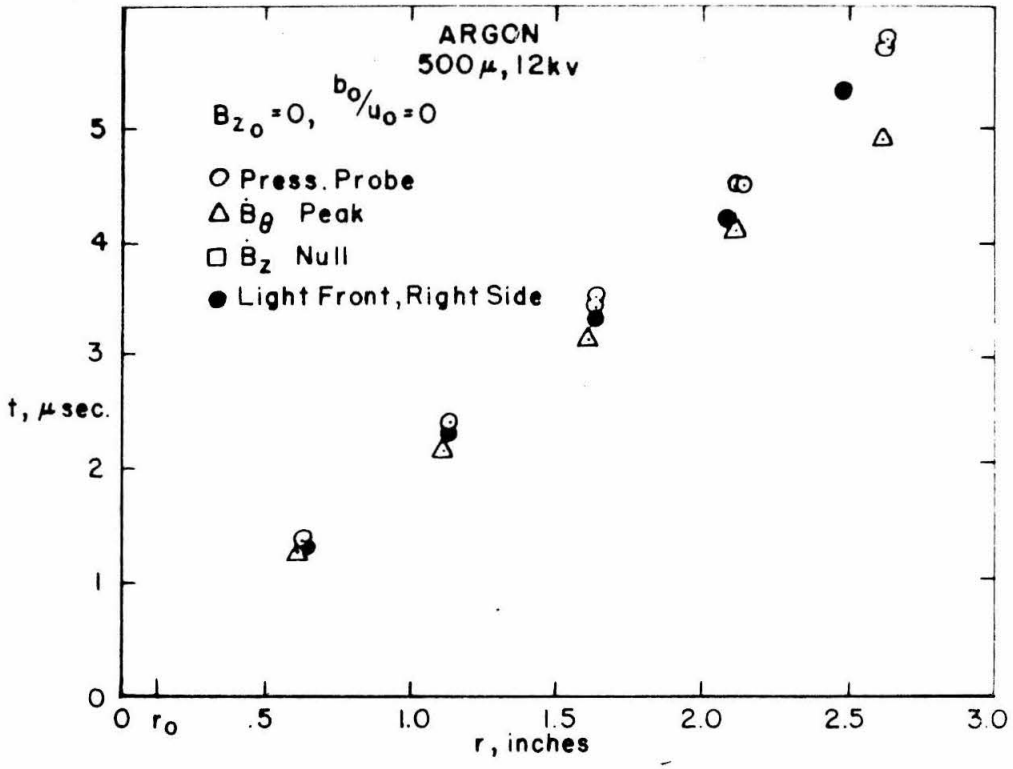

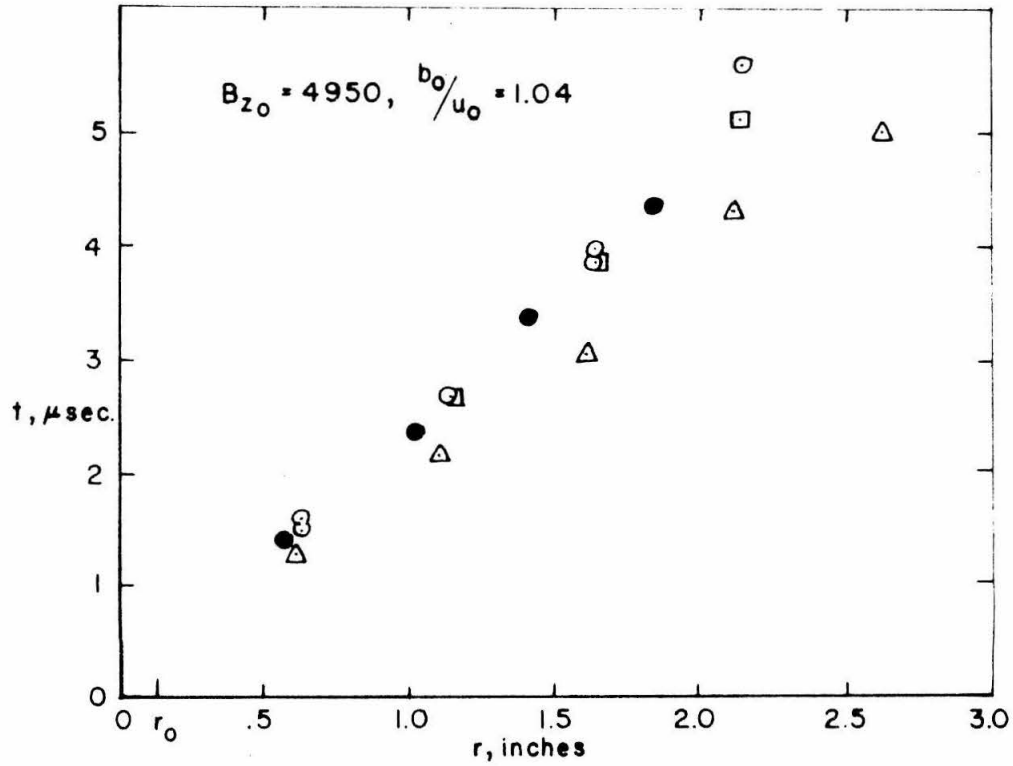

FIG. 10 RELATIVE FRONT POSITIONS

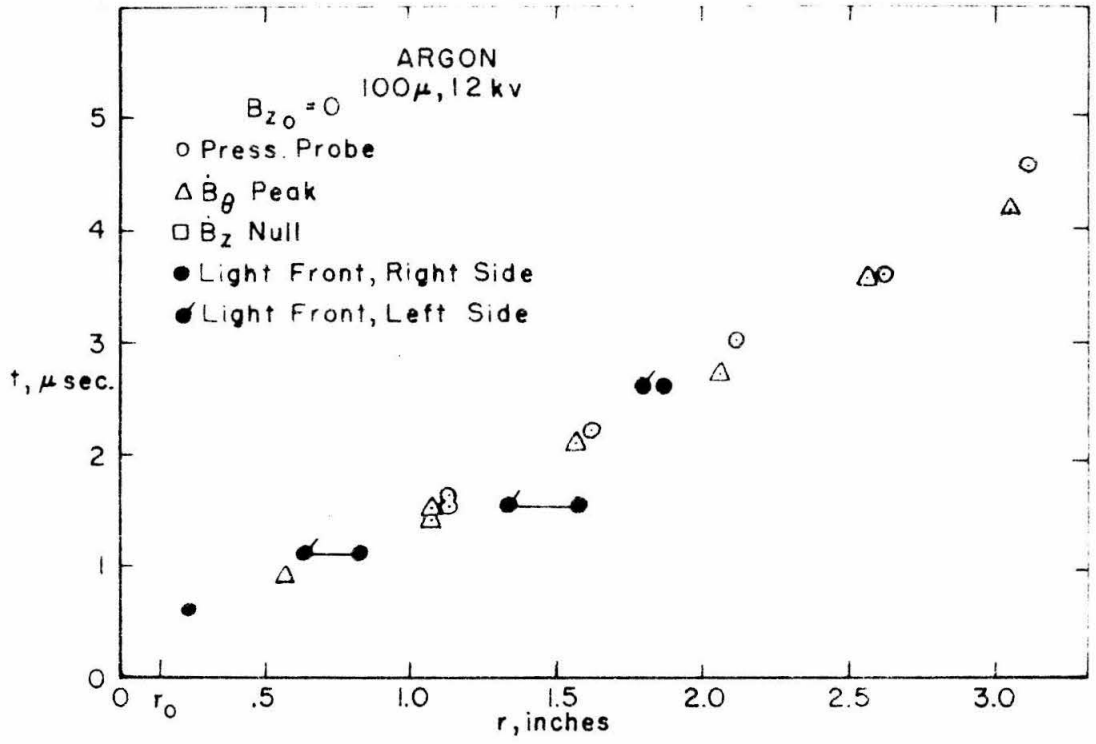

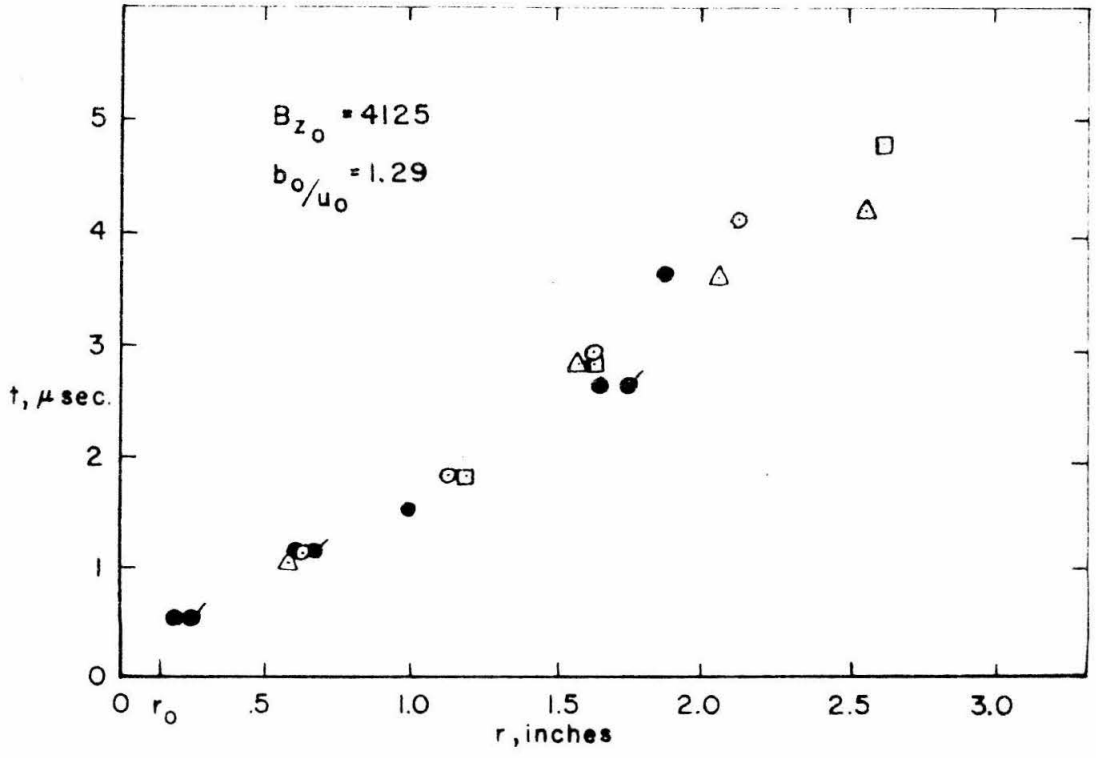

FIG. 11 RELATIVE FRONT POSITIONS

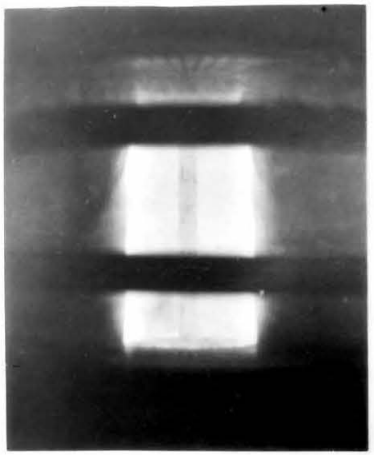

(a) $B_{z_o} = 0$, $p_o = 500\ \mu$

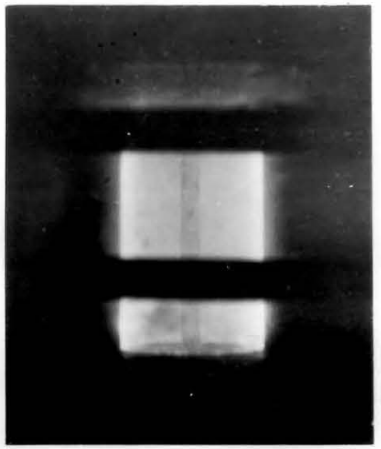

(b) $B_{z_o} = 1350$ g., $p_o = 500\ \mu$

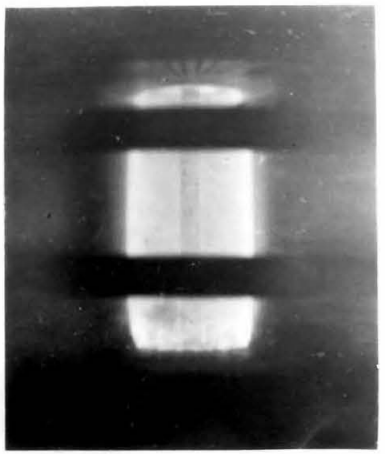

(c) $B_{z_o} = 4750$ g., $p_o = 500\ \mu$

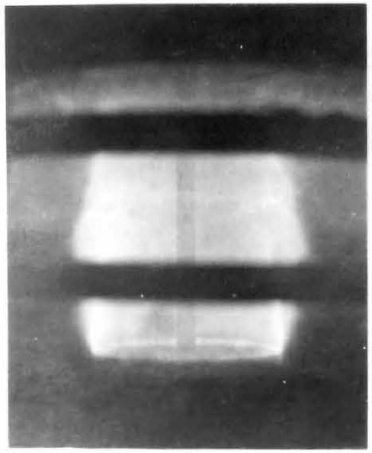

(d) $B_{z_o} = 0$, $p_o = 100\ \mu$

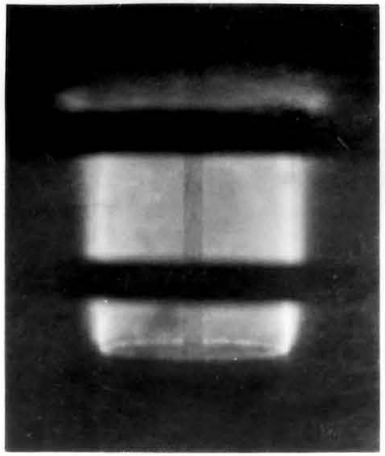

(e) $B_{z_o} = 1100$ g., $p_o = 100\ \mu$

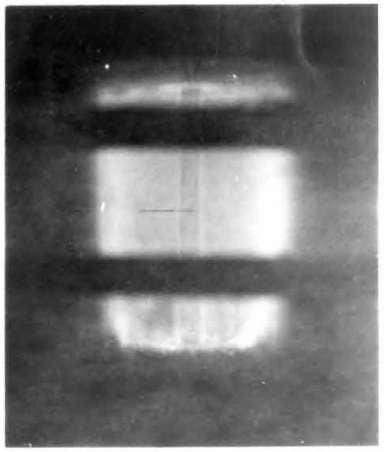

(f) $B_{z_o} = 4125$ g., $p_o = 100\ \mu$

Figure 12. Typical Kerr Cell Photographs in Argon

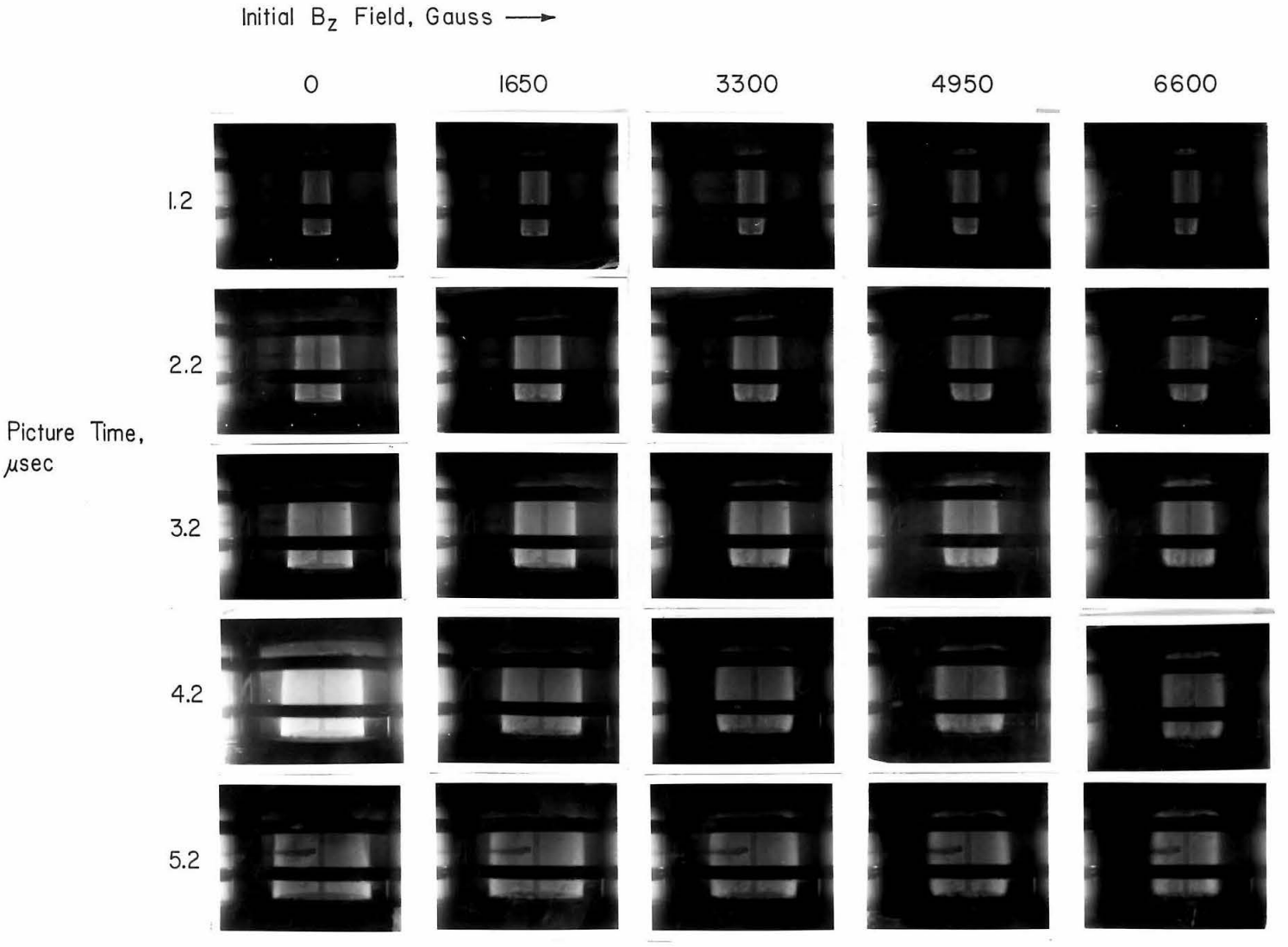

Figure 13. Kerr Cell Photographs in Argon at 500μ. Exposure Time .05μsec f16

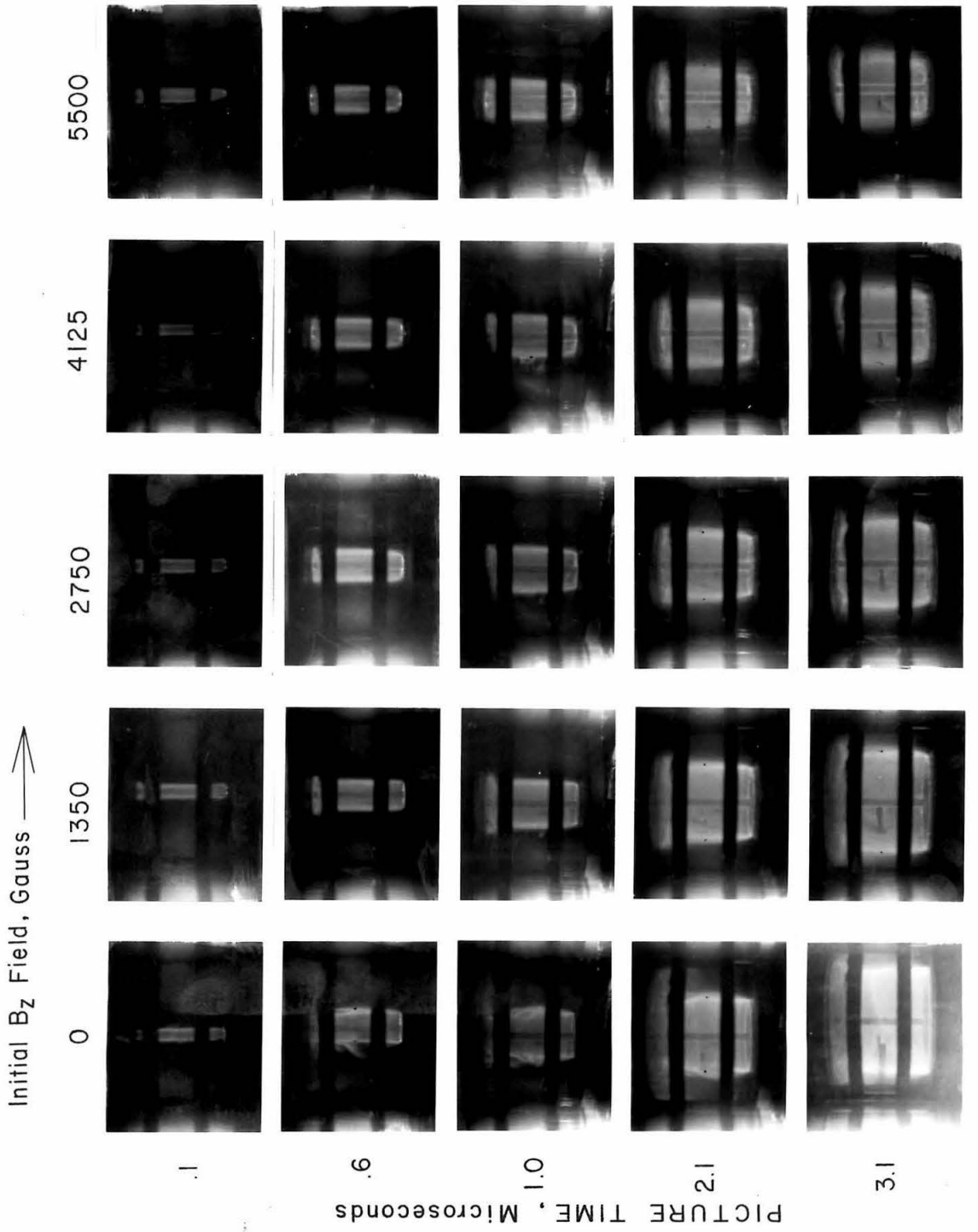

Figure 14. Kerr Cell Photographs in Argon at 100μ. Exposure Time .05μ sec f8

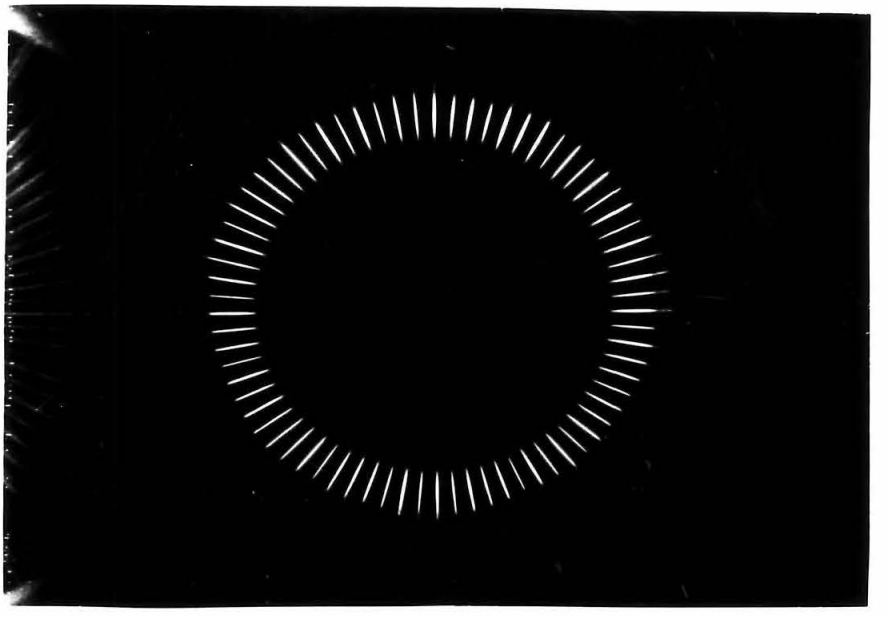

(a) $B_{z_o} = 0$

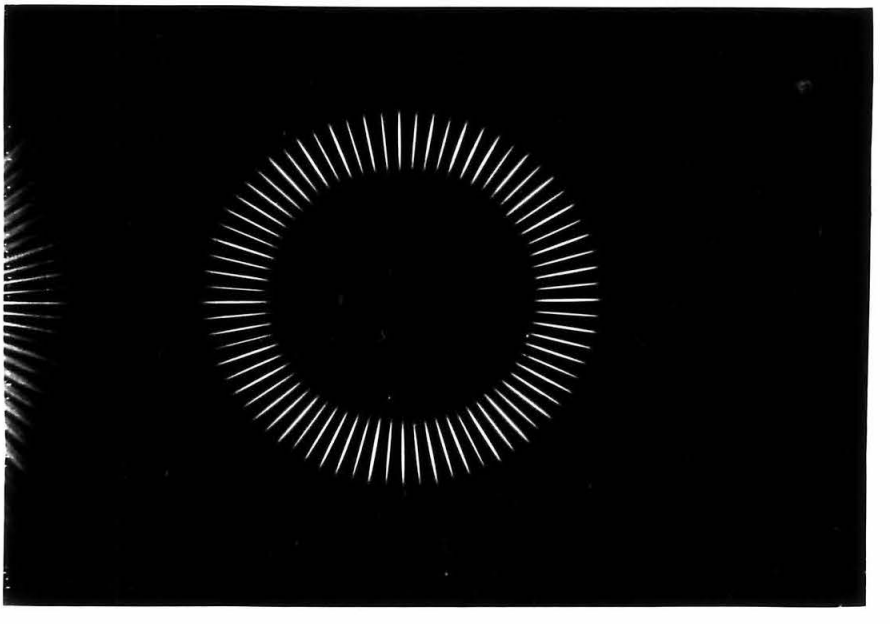

(b) $B_{z_o} = 4950$ g.

Fig. 15. Kerr Cell Photographs in Argon at 500μ Initial Pressure. Taken through the top electrode (anode) approximately 4.5 μ s after discharge. Exposure time .05 μ sec. Initial voltage 12 Kv.

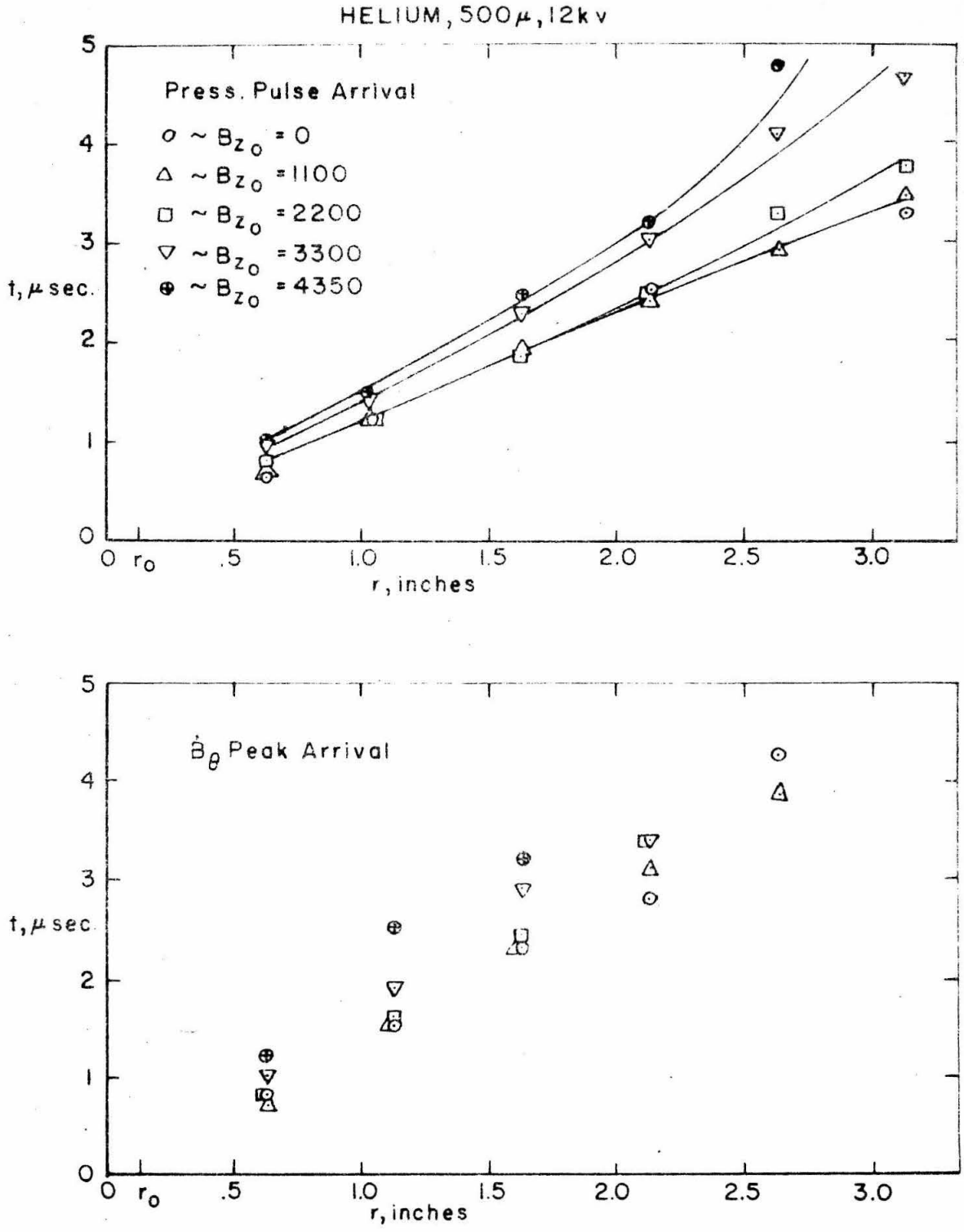

FIG. 16 EFFECT OF FIELD ON WAVE SPEEDS

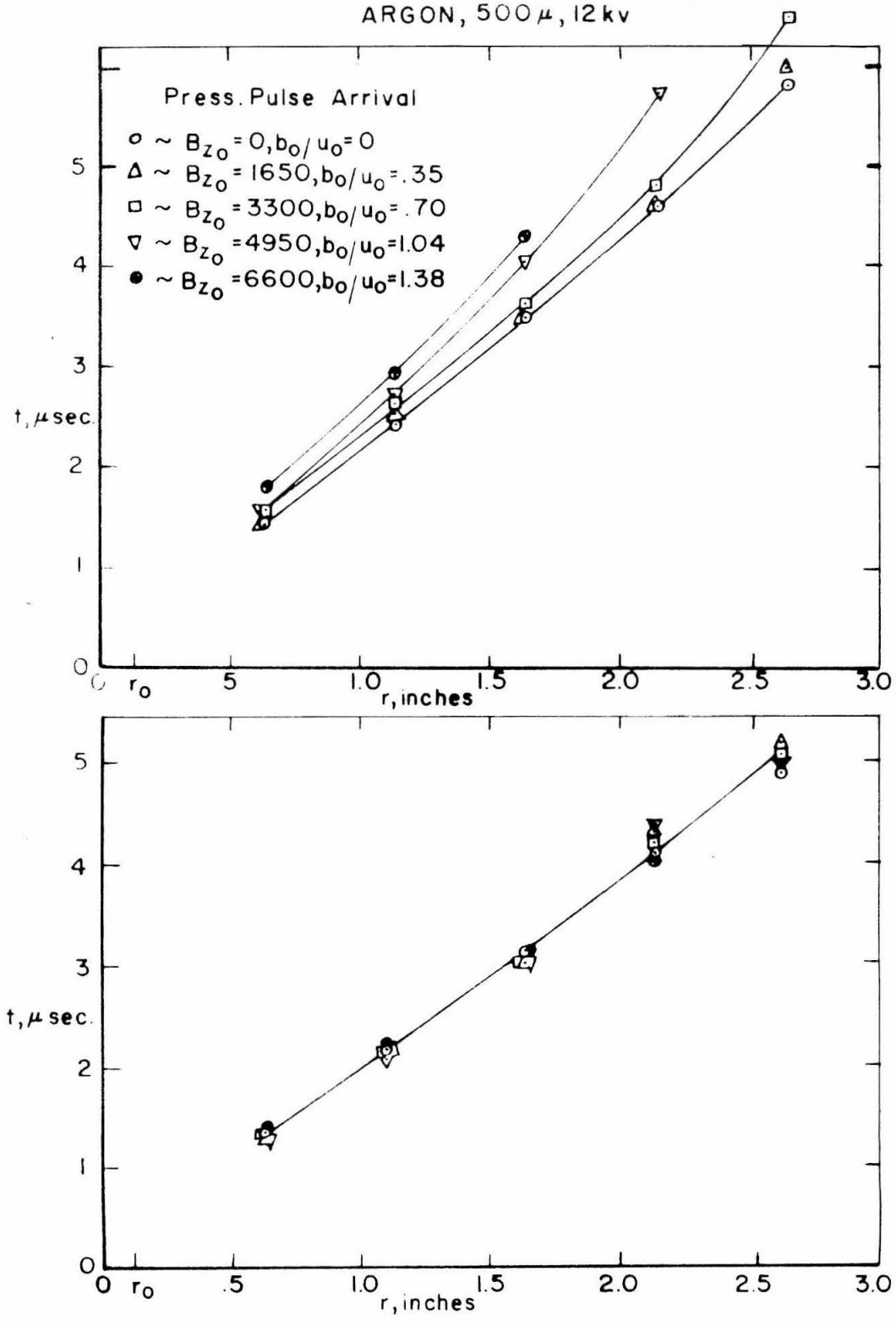

FIG. 17 EFFECT OF FIELD ON WAVE SPEEDS

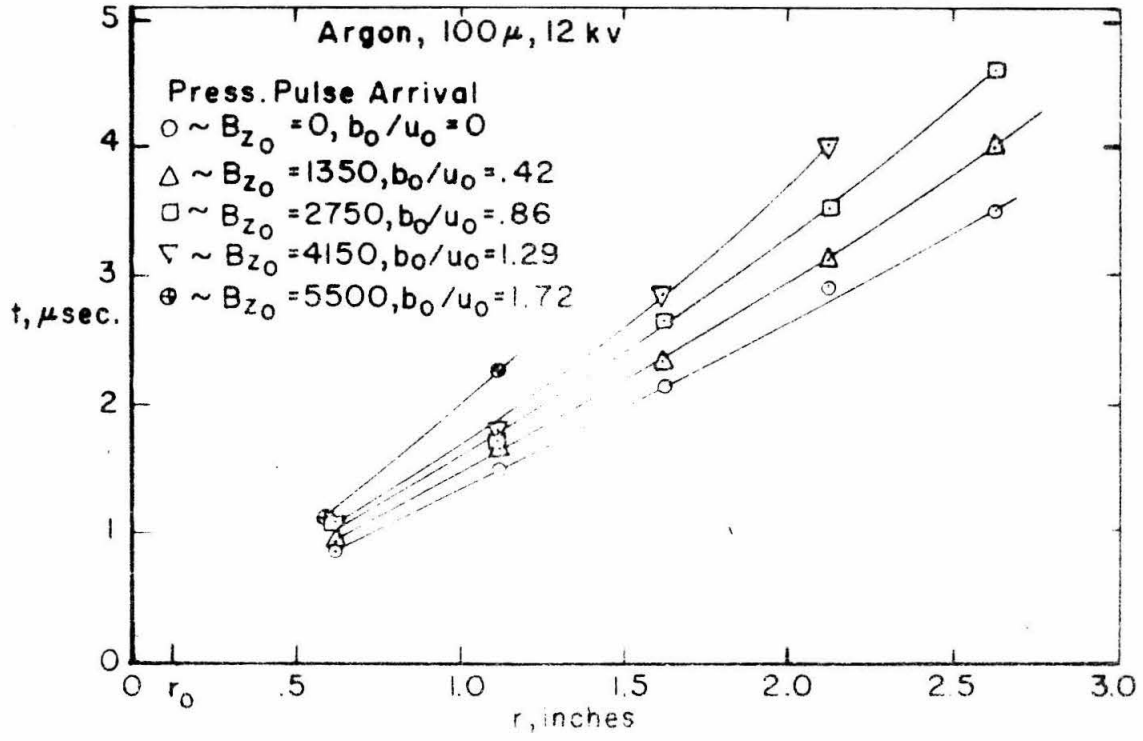

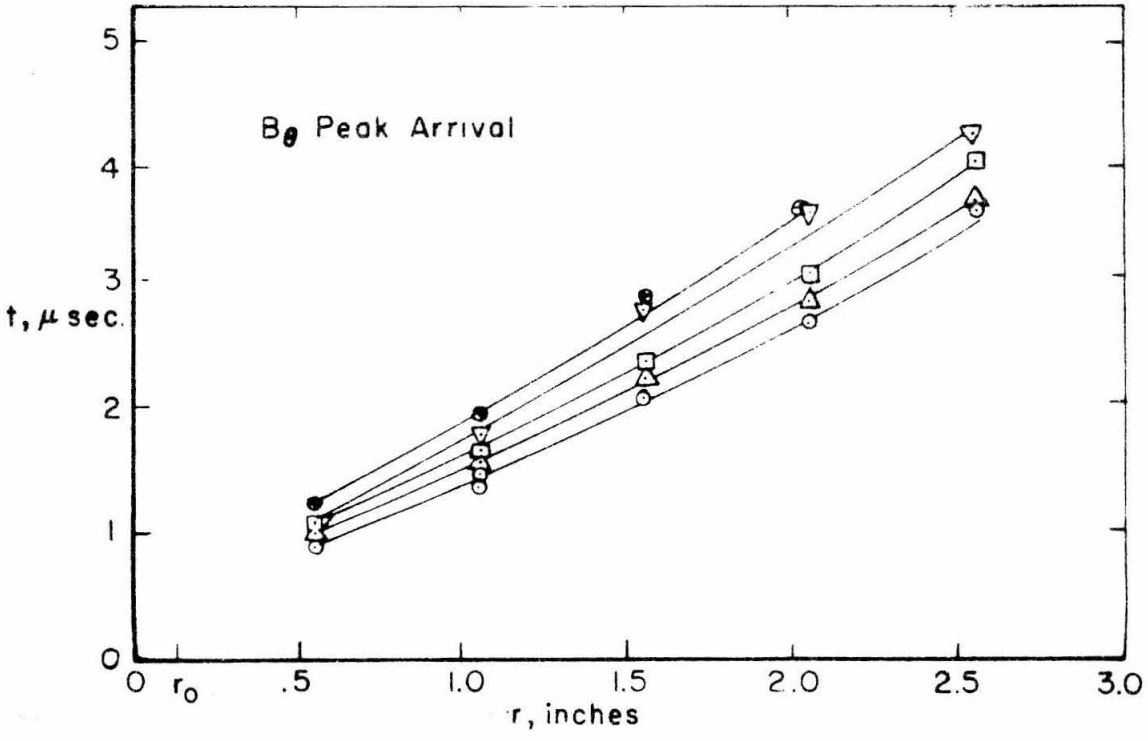

FIG. 18 EFFECT OF FIELD ON WAVE SPEEDS

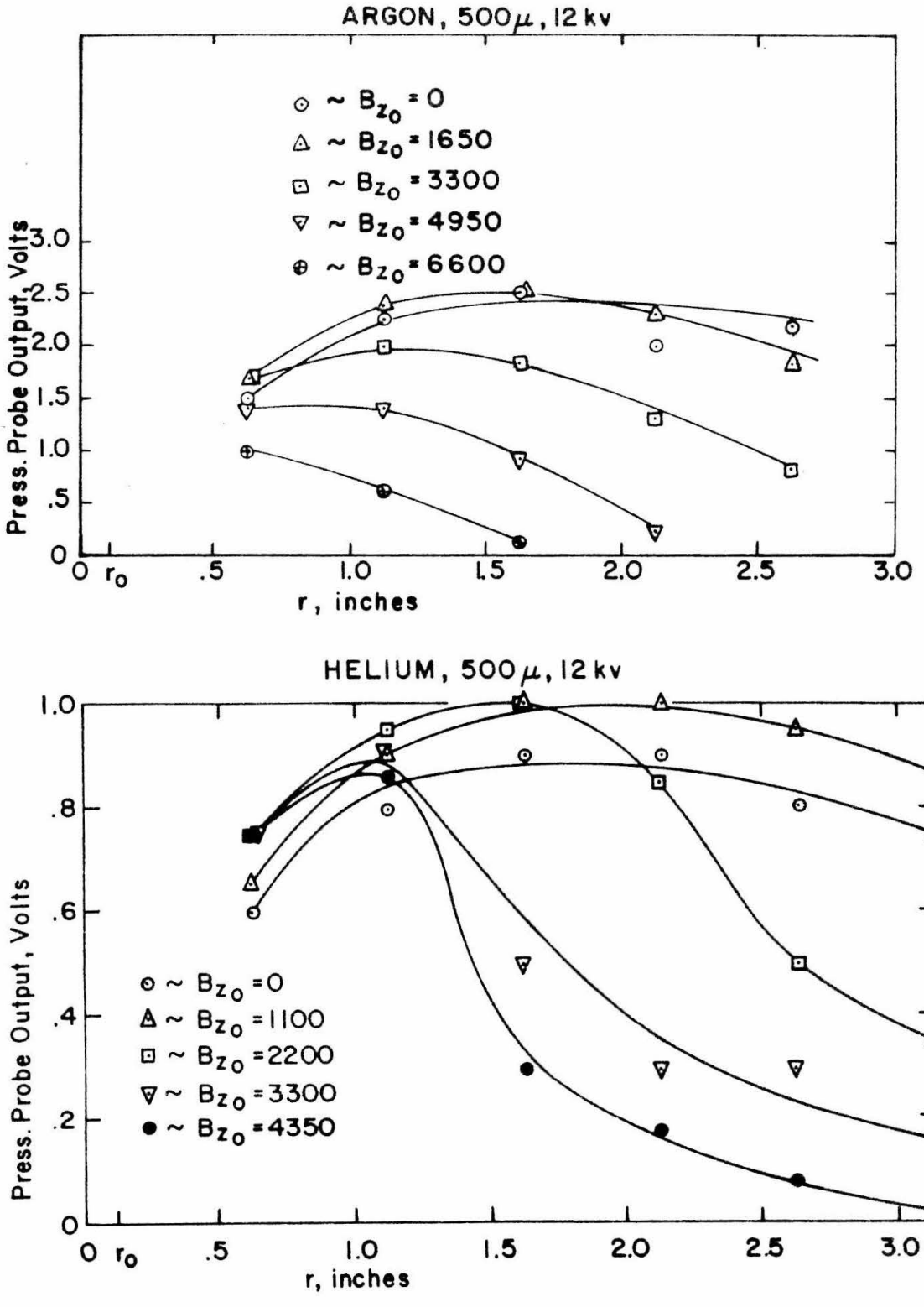

FIG. 19 DECAY OF PRESSURE PULSE AMPLITUDES

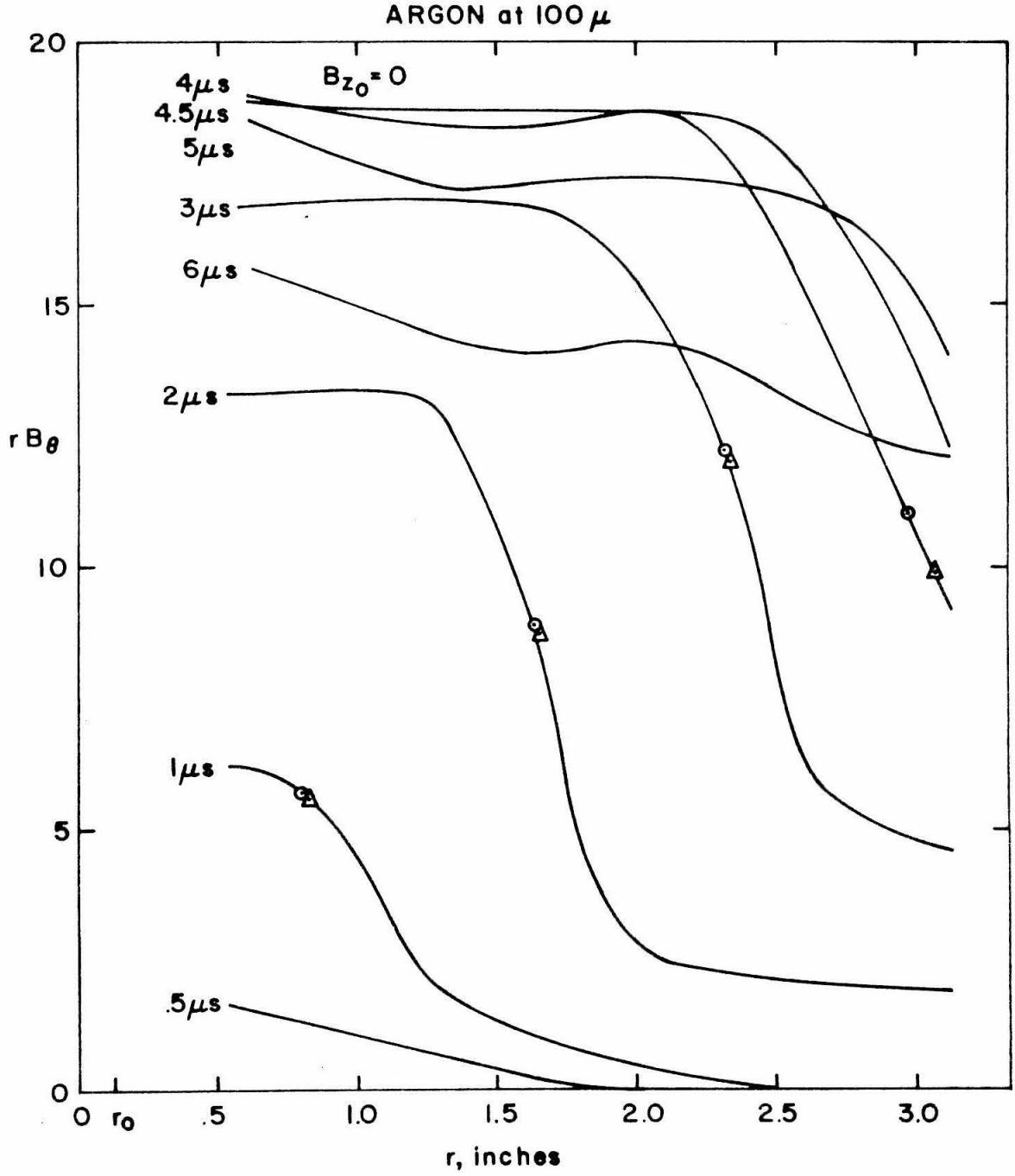

FIG. 20 PROFILES OF rB_θ

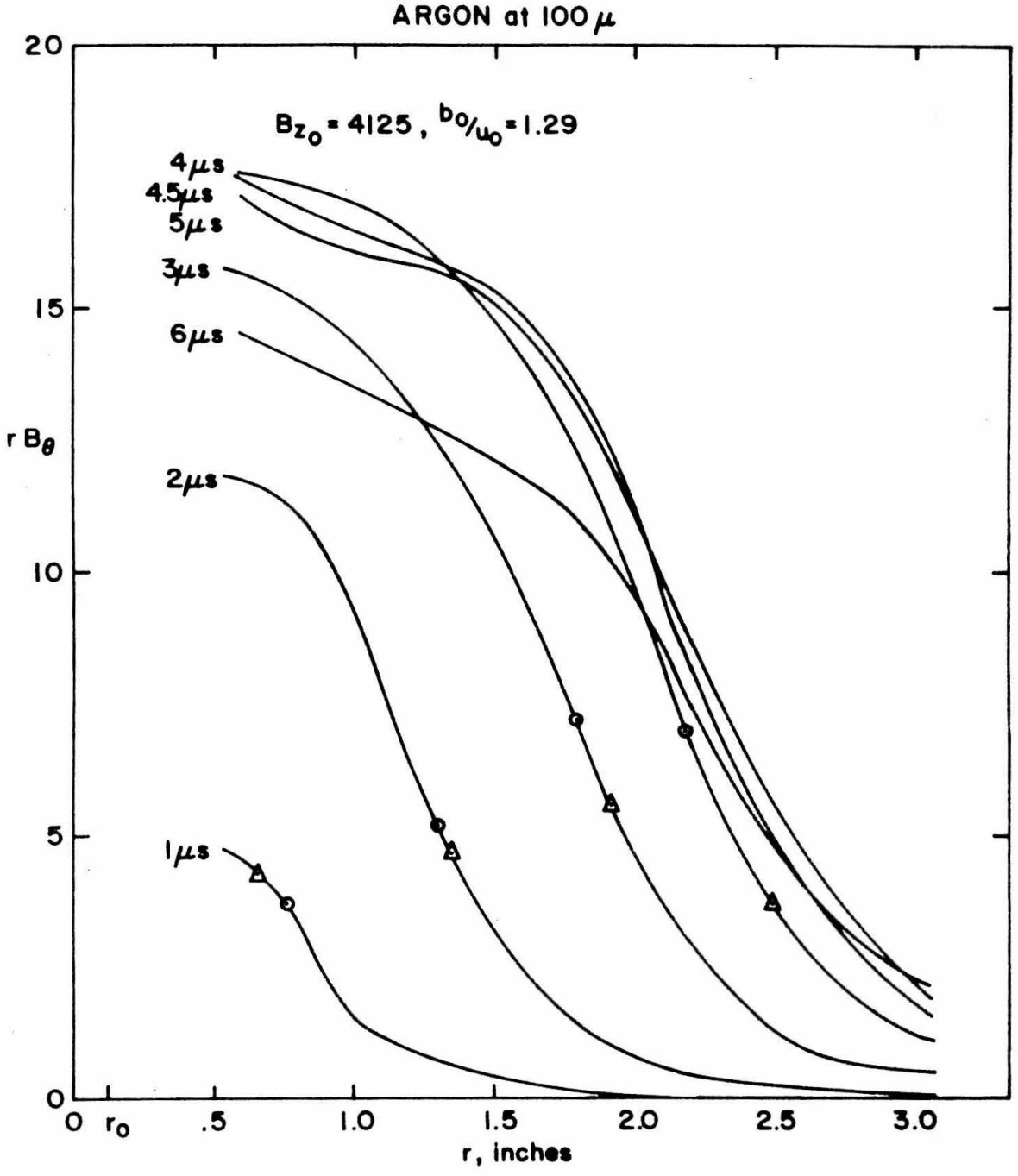

FIG. 21 PROFILES OF rB_θ

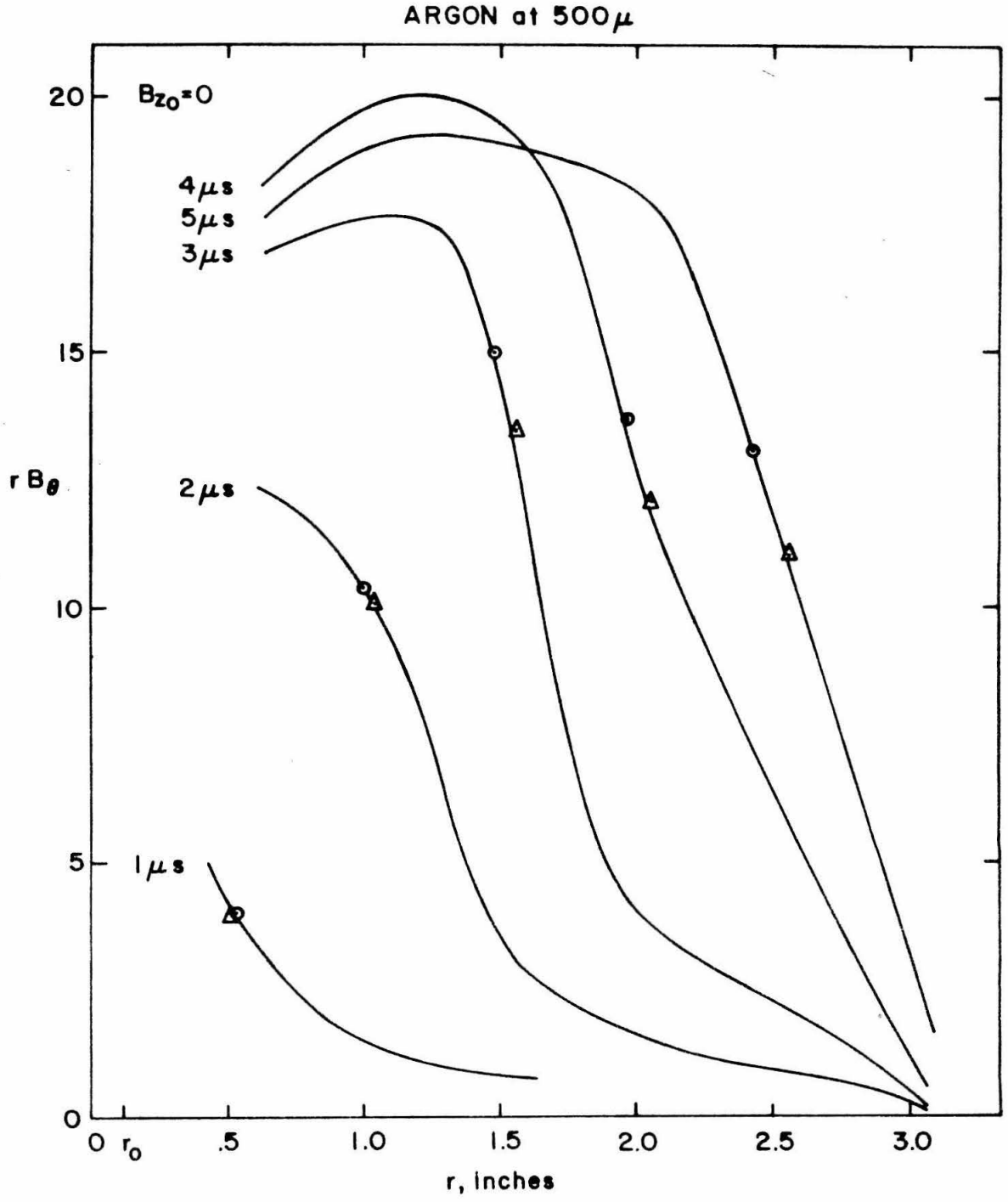

FIG. 22 PROFILES OF rB_θ

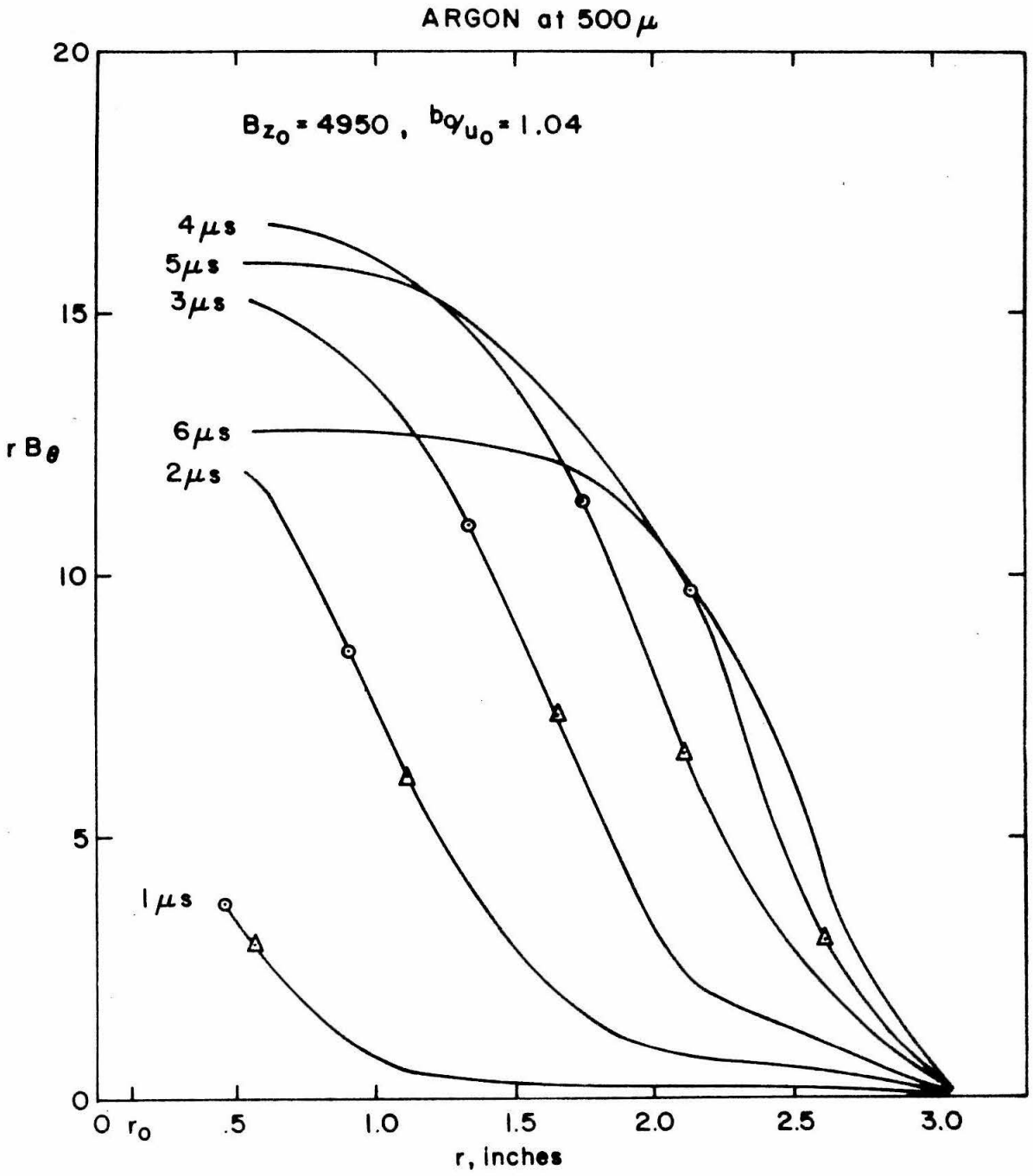

FIG. 23 PROFILES OF rB_θ

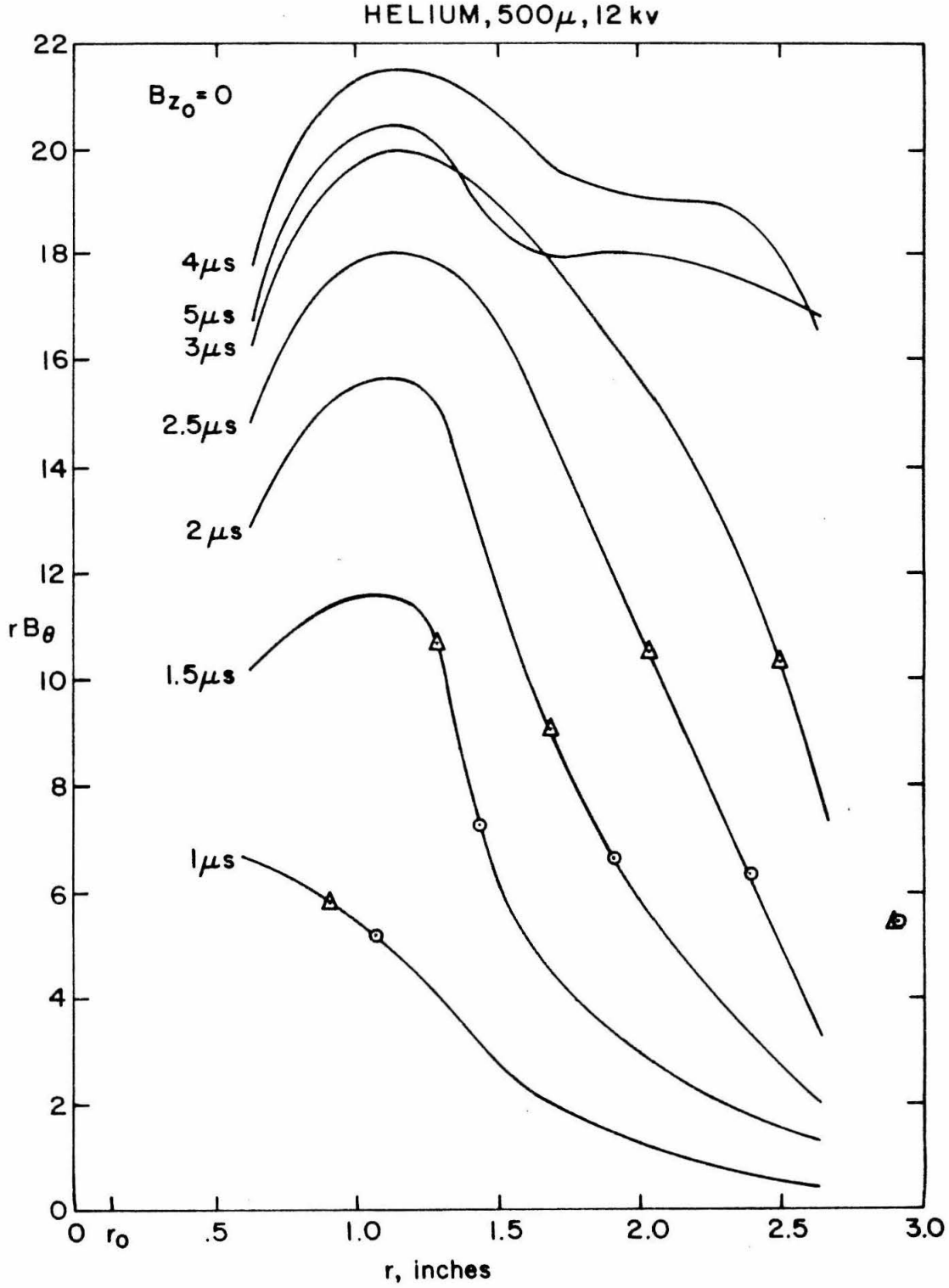

FIG. 24 PROFILES OF rB_θ

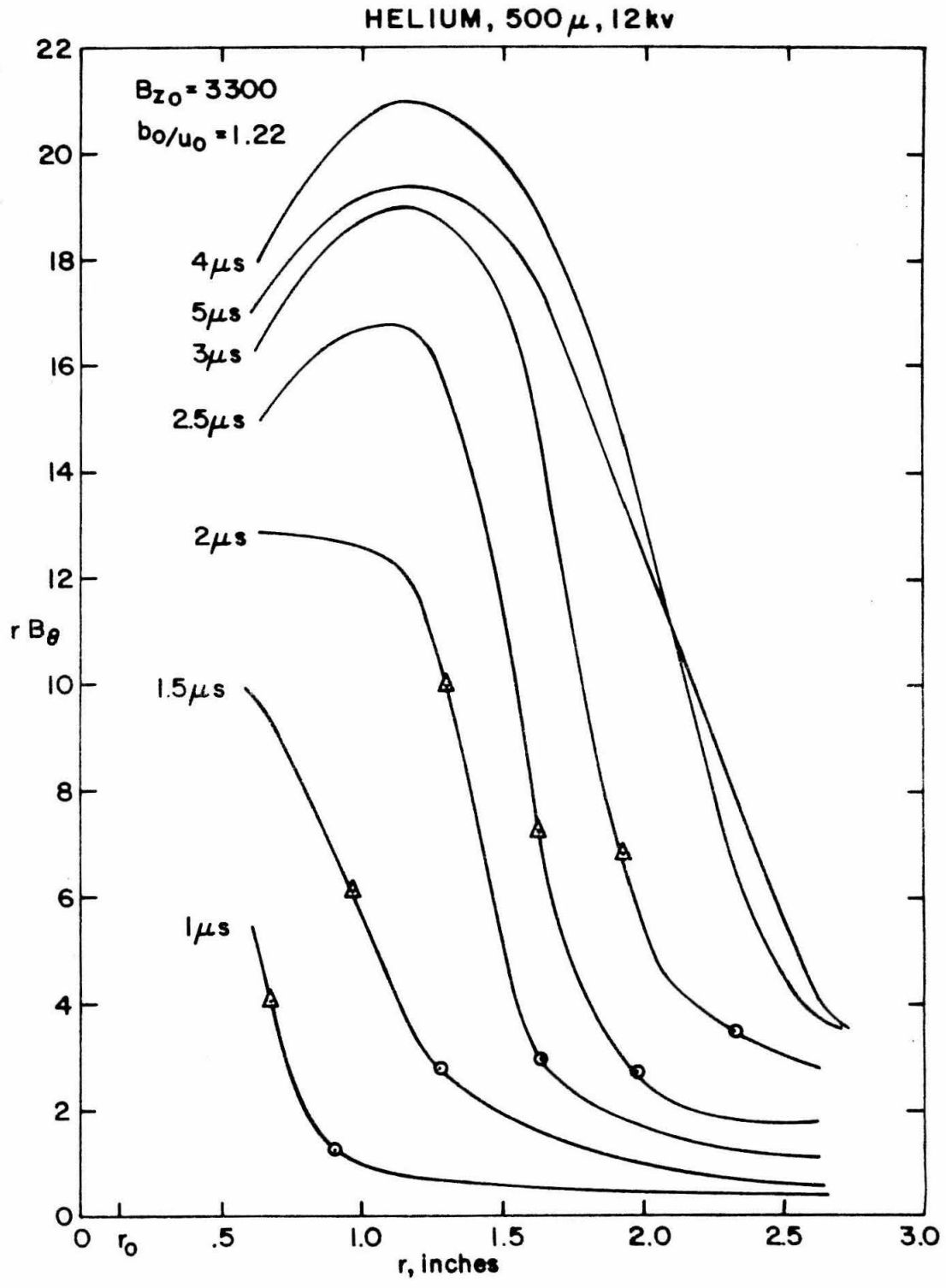

FIG. 25 PROFILES OF r B_θ

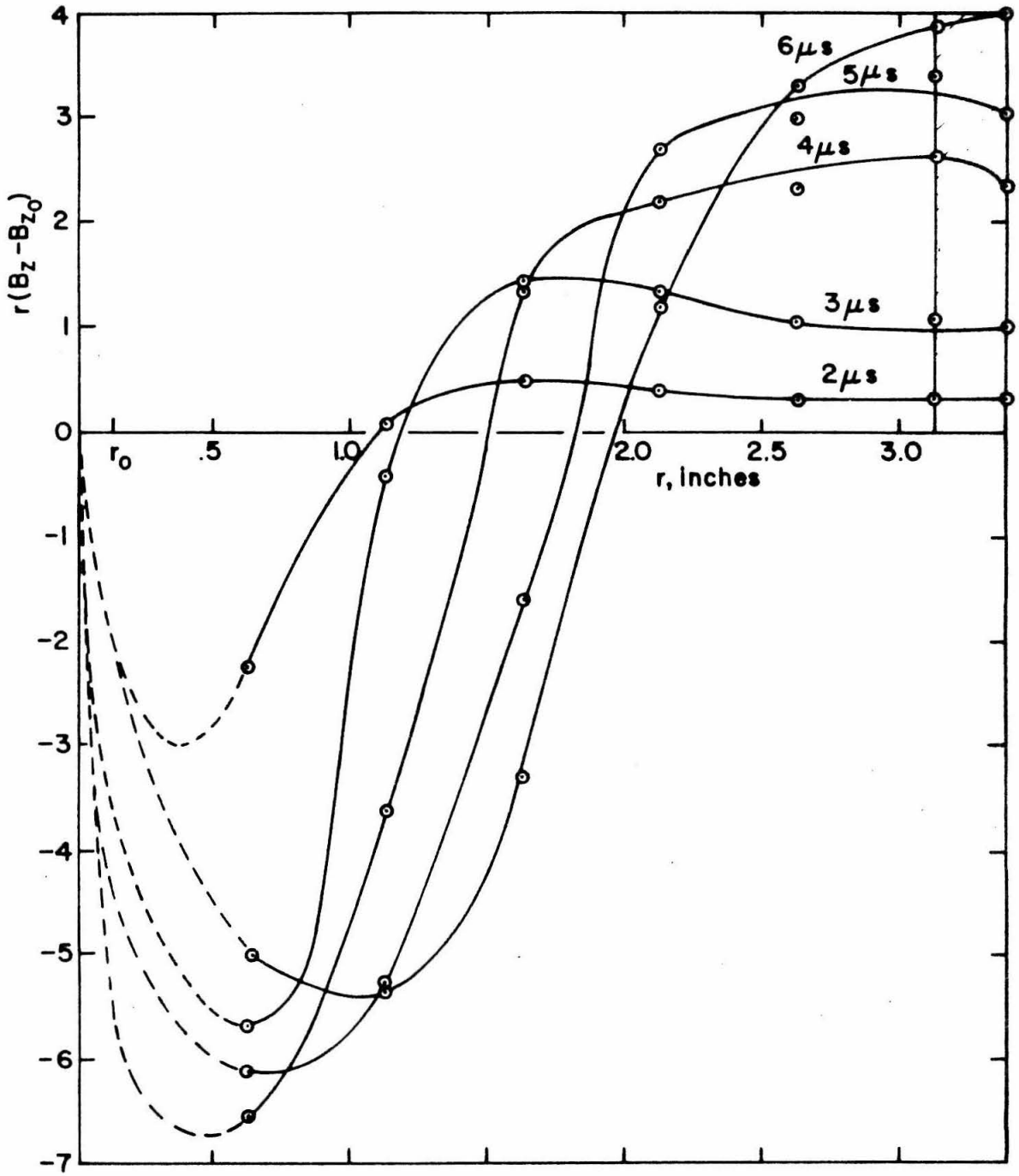

FIG. 26 CONSERVATION OF FLUX, ARGON, 500 μ

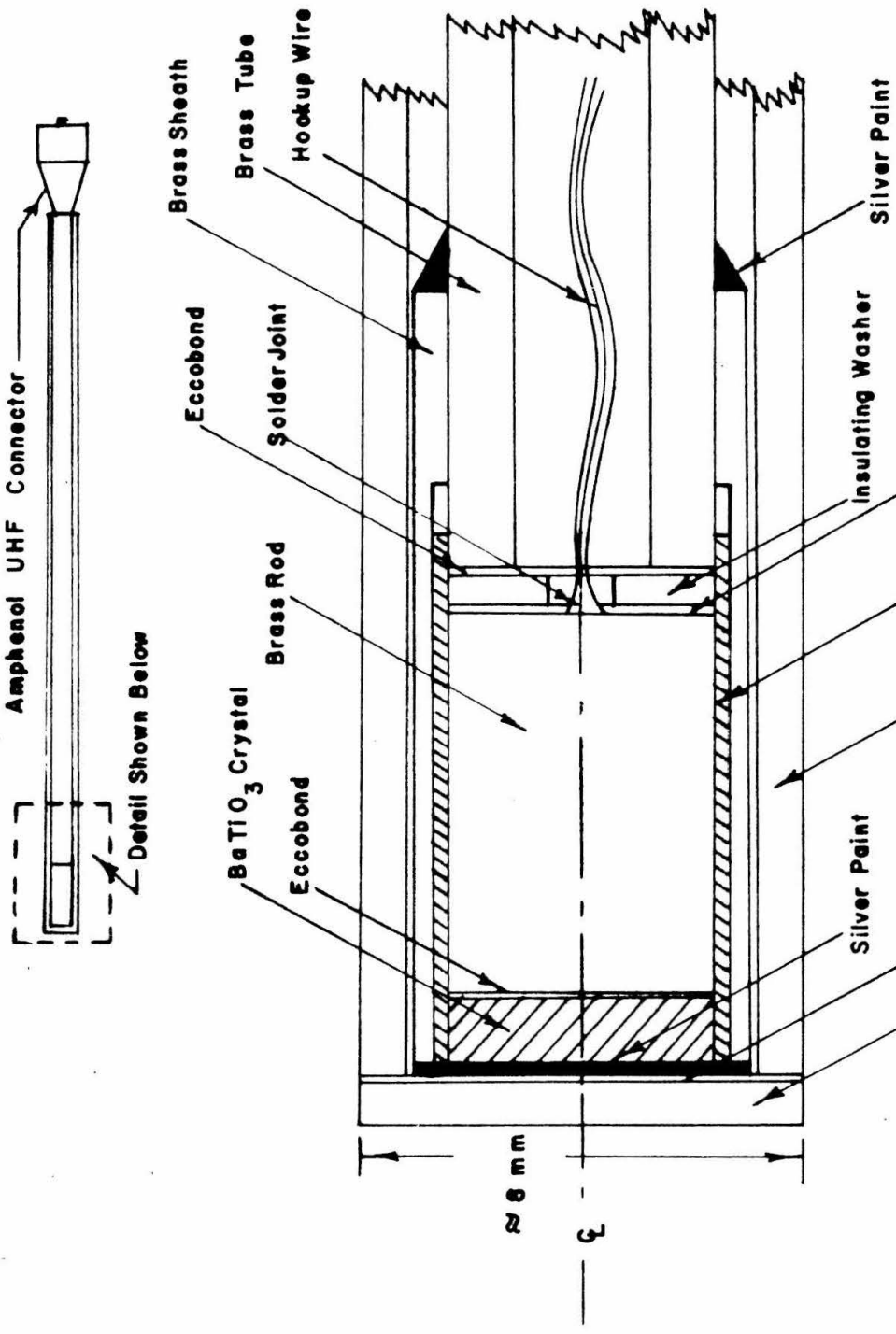

FIG.27 CROSS SECTION OF PRESSURE PROBE

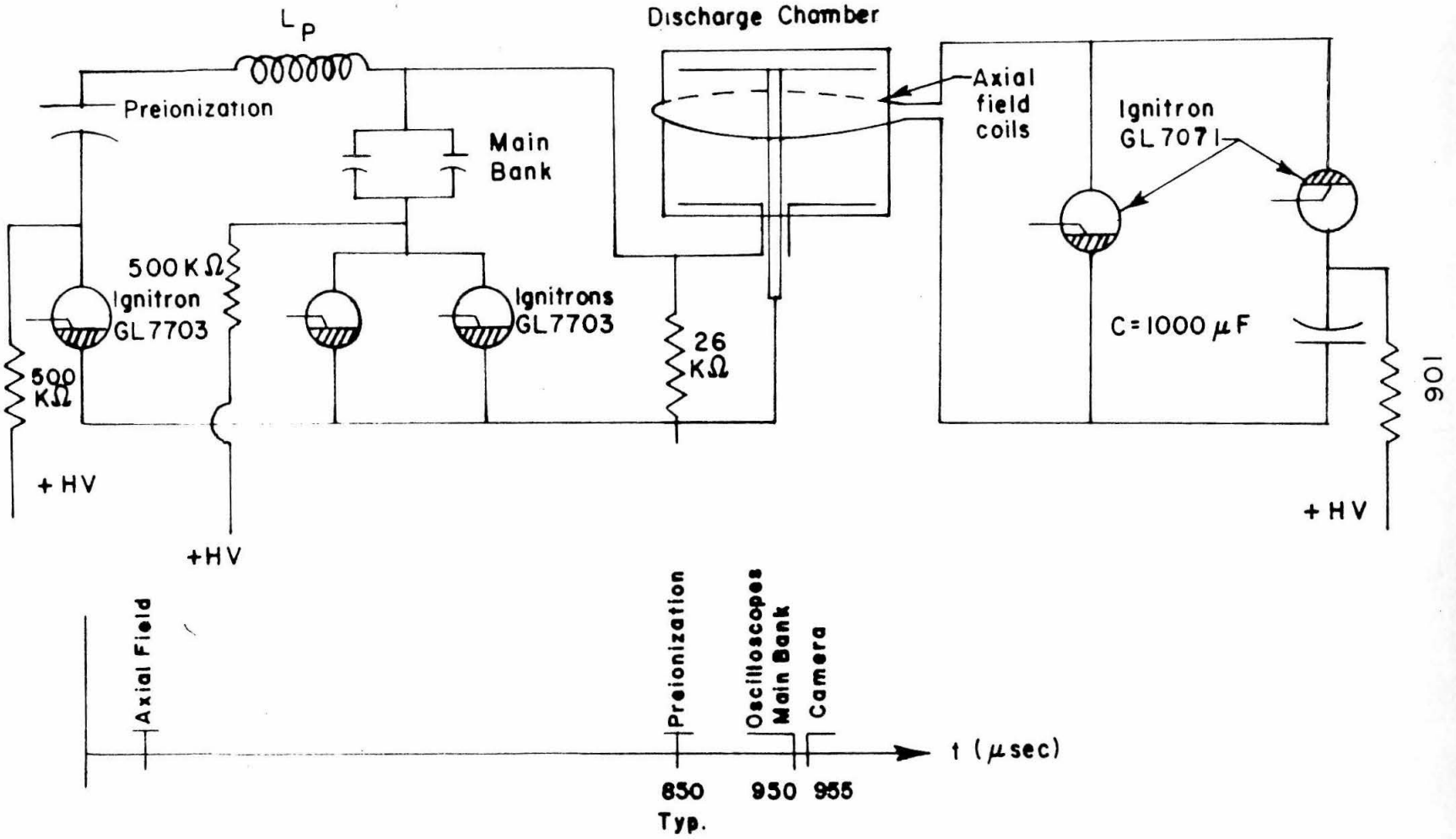

FIG.28 DISCHARGE CIRCUITS AND TYPICAL TIMING SEQUENCE

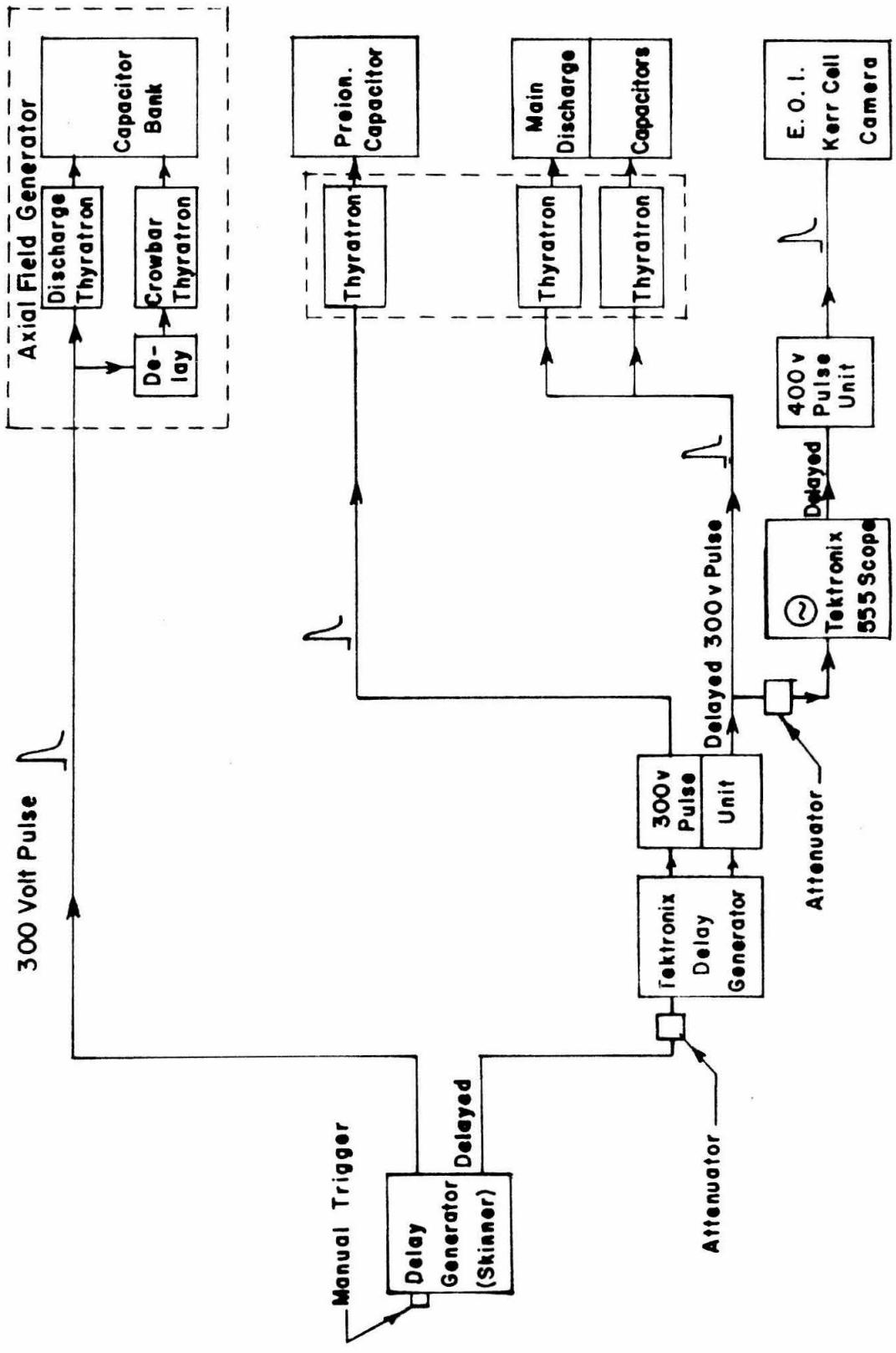

FIG. 29 BLOCK DIAGRAM OF TIMING AND TRIGGERING CIRCUITS

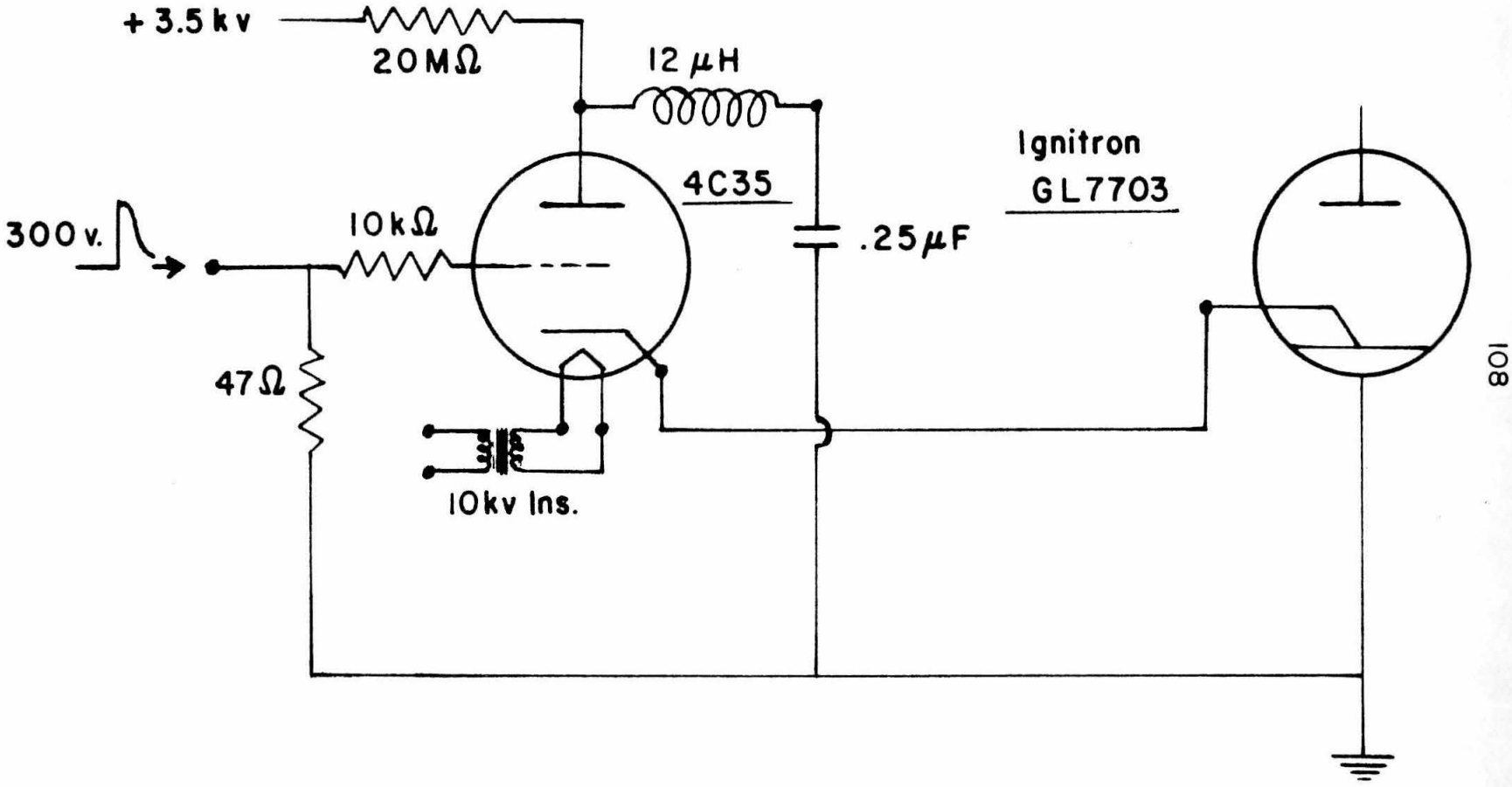

FIG. 30 IGNITRON FIRING CIRCUIT

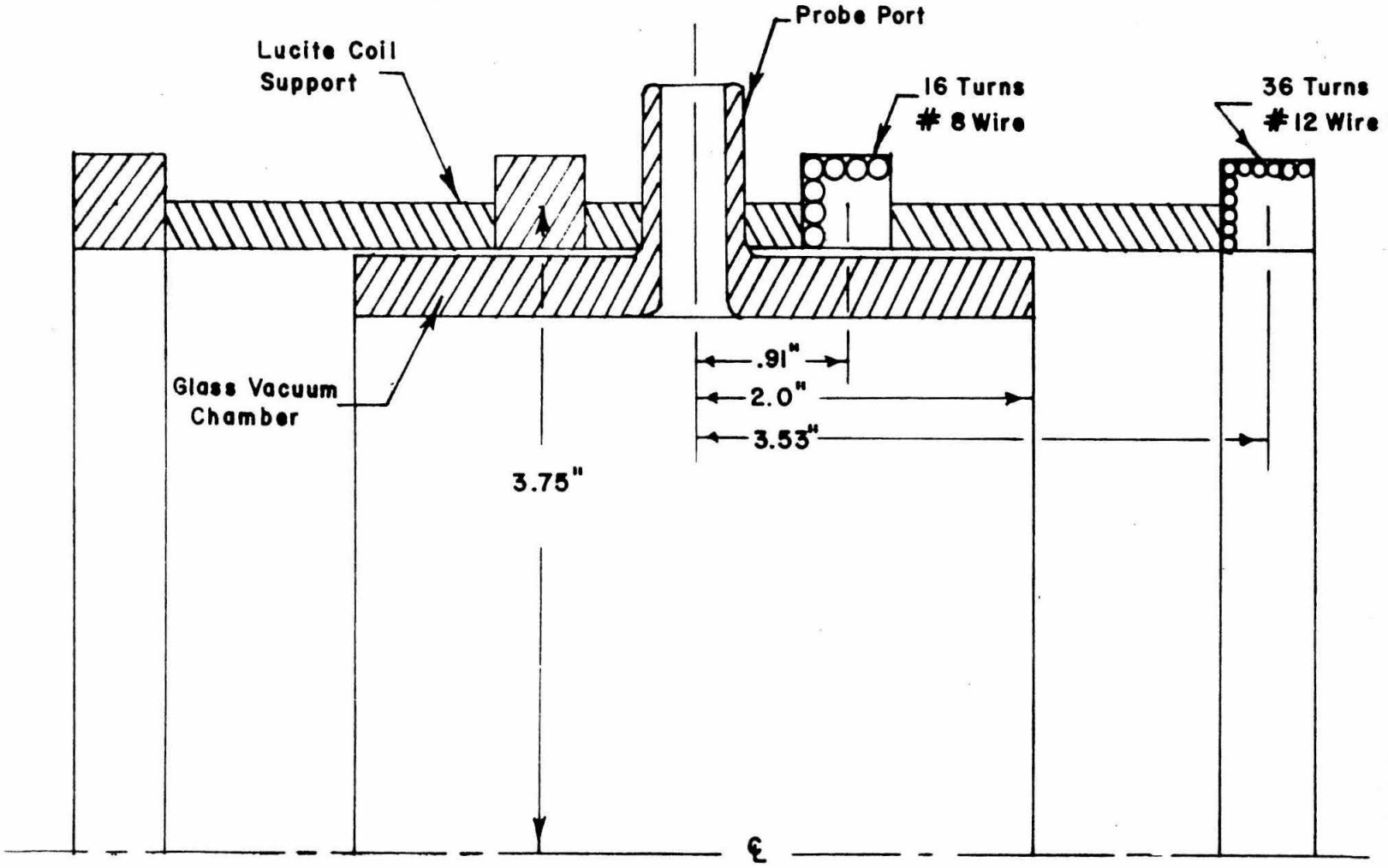

FIG.31 AXIAL FIELD COIL CONFIGURATION